INFORMATION TO USERS

This dissertation was produced from a microfilm copy of the original document. While the most advanced technological means to photograph and reproduce this document have been used, the quality is heavily dependent upon the quality of the original submitted.

The following explanation of techniques is provided to help you understand markings or patterns which may appear on this reproduction.

1. The sign or "target" for pages apparently lacking from the document photographed is "Missing Page(s)". If it was possible to obtain the missing page(s) or section, they are spliced into the film along with adjacent pages. This may have necessitated cutting thru an image and duplicating adjacent pages to insure you complete continuity.

2. When an image on the film is obliterated with a large round black mark, it is an indication that the photographer suspected that the copy may have moved during exposure and thus cause a blurred image. You will find a good image of the page in the adjacent frame.

3. When a map, drawing or chart, etc., was part of the material being photographed the photographer followed a definite method in "sectioning" the material. It is customary to begin photoing at the upper left hand corner of a large sheet and to continue photoing from left to right in equal sections with a small overlap. If necessary, sectioning is continued again — beginning below the first row and continuing on until complete.

4. The majority of users indicate that the textual content is of greatest value, however, a somewhat higher quality reproduction could be made from "photographs" if essential to the understanding of the dissertation. Silver prints of "photographs" may be ordered at additional charge by writing the Order Department, giving the catalog number, title, author and specific pages you wish reproduced.

University Microfilms

300 North Zeeb Road
Ann Arbor, Michigan 48106

A Xerox Education Company

Crack propagation velocities in NaCl crystals

by

Donald Lee Hindman

A Dissertation Submitted to the
Graduate Faculty in Partial Fulfillment of
The Requirements for the Degree of
DOCTOR OF PHILOSOPHY

Major: Ceramic Engineering

Approved:

Signature was redacted for privacy.

In Charge of Major Work

Signature was redacted for privacy.

For the Major Department

Signature was redacted for privacy.

For the Graduate College

Iowa State University
Ames, Iowa

1973

TABLE OF CONTENTS

INTRODUCTION

The study of crack propagation is of engineering importance because many materials fail by brittle fracture, frequently with serious consequences. Crack initiation alone does not imply brittleness since, for brittle fracture to occur, the crack must propagate rapidly (1). It therefore appears that the rate of crack propagation is the determining factor in the ductility or brittleness of materials.

It has recently become possible to relate the rate of crack propagation to the surface energy of solids (2,3). This is probably the most direct method of determining the surface energy (4). Surface energy has great bearing on the mechanical and chemical properties of materials (5). Therefore a knowledge of the surface energy is useful in such areas as the development of adhesives, studies of friction and lubrication, and development of glass to metal seals (6). Surface energy must also be considered in the study of filtration, sintering, wetting of surfaces, and the cleaning and polishing of surfaces.

Because of the key role that fracture velocity plays in determining the ductility or brittleness of materials, it was the object of this study to assess the effects of atmosphere and temperature on the crack velocity in NaCl. A second goal was to relate the cleavage energy of NaCl to crack velocity (and thereby determine its temperature and atmosphere depend-

ence).

NaCl was chosen for experimentation since it is particularly amenable to study of the cleavage process. Because of its transparency and simple structure, it has been used in numerous studies and much is already known about its behavior. Structures produced during cleavage are easily observed with optical microscopy with the aid of standard etching techniques. The solubility of NaCl in water also simplifies the replication techniques used in electron microscopy. Large, relatively pure single crystals are readily available. With the exercise of reasonable care, these crystals can easily be cleaved to obtain test specimens of uniform size.

LITERATURE REVIEW

A review of the literature reveals numerous methods for measuring the surface energy of materials. Kuznetsov (7), Gregg (8), and Partington (9) describe many of the methods and give a short historical review of the subject of surface energy. Duga (6) has compiled a comprehensive list of the surface energies of ceramic materials and the methods by which the results were obtained. He divided the methods of measurement into 2 broad categories, thermodynamic and mechanical. Among the thermodynamic methods are: heat of solution (10,11), heat of immersion (12), rate of solubility (7), and the critical surface tension for the wetting of a solid by a liquid (13,14,15). The mechanical methods include: measurement of the surface area produced by crushing (7,16,17,18), mutual grinding (7), and the measurement of the force required to balance the surface tension of a wire near its melting point (19). The mechanical method, cleavage and fracture of crystals and noncrystalline solids, which is of direct interest in this study, will be discussed in some detail.

Double Cantilever Method of Surface Energy Measurement

Obreimoff (20) is generally regarded as the first to apply the cleavage technique to the determination of surface energy. He carefully split sheets of mica with a glass wedge and was able to determine an energy required for the separation of the sheets. The amount of energy required appeared to be dependent

on the environment since the strength of mica was greater in vacuum than in air. In cases where the fresh surfaces were undisturbed by scratches or contamination, they could be rejoined so that a slightly smaller force was required to separate them a second time. Mica has since been studied by several others through use of the cleavage technique (21,22).

Gilman (4) applied the cleavage technique to materials of simpler crystal structure than mica and greatly extended its usefulness. His major modification was to sample geometry. He used crystals in the shape of partially cracked rectangular blocks as shown in Figure 1. This has since become the standard geometry for the cleavage technique. Gilman found that the use of a wedge to cleave crystals gave poor reproducibility. (This will later be discussed in more detail.) He developed a method by which the crystal could be pulled apart. The force required to cause the crack to begin to propagate was then measured. By treating the 2 halves of the partially cleaved crystals as cantilever beams, Gilman was able with the aid of simple elastic theory to relate the force at the instant of crack propagation to the deflection of the beams. He assumed that when the crack length was large with respect to the transverse crystal dimensions, deflection due to shearing forces and the kinetic energy associated with the sidewise motion of the beams were small and could be neglected. The surface energy was then calculated by equating the work done

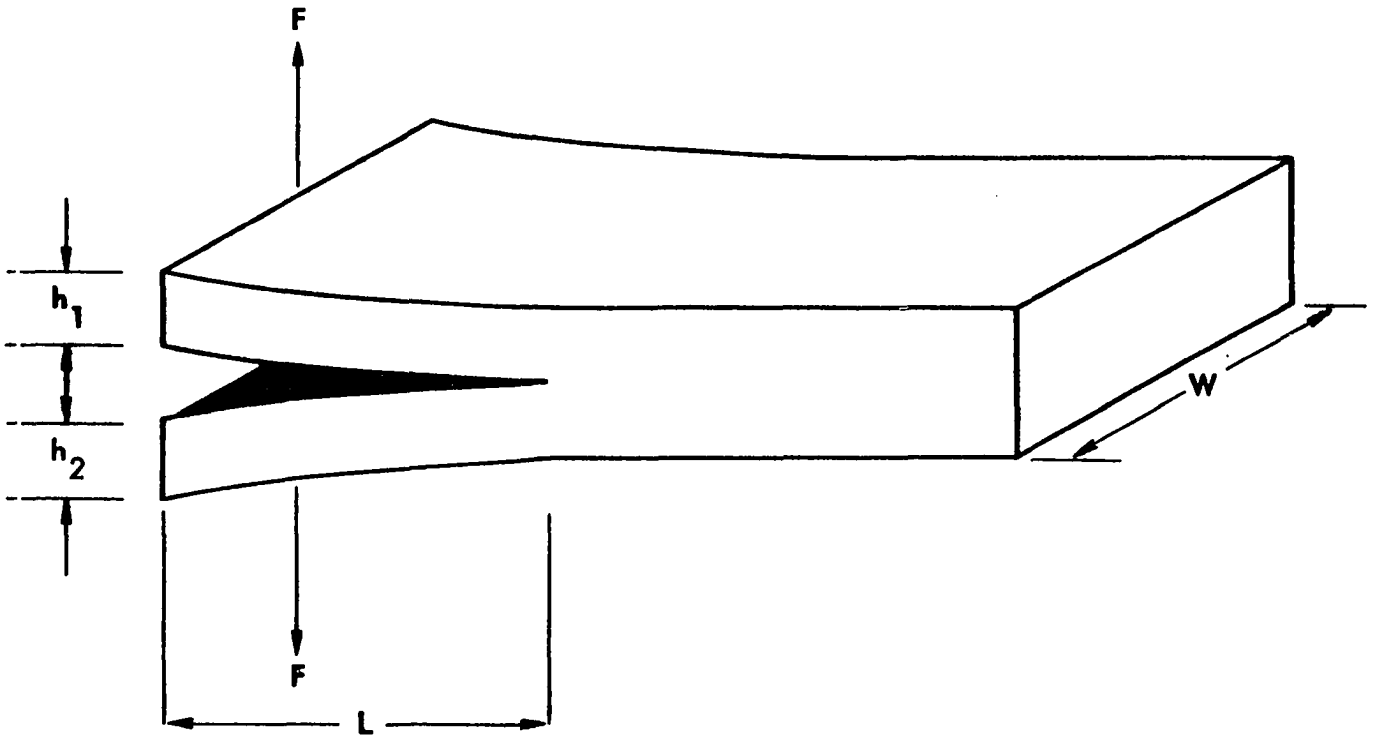

Figure 1. Typical double cantilever specimen

in causing an infinitesimal deflection of the beams to the change in the strain energy of the beams plus the energy required to increase the surface by an infinitesimal amount. Gilman's equation is

$$\gamma = 6F^2L^2/EW^2t^3$$

where γ is the cleavage energy, F is the force required to initiate crack growth, L is the initial crack length, E is the elastic modulus, W is the specimen width, and t is the height of one of the cleavage arms of the specimen.

Gilman found that, unlike mica, most of the materials he tested were not strongly influenced by the environment. He implied that the difference in behavior of mica from that of other materials was caused by the nature of the electrical charges on freshly cleaved surfaces of mica. He also noted that fairly high values of surface energy were obtained in LiF crystals unless the tests were conducted at very low temperatures. This was presumably due to absorption of energy in such processes as temperature enhanced plastic flow at the crack tip. When this occurred it was necessary to denote the energy as "effective surface energy" to signify that cleavage had occurred nonreversibly.

The Gilman cleavage technique has since been used by several workers to test the effects of environment and other factors on the surface energy. Jaccodine (23) measured the surface energy of germanium and silicon in air and liquid nitrogen. In air, he noted that oxidation products on the cleavage surfaces wedged open the crack and caused the apparent surface

energy to be low. Gutshall and Gross (24) measured the cleavage energies of NaCl and MgO single crystals in liquid nitrogen and in vacuum. They found that these environments had little influence on the cleavage energy and attributed this to the inability of contaminants to diffuse into an atomically sharp crack.

Shockey and Groves (25) tested MgO single crystals in air and in water. Water vapor in the air did not significantly affect the cleavage energy, but crystals cleaved in water showed an apparent increase in cleavage energy of about 30%. In all cases the cleavage energy was greater than the reversible surface energy by a factor of 2 or 3. In a later study (26) they found that if the cleavage crack was made to propagate slowly, the apparent increase in cleavage energy was as great as 60%. This was due to the fact that water roughened the surfaces during cleavage so that the surface area was greater than that produced by cleavage in air.

Brace and Walsh (27) determined a cleavage energy for quartz and orthoclase at room temperature. The cleavage energy of quartz ranged from 400 to 1000 ergs/cm^2, depending upon which crystallographic plane was cleaved. The cleavage energy of orthoclase was found to be 7800 ergs/cm^2. However, Brace and Walsh felt that this very high value for orthoclase might be too high by an order of magnitude. They assumed that it was caused by either plastic flow at the crack tip or by inhomogeneities acting as barriers to the crack.

Wiederhorn (28) measured the velocity of slow cracks in glass and sapphire in a moist atmosphere. He observed that crack velocity was a complex function of the stress and the water vapor content of the atmosphere. Crack motion in glass appeared to result from a thermally activated reaction between the glass and the water vapor at the root of the crack. The data on sapphire indicated an effect similar to that occurring in glass.

Gross and Gutshall (29) measured the cleavage energy of sodium chloride as a function of F-center concentration. Tests were carried out in both darkness and with optical radiation and in vacuum and liquid nitrogen. There appeared to be no discernible difference between tests in vacuum and liquid nitrogen or for tests in light or darkness up to F-center concentrations of $10^{15}/cm^3$. In all cases the cleavage energy increased with the square root of F-center concentration. For greater concentrations the cleavage energy of crystals exposed to light was about twice that of those cleaved in darkness. This was attributed to bleaching of F-centers by light. Bleaching freed electrons trapped at anion vacancies. This increased the effective charge on the vacancy and increased strain in the area of the vacancy which hindered dislocation motion.

Wiederhorn et al. (30) used the Gilman technique to measure the cleavage energy of NaCl crystals in the annealed and irradiated states. The cleavage energy depended on the type

and extent of plastic deformation and on whether the crack front was straight or curved.

Two types of plastic deformation, depending on which slip planes were active during cleavage, were described. Plastic deformation on {110} planes which intersected the cleavage plane parallel to the direction of cleavage was referred to as plane-stress deformation. This was due to the fact that the specimen width was small enough for stresses parallel to the cleavage plane to be approximately zero. Plastic deformation on {110} planes which intersected the cleavage plane normal to the direction of cleavage was called plane-strain deformation. This occurred in samples with great enough width for stresses parallel to the cleavage plane to develop so that the cleavage plane remained undeformed. This notation was adopted because of similar notation used to describe deformation in polycrystalline metals (31). (This notation appears to be contradictory to that used by Gilman (32).)

Straight cracks caused plane-stress deformation in radiation hardened crystals and thin annealed crystals, but caused plane-strain deformation in thick annealed crystals. Curved cracks produced plane-stress and plane-strain deformation simultaneously. The fracture surface energy could be divided into 2 ranges depending on the mode of deformation. The fracture energy ranged from 370 ergs/cm^2 to 3000 ergs/cm^2 for plane-stress deformation and straight cracks and for combined plane-strain-plane-stress deformation and curved cracks. When

only plane-strain deformation occurred in annealed crystals, the fracture energy ranged from only 80 ergs/cm^2 to 300 ergs/cm^2. This low range indicated that plastic deformation may not always hinder crack propagation. In the case of plane-strain in soft crystals, tensile stress fields may be formed at the crack tip by plastic deformation and aid crack growth.

The Gilman cleavage technique requires that the initial crack be large with respect to the transverse dimensions of the crystal so that the effects of shear forces may be neglected. It is valid only when the ratio of initial crack length to beam height is 1.50 or greater (33). However, Westwood and Hitch (34) have observed that long cracks in materials exhibiting appreciable ductility produce anomalously high values of cleavage energy. Accordingly, they modified Gilman's equation (4) to take into account the effects of shear and end effects. The equation they obtained is

$$\gamma = (6P^2L^2/EWt^3)[1+(\alpha E/4G)(t/L)^2],$$

where γ is the cleavage energy, P is the force required to initiate crack propagation, L is the initial crack length, E is the elastic modulus, W is the specimen width, t is the height of one of the cleavage arms of the specimen, α is a numerical constant determined by boundary conditions at the crack tip, and G is the shear modulus. If all terms, except the number 1, in the brackets are neglected, the equation is identical to Gilman's (4).

Westwood and Hitch (34) measured the cleavage energy of KCl at room temperature. They found that the "apparent" cleavage energy increased as the initial crack length in partially cleaved samples was increased. In order to determine the specific surface energy they extrapolated data to very long initial crack lengths where they assumed the double cantilever equations were more accurate. The extrapolated value for the surface energy agreed quite well with previously reported theoretical estimates (35). Westwood and Hitch found that the apparent cleavage energy was almost doubled if tests were performed on samples immersed in a solution of KCl and water. They suggested that this was due to an increase in the crack tip radius caused by formation of a polycrystalline precipitate at the crack tip.

Westwood and Goldheim (36) also used the same experimental procedure to determine the cleavage energy of MgO at room temperature. The value they obtained for the specific surface energy agreed well with earlier experimental values (4) but was lower than theoretical estimates (37).

Berry (38) observed that while Gilman's geometry works well for testing single crystals which cleave preferentially along specific planes, it must be modified for materials showing poor cleavage or no cleavage at all. This is because the tensile stress gradient at the crack tip tends to make the crack deviate from its original direction of propagation (39). This is prevented in crystals since cleavage tends to occur

along planes of weaker binding but is not prevented in materials in which the binding is isotropic. Other workers (40-42) overcame this handicap by applying constraints to the material being fractured to prevent deviation of the crack from its initial direction. Berry, however, simply modified the Gilman geometry (4) by milling thin slots on opposing faces of the fracture specimen so that the crack would be confined to the reduced cross section produced by the slots. With this new geometry Berry was able to determine a fracture energy for various glassy polymers and polystyrene. Berry's geometry has also been used in the determination of fracture energies of polycrystalline materials (43,44).

There has been some criticism about the simple analysis used by Gilman in the double cantilever technique. Gillis (45) felt that Gilman's neglect of strain energy in the uncleaved portion of the sample was inaccurate. He said that for long initial cracks the effect of strain in the post crack region of the crystal would be smaller than the effect of bending of the crystal "beams" but would not be negligible. In addition to the neglect of the strain energy, Berry (38) also criticized Gilman's use of elementary beam theory. This theory requires that the uncleaved portion of the crystal be rigidly fixed, which is not the case experimentally. Therefore Berry developed an empirical equation in which the deflection of the crystal arms is linearly proportional to the applied force. According to Berry, such factors as nonplan-

arity of the crack or dissymmetry of the sample are not important when this equation is used.

Dynamic Measurements of Surface Energy

The Gilman cleavage technique and the modifications to it heretofore presented have all dealt with the force needed to make a crack in a partially cracked sample begin to propagate. The process of propagation itself has not been considered to any great extent. However, Berry has extended the quasistatic treatment of cleavage to a dynamic treatment (46,47). He assumed that the precracked fracture specimen has only potential energy. The potential energy increases with applied force up to the force required to propagate the crack. During propagation the specimen contains both kinetic energy and potential energy. He was able to express the potential energy and the work done on the specimen in terms of the parameters of the system. He then took the kinetic energy as the difference between the potential energy and work done on the system and derived equations for crack velocity and acceleration from the expression for kinetic energy. He was then able to integrate the velocity equation to obtain an equation of motion for the case of constant applied force and for constant deformation. For the case of constant applied force the equation of motion became

$$A_c + 5V_c/2c = V_s^2 d^2 (3-N \frac{C_o^2}{C^2})/24C^3$$

where A_c is the acceleration of the crack, V_c is the crack velocity, c is instantaneous crack length, V_s is the velocity of sound in the specimen, d is the height of one of the cleavage arms of the specimen, N is a numerical factor, and C_o is the initial crack length. For the case of constant deflection, the equation was given by

$$A_c - \frac{V_c^2}{2\alpha C_o} = 35d^2V_s^2(3-N\alpha^4)/48\alpha^3C_o^3 ,$$

where $\alpha = C/C_o$, and all other terms remain the same. However, Berry was unable to obtain general solutions to either of the equations of motion.

Forwood (48) used dynamical cleavage to study the effect of small cavities in NaCl single crystals on the fracture energy. He used as-received crystals with the double cantilever geometry but formed cavities in the rear half of the samples by electrodiffusion of gold into the crystals. The crystals were cleaved with a knife attached to a pendulum and the progress of the crack was determined by the method developed by Gilman et al. (49). He found that when the crack left the normal region of the sample and entered the treated region, there was a marked drop in crack speed. Large cleavage steps were generated wherever the crack intersected a cavity. In samples containing large numbers of cavities, the fracture appeared to be non-crystallographic.

In order to estimate the energy required for cleavage, Forwood (48) used the equation of motion developed by Berry

(46), which assumes that the force applied by the cleavage knife is constant. He justified the use of this equation by showing that the variation in crack speed with position in the sample was approximately the same as would be observed for a constant loading force. Because of uncertainty in the crack speed measurements, Forwood was not able to assign absolute values to the fracture energy. Instead he estimated the ratio of the fracture energy in the treated region to that in the normal region to the nearest order of magnitude. He found the ratio varied from 10 to 100, showing that cavities markedly increase the cleavage energy.

The validity of the equations developed by Berry (46,47) has been questioned by several workers (50,51). Gillis and Gilman (50) stated that they are inaccurate for several reasons. Berry neglected the lateral inertia of the crystal arms and assumed that the end deflection is directly proportional to the applied force. Gillis and Gilman found this to be a "gross error" for cracks which are long and moving. They also stated that the bending moment at the crack tip is usually not constant during cleavage.

Burns (51) made a comparison between the equations of the constant force model treatment of double cantilever cleavage (46) and the equations of the constant deflection model (2). He believed that the constant deflection model is more accurate because the constraint that the beam arms remain in contact with the knife is more easily verified than the constraint

that the loading force remain constant during cleavage. However, he found that Forwood's data (48), which had been treated with the constant force model, agreed well with that model but not with the constant deflection model.

Burns (51) explained the poor agreement by stating that if the rate of deflection, V_e, of the ends of the cantilever beams is great enough, the cleavage crack may travel with flexure waves which travel down the cleavage specimen. In this case fracture growth is controlled by wave propagation rather than the deflection of the beam ends. Then, although the beam ends remain in contact with the knife, the static beam shapes used in the constant deflection model to determine the energy in the beams are not applicable. Thus the data may agree well with the constant force model, which applies improper constraints to the problem, and not agree with the constant deflection model, which applies the proper constraints.

The quasistatic equations for the double cantilever beam mode of crack propagation derived by Gillis and Gilman (50) have recently been extended to the dynamic case by Burns and Webb (2). A brief outline of their method of derivation is given here (a more detailed description may be found in the section on theory). Instead of treating the double cantilever mode of crack propagation as a problem in known forces, as is usually done, Burns and Webb treated it as a problem in known displacements. They formed a Lagrangian equation of motion

consisting of the kinetic energy of the outward moving arms of the crystal minus the strain energy of the arms and the reversible surface energy of the crystal. The nonreversible cleavage energy was taken as a dissipative energy in the equations of motion. For simplicity they neglected the effects of shear and end rotation in the derivation. A general solution to the equation was not found, but Burns and Webb obtained a particular solution which is

$$L^2/(t-t_0) = \{9EI_0V_e^2/(2W)[\gamma+(3/56)\rho h_o V_e^2]\}^{1/2},$$

where L = crack length

$(t-t_0)$ = time subsequent to introduction of the knife into the crystal

E = elastic modulus

$I_0 = 2I_1I_2/(I_1+I_2)$, where I_1 is the moment of inertia of one beam arm, and similarly for I_2

V_e = the velocity at which the ends of the beam arms are being separated

W = specimen width

γ = the cleavage energy

ρ = specimen density

$h_o = [(I_0/I_1)^2h_1 + (I_0/I_2)^2h_2]$, where h_1 is the height of one beam arm, and similarly for h_2.

This solution predicts that the square of the crack length is directly proportional to elapsed time so long as the cleavage energy remains constant. A plot of crack length squared versus time thus should yield a straight line. If the cleavage

energy varies continuously, the plot will yield a curve.

Burns and Webb (3) experimentally determined the cleavage energy of LiF with the equation they developed. They cleaved long slender single crystals of LiF over a range of temperatures using a knife attached to a pendulum. The crack was photographed with a high speed motion picture camera. Cleavage was performed in an evacuated chamber to prevent possible interference by the partial vacuum created by the moving crack. They found that absorption of energy by plastic flow occurred at temperatures as low as 90°K and increased rapidly with temperature. Plastic flow persisted at a crack velocity as high as 5×10^4 cm/sec at room temperature. In most cases a plot of the square of the crack length versus time yielded one or more straight segments as predicted for constant cleavage energy or brittle-ductile transitions. However, the amount of plastic absorption of energy was not as dependent on velocity as predicted. The specific surface energy was determined by extrapolating the data to maximum theoretical crack velocity and was found to be 480 ± 50 ergs/cm^2, a value differing from that of Gilman (4) by about 30%.

Factors Affecting Loss of Crack Energy

It is a well known fact that the specific surface energy is measured by the cleavage technique only if the material is completely brittle (4). In most cases the velocity of a cleavage crack is influenced greatly by the crystal perfection and

energy loss by several processes in addition to the creation of new surfaces (52). Gilman (1,32,53), Washburn et al. (54), and Forty (55) have found that a slowly moving crack nucleates dislocation loops ahead of the crack tip. Forty (55) observed that in NaCl and LiF the damage is confined to narrow "deformation zones" on the cleavage surface illustrating the velocity dependence of the plastic deformation. Plastic deformation is extensive wherever the crack slows down but occurs to a much lesser extent when the crack is moving fast.

The crack-nucleated dislocations must lie in glide planes that cross the cleavage plane at an oblique angle (1). This is true because the maximum tensile stress at the tip of the crack tends to be normal to the plane of the crack, making shear stresses in the plane of the crack small. If the cleavage plane in crystals of the sodium chloride structure is taken as the (010) plane, the (011), ($0\bar{1}1$), (110), and ($\bar{1}10$) planes would be the active glide planes (56). Dislocations lying in the (011) and ($0\bar{1}1$) planes intersect the cleavage plane parallel to the [100] direction and are able to glide along with the crack front. Dislocations lying in the (110) and ($\bar{1}10$) planes intersect the cleavage plane normal to the [100] direction and thus are unable to be pulled along by the crack front. However, they are able to expand on their own glide planes. Since the (101) and ($\bar{1}01$) glide planes are normal to the cleavage plane, no dislocations would be nucleated in them by the cleavage crack (1).

Those dislocations which are "grown in" or formed by deformation prior to cleavage and the cleavage steps associated with them can also affect crack propagation (53,57). The effect is quite dependent on whether the dislocations are edge or screw type. Local concentrations of edge dislocations have little influence on propagation. However, if the concentration is uniformly high, the cleavage surface develops numerous ragged steps. Screw dislocations appear to be much more effective in step formation and therefore in absorbing energy. Cleavage steps are probably formed by shear rather than by secondary cleavage so that even a step of atomic height can absorb appreciable energy (1). As height increases, the energy absorption increases rapidly. It is difficult to ascertain the magnitude of the shear stress producing a step, but even if it is fairly low, the energy absorbed in forming a step of typical height may easily be as large as the reversible surface energy.

Gilman et al. (49) measured the velocities of cleavage cracks in LiF single crystals and tried to correlate the damage produced by the crack to the crack speed. They stated that if the velocity is greater than some velocity, V*, no dislocations are nucleated. For LiF this velocity appeared to be about 6×10^3 cm/sec. However, Burns and Webb (3) have observed that dislocations in LiF interact with cracks traveling as fast as 5×10^4 cm/sec. The data on the velocity of dislocations in LiF as a function of applied stress indicate that

crack-dislocation interaction may occur at crack speeds approaching the speed of sound (58).

Gilman et al. (49) also found that as the crack velocity decreases below V* more and more dislocations are nucleated until at some point the velocity begins to oscillate. The oscillation is caused in the following manner. As a crack slows down it begins to nucleate dislocations. This process absorbs energy from the crack and slows it down further. The arms of the crystal, however, are being moved apart by the cleavage knife at more or less constant velocity and the force driving the crack forward begins to build up. At some point the force is great enough to cause the crack to surge ahead again. Once more the crack begins to slow down as dislocations are nucleated and the process starts over again.

Finkel' et al. (52) found that cleavage cracks in NaCl could also be slowed and even stopped for short periods of time by slip bands formed by compressing the crystal normal to the direction of cleavage. The ability of the bands to stop the crack depended upon the width of the bands and the crack velocity. Cracks traveling at less than 4×10^3 cm/sec were often stopped by a single band. Cracks traveling at about 7×10^3 cm/sec hesitated only for a short time at a single band, but were often stopped before entering a second band. A similar effect was observed by Stokes et al. (59) in plastically deformed MgO. They found that cracks nucleated at the intersection of 2 slip bands were able to propagate rapidly

if adjacent slip bands were narrow and widely spaced. If the number of slip bands was large, the cracks were often stabilized.

Finkel', Savel'ev et al. (60) investigated the ability of different types of boundaries and sub-boundaries to absorb energy from a moving crack in NaCl and LiF. Prior to testing, each crystal was partially cleaved. It was found that usually the crack initially halted at a twist boundary and that later the crack hesitated during propagation at each twist boundary, forming numerous cleavage steps when it passed through the boundary. The period of crack stoppage was as much as 16×10^{-6} seconds for cracks traveling at about 2×10^{3} cm/sec. In general the time of stoppage was directly related to the energy of the boundary. As a rule low angle tilt boundaries had little effect on crack velocity.

Effects of Atmosphere on the Mechanical Properties of NaCl

There has apparently been little systematic study of the effects of atmosphere on the cleavage energy of NaCl although it has been observed that the value of cleavage energy in liquid nitrogen is only slightly different from the value in vacuum (24). However, the literature on the interaction of sodium chloride with air and various gases is voluminous. The intimate relation between surface energy and mechanical properties of materials requires consideration of these effects whenever cleavage energy measurements are made in

different atmospheres.

Sodium chloride has been shown to react with several components of the atmosphere (24,60-67), although some of the observations are contradictory. Gorum et al. (61) and Aerts and Dekeyser (68) reported that freshly cleaved NaCl is embrittled by nitrogen while Machlin and Murray (63) reported that these gases have no effect. However Machlin and Murray did find that ozone, nitrous oxide, and atomic oxygen embrittle NaCl.

An interesting fact that has been observed by Machlin et al. (63,66) is that air embrittlement of NaCl occurs chiefly in summer. This is probably due to increased ozone in the atmosphere from thunderstorm activity. They reported that mechanical behavior was very erratic when samples were exposed to air. On certain days the atmosphere embrittled samples, while on other days no embrittlement occurred. Some samples previously embrittled became ductile.

There are several proposed mechanisms by which sodium chloride is embrittled in the atmosphere. The exact mechanism depends upon the contaminant, but in general the effect is due to some change in surface structure rather than a change in the volume. However, at high pressure, nitrogen reportedly diffuses into the crystal to cause dislocation pinning (68). Oxygen and ozone react with the crystal surface to form a $NaClO_3$ layer (66). This layer acts either to prevent dislocation egress through the surface or to cause a coherency stress due to differences in the sizes of the NaCl and $NaClO_3$

lattices. Otterson (64) has indicated that CO_2 may react with hydroxide ions in the surface of NaCl to cause embrittlement. The hydroxide is necessary for the process since crystals free from it are not embrittled by dry CO_2. A similar observation has been made by Stokes et al. (65) who reported that water polished crystals remain ductile for long periods of time so long as they are stored in desiccated air.

In view of the fact that NaCl is often treated by surface dissolution to remove flaws (the well known Joffe effect (69)), one possible mechanism of embrittlement not specifically related to the atmosphere should be mentioned. Metz and Lad (70) and Lad (71) have indicated that microcracks form apparently spontaneously on the surfaces of NaCl crystals which have been water polished. At room temperature microcrack formation may take months, but does occur whether the crystals are stored in vacuum or desiccated air. However, if the crystals are heated to 130°C or above, the process is complete within about an hour. The microcrack formation probably results from the smaller equilibrium spacing of the surface layers with respect to the interior of the crystal.

If microcracks do indeed form by this process there should be a noticeable decrease in ductility. From this viewpoint there is evidence that microcrack formation does not occur in this manner. Stearns et al. (72) tested NaCl crystals which had been subjected to various treatments. They found

that crystals which had been water polished and heated to 135°C were more ductile in flexure tests than crystals which were water polished but not heated.

THEORY

It has been shown by Gilman (4) that the force needed to propagate cracks in crystals can be related to the surface energy through elementary beam theory. The quasistatic equations of Gillis and Gilman (50) have been extended to the dynamic case by Burns and Webb (2). In both treatments the effects of shear forces have been neglected, presumably for simplicity.

The neglect of shear imposes the restriction on the experimental geometry that the crack be long with respect to the heights of the cantilever beams (3,4). Otherwise the treatments are not valid. As was stated earlier, this limitation poses no problems for many materials but in materials exhibiting appreciable ductility long cracks tend to be blunted by plastic flow (4,34,73). This results in values for the cleavage energy which can easily be many times greater than the reversible surface energy (34,36). The logical approach to the study of the more ductile materials would be to use shorter cracks with respect to the cross-sectional dimensions. This necessitates consideration of the effects of shear to prevent underestimation of the surface energy (34,50).

An attempt was made in this study to include the effects of shear in the derivation of a Lagrangian equation of crack motion. The work of Gillis and Gilman (50) and work and notation of Burns and Webb (2) were used to facilitate the deriva-

tion. The coordinate system of Burns and Webb, in which the origin moves with the crack tip, was adopted and is shown in Figure 2. The crystal geometry in Figure 2 is the one used in this study and differs from that of Burns and Webb in that the transverse dimensions are much larger, with respect to the length.

The Deflection Equation

The equation for the deflection of one beam arm is given by Gillis and Gilman (50) as:

$$y(x) = \frac{3Lx^2F - x^3F}{6EI} + \frac{KFx}{AG} + \theta x \qquad (1)$$

where $y(x)$ = deflection of the beam at x

L = crack length

F = force acting on the free end of the beam

E = modulus of elasticity

I = moment of inertia

K = a shape factor = 3/2 for rectangular beams

A = cross sectional area of the beam

G = shear modulus

θ = a rotational term

The Strain Energy Equation

The strain energy for the beam arm is given by:

$$U = -\int_L^0 \frac{M^2dx}{2EI} - \int_L^0 \frac{KV^2dx}{2AG} \qquad (2)$$

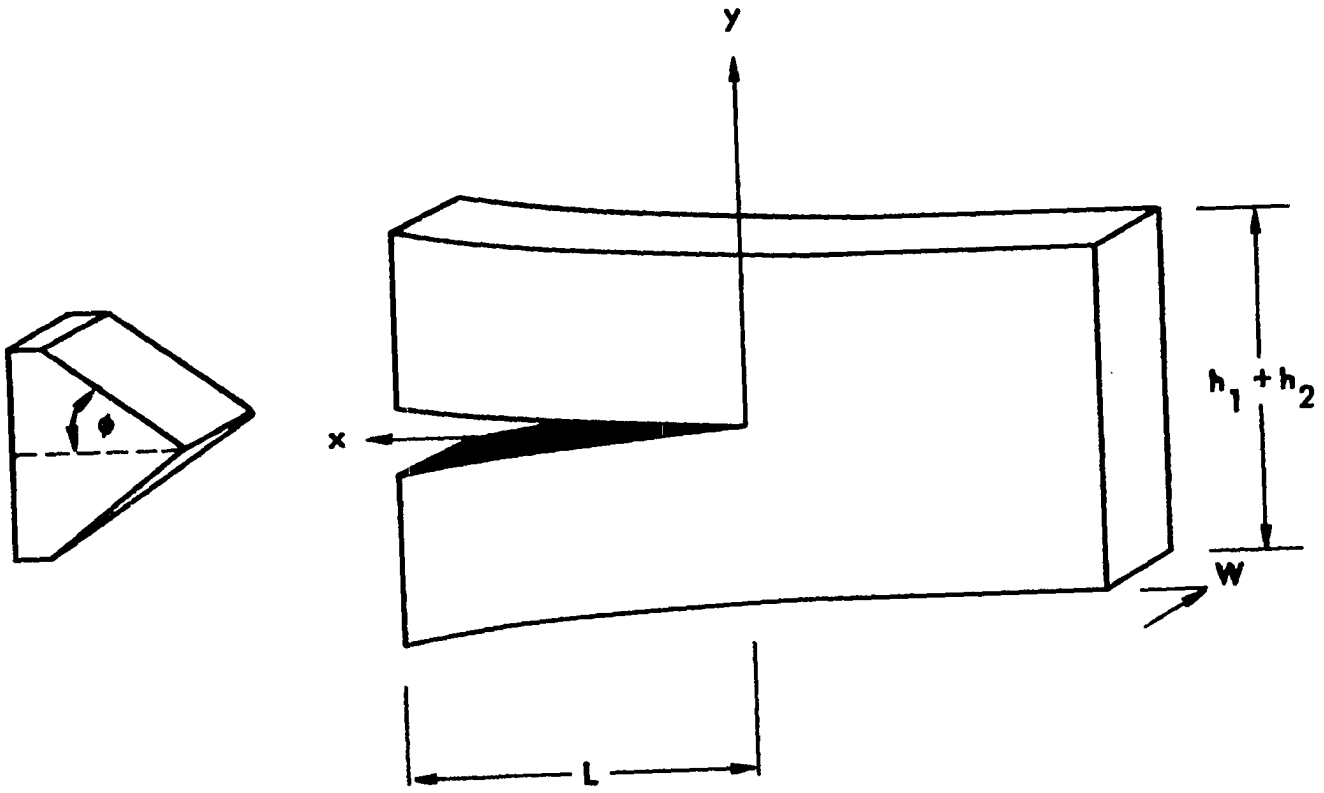

Figure 2. Modified double cantilever specimen

where U = strain energy

M = bending moment = -F(L-x)

V = shearing force = F.

Thus

$$U = -\int_L^0 \frac{F^2}{2EI}(L^2-2Lx+x^2)dx - \int_L^0 \frac{KF^2}{2AG}\,dx \tag{3}$$

Integration of Equation 3 yields

$$U = \frac{F^2L^3}{6EI} + \frac{KF^2L}{2AG} . \tag{4}$$

If the last two terms in Equation 1 are dropped, one has the equation of deflection used by Burns and Webb (2). However, in order to determine the effects of shear, only the rotation term is dropped here. Thus the deflections of the two beams are now described by:

$$y_1(x) = \frac{3Lx^2F_1 - F_1x^3}{6EI_1} + \frac{KF_1x}{A_1G} . \tag{5}$$

$$y_2(x) = \frac{3Lx^2F_2 - F_2x^3}{6EI_2} + \frac{KF_2x}{A_2G} . \tag{6}$$

If 2Y is the height of the crack opening at x = L (i.e. at the free end of the crystal), then

$$2Y = y_1(L) + y_2(L) \tag{7}$$

or

$$2Y = \frac{2F_1L^3}{6EI_1} + \frac{KL}{G}\left(\frac{F_1}{A_1} + \frac{F_2}{A_2}\right) + \frac{2F_2L^3}{6EI_2} . \tag{8}$$

Allowing the crystal to pivot about the unloaded end

maintains equal forces across the knife edge used in cleavage. Therefore

$$F_1 = F_2 = F \tag{9}$$

and Equation 8 now becomes

$$Y = \frac{L^3F}{6E}\left(\frac{1}{I_1} + \frac{1}{I_2}\right) + \frac{KLF}{2G}\left(\frac{1}{A_1} + \frac{1}{A_2}\right). \tag{10}$$

If we assume that the ends of the beam arms are in contact with the cleavage knife, then Y is determined by the motion of the knife. If the knife moves with constant velocity then we can define Y by

$$Y = V_W \tan \phi(t-t_0) = V_e(t-t_0) \tag{11}$$

where V_W = velocity of the knife

ϕ = half-angle of the knife edge

$t-t_0$ = time elapsed since introduction of the knife into the crystal

V_e = velocity of the outward moving ends of the crystal halves.

We now write Equation 10 as:

$$Y = F\left(\frac{L^3}{3EI_0} + \frac{KL}{A_0G}\right) \tag{12}$$

where $I_0 = \frac{2I_1I_2}{I_1+I_2}$

$$A_0 = \frac{2A_1A_2}{A_1+A_2}.$$

Equation 12 is rearranged to give:

$$F = \frac{Y}{(\alpha L^3+\beta L)} \tag{13}$$

where $\alpha = \frac{1}{3EI_0}$

$$\beta = \frac{K}{A_0 G} .$$

The Kinetic Energy Equation

The kinetic energy associated with the two beams being pushed apart by the knife can be found by integration of the squares of the local velocities over the crystal. The velocity of the first beam is found by taking the time derivative of Equation 5. Thus

$$\dot{y}_1(x) = \frac{\dot{F}}{6EI_1}(3Lx^2-x^3) + \frac{F}{6EI_1}(6Lx\dot{L}) + \frac{K}{A_1 G}(\dot{F}x+F\dot{L}) \tag{14}$$

where $\dot{y}$, $\dot{F}$, and $\dot{L}$ are the time derivatives. From Equation 13,

$$\dot{F} = \frac{(\alpha L^3+\beta L)\dot{Y} - Y(3\alpha L^2+\beta)\dot{L}}{(\alpha L^3+\beta L)^2} . \tag{15}$$

The velocity of the second beam is found similarly. The squared velocity of the first beam arm is given by:

$$[\dot{y}_1(x)]^2 = \frac{\dot{F}^2}{(6EI_1)^2}(3Lx^2-x^3)^2 + \frac{2F\dot{F}}{(6EI_1)^2}(3Lx^2-x^3)(6xL\dot{L})$$

$$+ \frac{2K\dot{F}}{6EI_1A_1G}(3Lx^2-x^3)(\dot{F}x+F\dot{L}) + \frac{2KF}{6EI_1A_1G}(6Lx\dot{L})(\dot{F}x+F\dot{L})$$

$$+ \frac{K^2}{(A_1G)^2}(\dot{F}x+F\dot{L})^2 + \frac{F^2}{(6EI_1)^2}(6Lx\dot{L})^2, \tag{16}$$

and similarly for the second beam arm. Then

$$\int_0^L [\dot{y}_1(x)]^2 dx = \frac{1}{(6EI_1)^2} [\dot{F}^2(\frac{33L^7}{35}) + F\ddot{F}L(\frac{66L^6}{10}) + F^2(12L^5\dot{L}^2)]$$

$$+ (\frac{K}{3EI_1A_1G})[\dot{F}^2(\frac{11L^5}{20}) + F\ddot{F}L(\frac{11L^4}{4}) + 3F^2\dot{L}^2L^3]$$

$$+ (\frac{K}{A_1G})^2[\frac{\dot{F}^2L^3}{3} + F\ddot{F}LL^2 + F^2\dot{L}^2L] \qquad (17)$$

and similarly for the second beam arm. We are now ready to write an expression for the kinetic energy K*.

$$\frac{K^*}{\rho} = \int_0^L \{[\dot{y}_1(x)]^2h_1 + [\dot{y}_2(x)]^2h_2\}Wdx \qquad (18)$$

where ρ = density of the beam arms

h_1, h_2 = heights of the beams

W = width of the beams.

Substitution of Equation 17 and the similar expression for the second beam into Equation 18 yields:

$$\frac{K^*}{\rho} = C_1^*[\dot{F}^2(\frac{33L^7}{35}) + F\ddot{F}L(\frac{66L^6}{10}) + F^2(12L^5\dot{L}^2)] + C_2^*[\dot{F}^2(\frac{11L^5}{20})$$

$$+ F\ddot{F}L(\frac{11L^4}{4}) + 3F^2\dot{L}^2L^3] + C_3^*[\frac{\dot{F}^2L^3}{3} + F\ddot{F}LL^2 + F^2\dot{L}^2L] \qquad (19)$$

where

$$C_1^* = \frac{W}{(6E)^2}[\frac{h_1I_2^2 + h_2I_1^2}{I_1^2I_2^2}]$$

$$C_2^* = (\frac{KW}{3EG})[\frac{h_1I_2A_2 + h_2I_1A_1}{I_1A_1I_2A_2}]$$

$$C_3^* = \left(\frac{K^2W}{G^2}\right)\left(\frac{h_1A_2^2 + h_2A_1^2}{A_1^2A_2^2}\right].$$

For the moment, let

$$\underline{A} = \left[\frac{33C_1^*L^7}{35} + \frac{11C_2^*L^5}{20} + \frac{C_3^*L^3}{3}\right]$$

and

$$\underline{N} = \left[\frac{66C_1^*L^6}{10} + \frac{11C_2^*L^4}{4} + C_3^*L^2\right].$$

Equation 19 can be rewritten as:

$$\frac{K^*}{\rho} = \frac{\dot{Y}^2A}{(\alpha L^3+\beta L)^2} - \frac{2Y\dot{Y}\dot{L}(3\alpha L^2+\beta)A}{(\alpha L^3+\beta L)^3} + \frac{Y^2\dot{L}^2(3\alpha L^2+\beta)^2A}{(\alpha L^3+\beta L)^4} + \frac{Y\ddot{Y}LN}{(\alpha L^3+\beta L)^2}$$

$$- \frac{Y^2\dot{L}^2(3\alpha L^2+\beta)N}{(\alpha L^3+\beta L)^3} + \frac{Y^2\dot{L}^2}{(\alpha L^3+\beta L)^2}\left[12C_1^*L^5 + 3C_2^*L^3 + C_3^*L\right]. \qquad (20)$$

The total effective surface energy required for cleavage is a combination of a reversible energy associated with the equilibrium surface energy of the material and a nonreversible energy. The nonreversible energy is energy dissipated in plastic flow. The reversible part is denoted by Burns and Webb (2) as

$$S = 2\gamma_0WL \qquad (21)$$

where γ_0 = reversible specific surface energy

W = beam width

L = crack length.

The nonreversible part is denoted by:

$$Q_f = -2\gamma_p W \tag{22}$$

where γ_p = an incremental change in plastic work divided by the incremental increase in the fractured area.

The Lagrangian Equation

The Lagrangian is now written as

$$\mathcal{L} = K^* - U_1 - U_2 - S \tag{23}$$

where U_1 and U_2 are the strain energies associated with the two beams. From Equation 4 and the definitions of I_0 and A_0 in Equation 12 and the definitions of α and β in Equation 13

$$U_1 + U_2 = \frac{F^2L^3}{3EI_0} + \frac{KF^2L}{A_0G} \tag{24}$$

and the Lagrangian becomes:

$$\mathcal{L} = K^* - F^2(\alpha L^3+\beta L) - 2\gamma_0 WL. \tag{25}$$

The equation of crack motion, the equation that remains to be solved, is given by:

$$\frac{d}{dt}\left(\frac{\partial \mathcal{L}}{\partial \dot{L}}\right) - \left(\frac{\partial \mathcal{L}}{\partial L}\right) = Q_f = -2\gamma_p W. \tag{26}$$

Keeping in mind the definition of $\underline{A}$ in Equation 20, let

$$\underline{B} = \left[\frac{24C_1^*\alpha^2L^{11}}{35} + \frac{114C_1^*\alpha\beta L^9}{35} + \frac{222C_1^*\beta^2L^7}{35} - \frac{6C_2^*\alpha^2L^9}{20}\right.$$

$$\left. - \frac{34C_2^*\alpha\beta L^7}{20} + \frac{16C_2^*\beta^2L^5}{20} + C_3^*\alpha^2L^7 + \frac{C_3^*\beta^2L^3}{3}\right] \tag{27}$$

and

$$\underline{C} = \left[\frac{33C_1^*\alpha L^9}{35} + \frac{165C_1^*\beta L^7}{35} - \frac{11C_2^*\alpha L^7}{20} + \frac{33C_2^*\beta L^5}{20} - C_3^*\alpha L^5 + \frac{C_3^*\beta L^3}{3}\right]. \tag{28}$$

Then with the aid of Equation 13 and the definitions of $\underline{A}$, $\underline{B}$, and $\underline{C}$, Equation 25 can be written as:

$$\mathcal{L} = \frac{\dot{Y}^2 A\rho}{(\alpha L^3+\beta L)^2} + \frac{Y^2\dot{L}^2 B\rho}{(\alpha L^3+\beta L)^4} + \frac{\dot{Y}\dot{Y}LC\rho}{(\alpha L^3+\beta L)^3} - \frac{Y^2}{(\alpha L^3+\beta L)} - 2\gamma_0 WL\ . \tag{29}$$

By taking the proper derivatives, Equation 26 becomes:

$$\frac{d}{dt}\left(\frac{\partial\mathcal{L}}{\partial\dot{L}}\right) - \left(\frac{\partial\mathcal{L}}{\partial L}\right) = \frac{\dot{Y}^2\rho}{(\alpha L^3+\beta L)^3}\left[C - (\alpha L^3+\beta L)\frac{\partial A}{\partial L} + (6\alpha L^2+2\beta)A\right] +$$

$$\frac{4\dot{Y}\dot{Y}L\rho B}{(\alpha L^3+\beta L)^4} + \frac{2Y^2\ddot{L}\rho B}{(\alpha L^3+\beta L)^4} + \frac{Y^2\dot{L}^2\rho}{(\alpha L^3+\beta L)^5}\left[(\alpha L^3+\beta L)\frac{\partial B}{\partial L} - 4B(3\alpha L^2+\beta)\right] -$$

$$\frac{Y^2(3\alpha L^2+\beta)}{(\alpha L^3+\beta L)^2} + 2\gamma_0 W = -2\gamma_p W. \tag{30}$$

For compactness let:

$$\text{Term 0} = \left(\frac{1}{\alpha L^3+\beta L}\right)^3\left[C-(\alpha L^3+\beta L)\frac{\partial A}{\partial L} + (6\alpha L^2+2\beta)A\right],$$

$$\text{Term I} = \frac{4B}{(\alpha L^3+\beta L)^4}\ ,$$

$$\text{Term II} = \frac{2B}{(\alpha L^3+\beta L)^4} = \frac{1}{2}\ \text{Term I},$$

$$\text{Term III} = \left(\frac{1}{\alpha L^3+\beta L}\right)^5\left[(\alpha L^3+\beta L)\frac{\partial B}{\partial L} - 4B(3\alpha L^2+\beta)\right],$$

$$\text{Term IV} = \frac{(3\alpha L^2+\beta)}{(\alpha L^3+\beta L)^2} .$$

Then Equation 30 can be rewritten as:

$$\frac{d}{dt}\left(\frac{\partial \mathcal{L}}{\partial \dot{L}}\right) - \left(\frac{\partial \mathcal{L}}{\partial L}\right) = \dot{Y}^2\rho \text{ Term 0} + Y\dot{Y}\dot{L}\rho \text{ Term I} + Y^2\ddot{L}\rho \text{ Term II}$$

$$+ Y^2\dot{L}^2\rho \text{ Term III} - Y^2 \text{ Term IV} = -2\gamma_0 W - 2\gamma_p W = -2\gamma W. \qquad (31)$$

It can easily be shown that Term 0 = 0. With this in mind, Equation 31 can be rewritten as:

$$\ddot{L} = -\dot{L}^2\left(\frac{\text{Term III}}{\text{Term II}}\right) - \frac{2\dot{Y}\dot{L}}{Y} + \frac{1}{\rho}\left(\frac{\text{Term IV}}{\text{Term II}}\right) - \left(\frac{2\gamma W}{Y^2\rho}\right)\left(\frac{1}{\text{Term II}}\right). \qquad (32)$$

The final equation relating crack velocity, $\dot{L}$, to surface energy is obtained by substituting for Y and $\dot{Y}$ in Equation 32. Thus:

$$\ddot{L} = -\dot{L}^2\left(\frac{\text{Term III}}{\text{Term II}}\right) - \frac{2\dot{L}}{t-t_0} + \frac{1}{\rho}\left(\frac{\text{Term IV}}{\text{Term II}}\right) - \left[\frac{2\gamma W}{\rho V_e^2 (t-t_0)^2}\right]\left(\frac{1}{\text{Term II}}\right). \qquad (33)$$

A general solution to the equation of motion has not been found. An attempt was made to find a particular solution with the aid of an IBM 360 computer. The computer program developed for searching for the solution is presented in APPENDIX E. The method used in the search was to guess a solution and substitute it into Equation 33. The right-hand side of the equation was subtracted from the left-hand side under the assumption that the difference would be 0 when a solution was found. This was done for many different combin-

ations of beam dimensions and crack lengths ranging from $(h_1+h_2)/20$ to about $5(h_1+h_2)$. In this manner it was found that for $L \geq (h_1+h_2)/2$ one approximate solution is:

$$\frac{(\alpha L^3+\beta L)^2}{(3\alpha L^2+\beta)(t-t_0)^2} = V_e^2/2W[\gamma + \frac{35}{3328}\rho h_o V_e^2] \tag{34}$$

where

$$h_o = [(\frac{I_0}{I_1})^2 h_1 + (\frac{I_0}{I_2})^2 h_2].$$

This solution is well within 1% of the numerical solution obtained from the computer. For $(h_1+h_2)/4 \leq L \leq (h_1+h_2)/2$. A numerical solution of the form

$$\frac{(\alpha L^3+\beta L)^2}{(3\alpha L^2+\beta)(t-t_0)^2} = V_e^2/2W[\gamma + \frac{35}{3328}\rho V_e^2 x] \tag{35}$$

was found where x has dimensions of length. Values of x for different beam heights are plotted versus crack length in Figure 3. Figure 4 shows a hypothetical plot of the square of crack length versus time for a constant cleavage energy. The most striking feature of the figure is that initially, L^2 is not linear with time. Instead, for $L \leq (h_1+h_2)/2$, L is approximately linear with time. The reason for this becomes apparent upon examination of the solution. The term β is dominant when the crack length is short. While x is not constant, the effect of it is very small so that initially the form of the solution is essentially

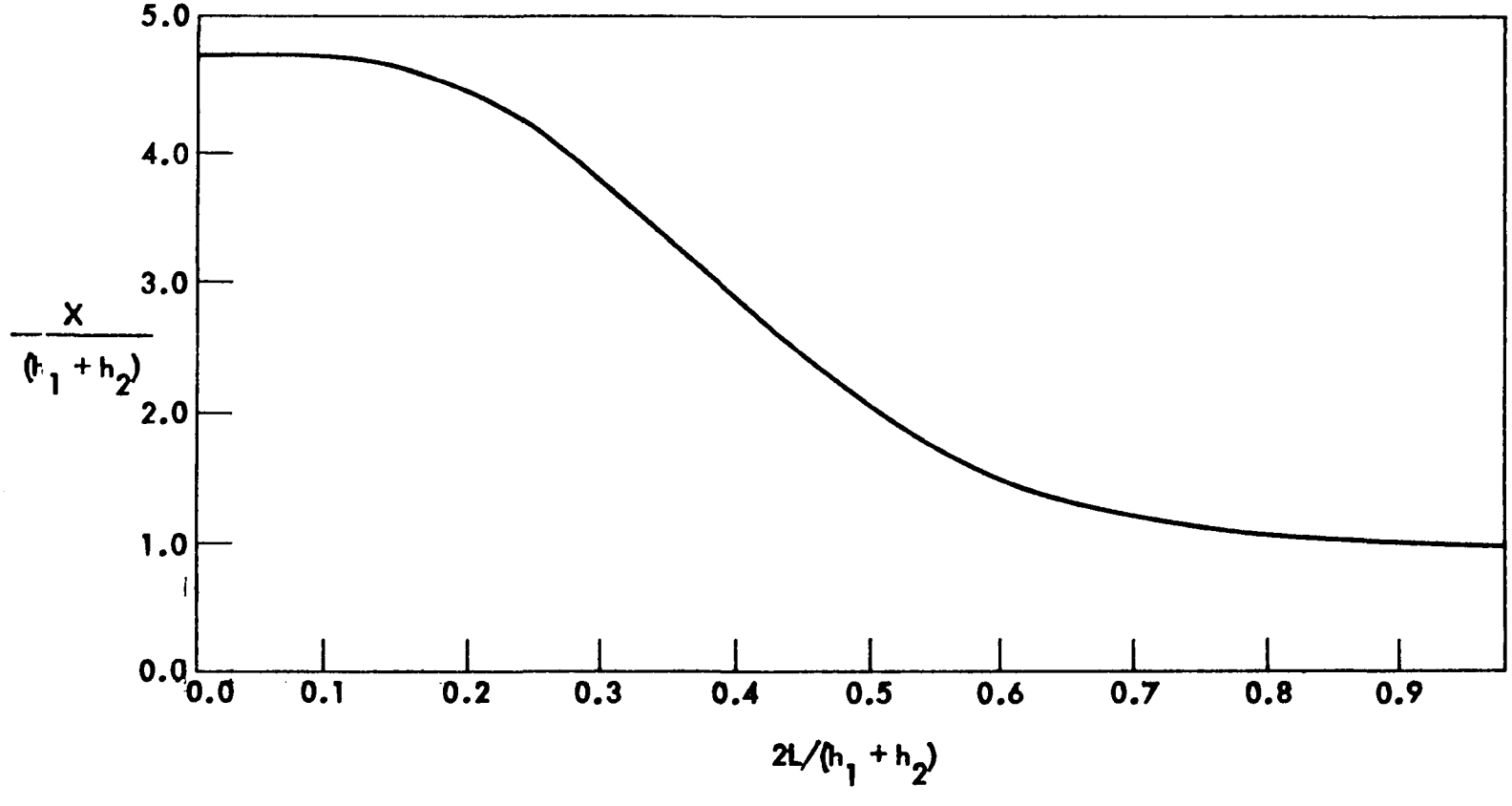

Figure 3. Variation of "x" factor with crack length for the condition $h_1=h_2$

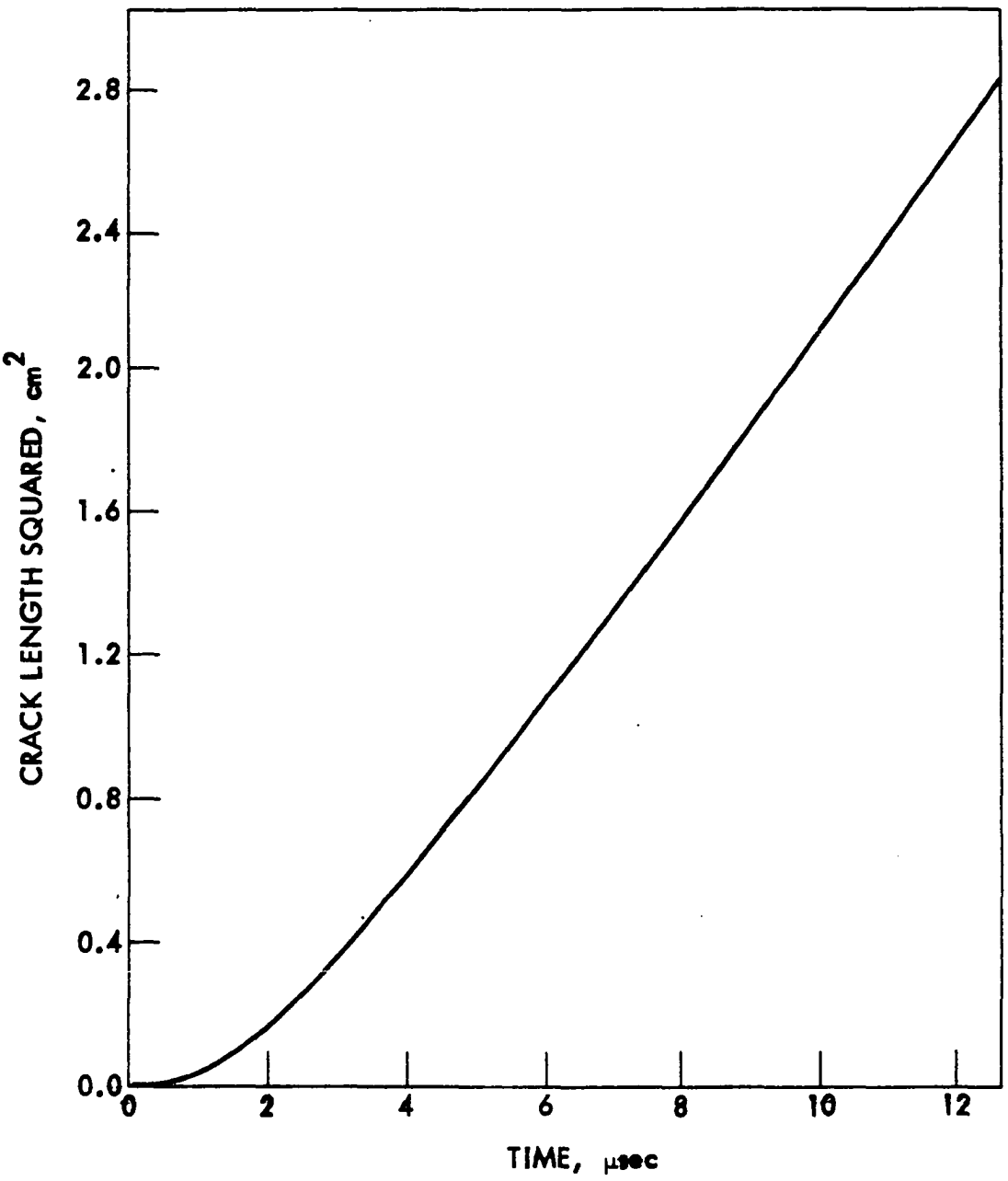

Figure 4. Theoretical relation between crack length and time for constant cleavage energy

$$\frac{L^2}{(t-t_0)^2} = \frac{V_e^2}{2W\gamma} . \qquad (36)$$

The equation of crack motion is an improvement over the equation developed by Burns and Webb (2) in that the effects of shear can now be taken into consideration. Whereas their equation is valid only for cracks with length greater than about $3(h_1+h_2)/2$ (50), this equation should be valid for cracks with length greater than about $(h_1+h_2)/4$.

The accuracy of the solution for short cracks is reduced somewhat because of neglect of strain energy in the uncleaved portion of the specimen (38). Elementary beam theory requires that the uncleaved portion of a specimen be rigidly fixed and therefore that the amount of stored energy be nil. Experimentally, however, it is found that deformation occurs in the post crack region. This strain energy in the post crack region can be important, especially for short cracks (45). Even for cracks which approach the specimen length in size, the strain energy in the post crack region is significant.

Another limitation is the failure to account for end rotation. Inclusion of the end rotation term in the deflection equation makes the derivation of the Lagrangian exceedingly complex. For this reason it was neglected. However, it should be noted that the end rotation is usually significant (50).

It will be remembered that the assumption was made in the

derivation that the cleavage knife moves with constant velocity. Practically, this means that if cleavage is accomplished by a pendulum, the kinetic energy of the pendulum must be many times greater than the cleavage energy of the specimen. It also requires that the pendulum travel a very short distance during the cleavage process. Only under these conditions will the assumption of constant velocity be valid. However, Burns (51) has determined upper limits to the pendulum velocity beyond which the theory no longer applies. The first upper limit is defined by

$$V_e < 1.56[\gamma/\rho(h_1+h_2)]^{1/2}. \qquad (37)$$

If this limit is exceeded the crack will travel with flexure waves propagating through the crystal and the use of static beam shapes in the derivation of the equation of motion will not be valid. The second upper limit is defined by

$$V_e < 2.9[\gamma/\rho(h_1+h_2)]^{1/2}. \qquad (38)$$

If this limit is exceeded the crack will propagate because the bending moment at the crack tip exceeds the critical bending moment for fracture.

EXPERIMENTAL PROCEDURE AND DESCRIPTION OF EQUIPMENT

Sample Preparation

Large cubes of Kyropoulous-grown NaCl and small random sized samples of Stockbarger NaCl were obtained from Harshaw Chemical Company, Cleveland, Ohio. The purity of the crystals was not determined but an analysis performed by Long (74) on similar crystals showed the major impurities to be Si (<10 ppm), Cu (<50 ppm), Al (<100 ppm), and Mg (<20 ppm).

An attempt was made to reduce the crystals to the desired dimensions with a string saw using distilled water as a cutting agent. It was felt that the use of a string saw would minimize mechanical damage to the specimens. However, it proved to be very difficult to produce {100} faces on the samples. The misalignment of the longitudinal axes of the specimens from a true [100] direction was typically less than 2°. Nevertheless, this was sufficient to cause extreme problems in obtaining reproducible crack speeds during cleavage. The Kyropoulous-grown crystals also were relatively imperfect. They contained large numbers of subgrain boundaries and tilt-twist boundaries, as evidenced by the large steps formed on the cleavage surfaces (53). For this reason it was decided to use only samples cleaved from the parent blocks of Stockbarger NaCl for velocity measurements.

Single crystals with approximate dimensions 0.4 cm x 1.2 cm x 2.0 cm were cleaved from the random sections. This was

accomplished by placing a knife edge against the crystal and lightly tapping it with a hammer. The crystals were placed in lots of 25 on platinum foil and annealed for 12 hours at 580°C in air. They were cooled to room temperature at a maximum rate of 0.5°C/min.

After the anneal the crystals were polished on a nylon lap with a 30% (volume) solution of absolute methanol in deionized water. This solution dissolved the surface from a crystal more slowly than pure water and therefore allowed greater control over the polishing process. Each crystal was then rinsed in the methanol-water solution and then in acetone and wiped dry with tissue paper. The crystal was immediately placed in a desiccator and stored for a period of several days.

Gold was vapor deposited on one of the large faces of each crystal to form a series of electrically conductive stripes. The stripes were formed with the aid of a mask made of aluminum sheet 0.0051 cm in thickness. The mask contained slots 0.0127 $\pm$ 0.0025 cm in width and separated from one another by 0.147 cm. The gold stripes were approximately 200 Å thick and varied in resistance from 200 to 4000 ohms, depending upon whether cleavage steps remained on the surface after polishing.

The configuration of the stripes was similar to that used by Gilman *et al.* (49). However, the stripes were placed on one of the large crystal faces so that the cleavage geometry would

produce a crack of short length relative to the crystal height (36). The two stripes nearest the front of the crystal were connected in parallel with Dotite Type D-550 paint (Jeolco, U.S.A., Inc., Medford, Massachusetts) to form the "trigger". It was necessary to use a dual stripe trigger rather than a single stripe trigger due to the instability of the stripes when a voltage was applied to them.

It was found that when as little as 0.03 volts DC was applied to a single trigger stripe, the gold tended to migrate from one side of the crystal to the other, causing a break in the stripe. This migration occurred often within 10 seconds of the application of voltage and seemed to be enhanced when the relative humidity was 50% or greater. Crystals stored for more than a week after vapor deposition also showed the same tendency. The use of a dual stripe trigger reduced the problem, presumably due to decreased electrical resistance. It was noted that none of the deflection stripes were ever broken in this manner. This was because the parallel resistance of the deflection stripes was considerably less than for the trigger since there were 8 to 12 deflection stripes connected in parallel.

It was found necessary to place the trigger stripe approximately 0.2 cm away from the front of the crystal. When the trigger was placed exactly at the front of the crystal it was noted that an extremely long time (about 40 microseconds) often passed between breakage of the trigger and breakage of the

first deflection stripe. This was at first attributed to "early triggering" due to some malfunction in the electrical circuit. However, examination of the cleavage surface showed that the crack often hesitated within the first 0.2 cm of crack growth. In order to observe crack motion throughout the entire crystal length, it was necessary to use slow sweep rates for the oscilloscope trace. (The procedure for crack speed measurement is explained later.) In later stages of crack growth when the crack velocity was high, it was impossible to identify breakage of individual deflection stripes since the oscilloscope trace was "bunched up". To overcome the problem, the trigger stripe was placed beyond the region of slow crack growth so that faster sweep rates could be used. The deflection stripes were placed behind the trigger and connected in parallel but isolated from the trigger.

Two small diameter wires were attached to the crystal (one on each side of the deflection stripes) with the Dotite paint and 2 other wires were attached to the trigger in a similar manner. If the crystal was to be cleaved at a temperature above 100°C, the connections were reinforced with a small drop of Dupont silver preparation 7713 (E. I. Dupont de Nemours and Co., Wilmington, Delaware). The silver preparation provided a degree of adherence at higher temperatures which the Dotite paint lacked. A typical sample is shown in Figure 5.

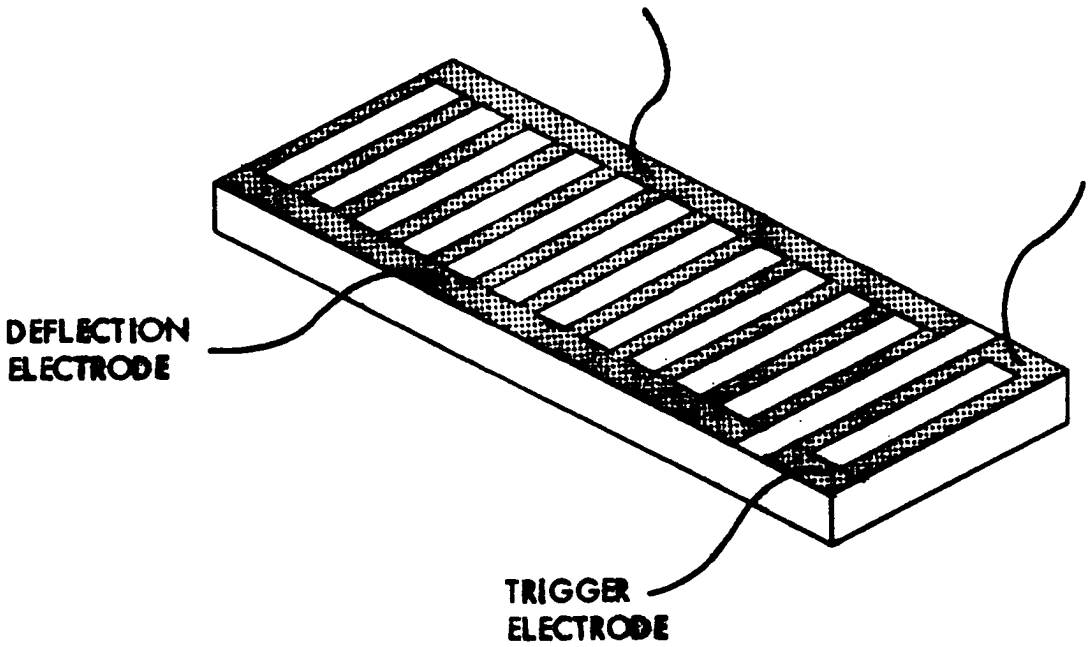

Figure 5. Typical cleavage specimen

The Sample Holder

The sample holder is shown in Figure 6. It was fabricated from a stainless steel block with top and bottom face dimensions 10.10 x 10.10 cm and side face dimensions 10.10 x 6.00 cm. A slot 0.69 cm wide and 1.27 cm deep was milled across the top face for a distance of 2.54 cm, beginning at the center of one side. Beyond this distance the slot was widened to 5.10 cm with a depth of 0.69 cm for the remainder of the distance across the top face. The narrow part of the slot was covered with a 0.60 cm thick stainless steel plate which contained a slot 0.60 cm long and 0.3 cm wide. This slot allowed the cleavage knife to strike the crystal without ever touching the block. Two stainless steel braces were bolted to the block, one on each side of the wider section of the slot. Each brace contained a set screw for locking the slide (described below) in the slot and facilities for holding the electrical wires leading to the crystal sample.

The slide was a stainless steel plate with dimensions 5.08 x 5.08 x 5.08 x 0.69 cm. A small block rounded on the front end was fastened to the front of the slide to hold the crystal in place and to allow the two arms formed during cleavage to rotate freely. Since the slide position was adjustable, it was possible to place each specimen precisely as desired even though the crystal length might vary slightly from specimen to specimen.

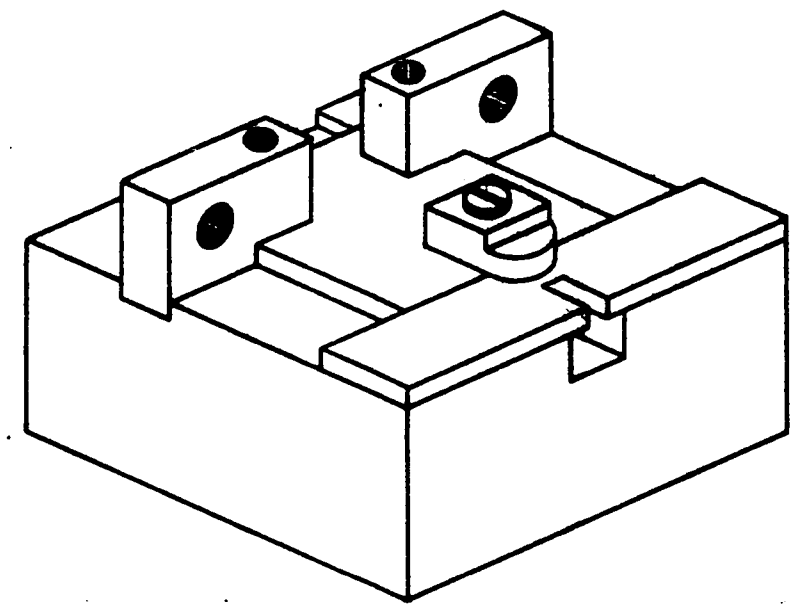

Figure 6. The specimen holder

The crystal was carefully placed on the holder above the narrow slot with the back of the crystal toward the slide. The deflection wires and trigger wires were then connected to the crystals in the manner described earlier and also were connected to terminals on the holder. The slide was moved forward so that the pivot block rested against the back face of the crystal while the front face of the crystal was collinear with the front face of the sample holder. With the sample thus positioned, the slide was locked in place.

The electrical resistance of the trigger stripes and deflection stripes were checked with a Hewlett Packard Model 410B vacuum tube voltmeter (Hewlett Packard, Loveland, Colorado). If the stripes were conductive, the holder was placed in the cleavage apparatus.

The Cleavage Apparatus

The cleavage apparatus consisted of a small electrical furnace and a pendulum mounted together on a heavy steel base plate and enclosed in a gastight plexiglas box. The inside dimensions of the furnace were 20 cm x 15 cm x 10 cm. Two stainless steel rails running the length of the furnace were bolted to the bottom. A stainless steel rod was bolted transversely across the rails to prevent the sample holder from moving backward during cleavage.

The heating element consisted of Kanthal "A" ribbon laced through holes drilled in the refractory lining of the furnace.

The heating element was isolated from the furnace interior in order to give more uniform radiant heating.

Power for heating was supplied by an SCR Stepless Power Unit (West Instrument Company, Schiller Park, Illinois). The temperature was measured with a Pt/Pt-10% Rh thermocouple placed approximately 1 cm above the sample and connected to a West Model JSCR controller. The temperature indicated by the JSCR controller was calibrated against a chromel-alumel thermocouple placed exactly at the sample position and connected to a millivolt potentiometer (Leeds and Northrup Co., Philadelphia, Pennsylvania). The calibration was done in air and also with nitrogen flowing over the sample position at a rate of 12.2 ℓ/min. It was found that temperature stabilized within 60 minutes after the JSCR controller indicated that the desired temperature had been reached.

The furnace wall facing the pendulum contained a 2.5 cm x 5.5 cm access slot to allow entrance of the cleavage knife into the furnace. The pendulum had an arm length of 38 cm. A 10.5 cm long rod was mounted on the bob end of the pendulum by a pin and set screw. This allowed adjustment of the rod so that the cleavage knife, which was attached to the end of the rod, would be exactly vertical when it struck the crystal. The total mass of the pendulum system was 4900 grams. The cleavage knife was made of steel hardened to Rockwell 55C and ground to a 15° chisel edge with a radius of curvature of 1.27 cm.

The pendulum could be held at any angle up to about 40° from the equilibrium position by a wire. Cleavage of the crystal was accomplished by cutting the wire with wire cutters. The pendulum velocity was calculated from the period which was measured approximately 500 times at drop angles ranging from 5 to 15°. The period was found to be independent of the drop angle to within less than 1% error. The velocity of the knife was then calculated to be 90 cm/sec.

Cleavage Tests in Various Atmospheres

Single crystal specimens with the dimensions mentioned earlier were cleaved in nitrogen at temperatures ranging from room temperature to 300°C. The upper temperature was limited because of damage to the bearings in the pendulum assembly by heat. Samples were also cleaved at room temperature in argon, carbon dioxide and air. Several samples were irradiated to a dose of about 3×10^8 rads at the rate of 1.96 rads/hour (γ-irradiation) and then cleaved in nitrogen. In an attempt to determine the effect of sample dimensions on crack speed several samples about 0.3 cm x 0.8 cm x 2.0 cm were also cleaved in air. The composition of the gases is given in Table I.

For testing in nitrogen and argon atmospheres the gas was delivered from a pressurized tank by Tygon tubing (Norton Company, Akron, Ohio) through 4 steel drying tubes, 61 cm long and 3.8 cm in diameter, filled with anhydrone (J. T. Baker

Table I. Composition of the gases

	Argon	Nitrogen	Carbon dioxide
Dew point	-100°F	-90°F	
O_2	0.0005%	0.0015%	
H_2	0.0001%	0.0005%	
N_2	0.0020%		
CH_4	0.0001%	nil	
CO_2	0.0001%	nil	
CO			0.1%

Chemical Co., Phillipsburg, New Jersey). The gas flow was then split into 2 parts and flowed through flow meters into the plexiglas box. A flow of 12.2 ℓ/min went directly into the furnace while the other flow, also 12.2 ℓ/min, was directed around the exterior of the furnace. The pressure in the plexiglas box was measured with a manometer filled with oil of known density. The rate of escape of the gas from the box was regulated to maintain a positive pressure of less than 0.01 psi. The gas flow was maintained for a period of time sufficient to allow a volume of gas 5 times that of the box to flow through the system.

The procedure used with carbon dioxide was identical to that outlined above except that drying tubes filled with silica gel, rather than anhydrone, were used. Cleavage in air was accomplished by leaving the system open to the atmosphere.

In all the tests the humidity was checked with a Lab-Line Electro-Hygrometer (Lab-Line Instruments, Inc., Melrose Park, Illinois). The tests in air were conducted within the relative humidity range 45-54 percent. For tests in other atmospheres the lower limit of the electro-hygrometer, 30 percent, was reached within the time a volume of gas equal to that of the plexiglas box had passed through the system. The true amount of moisture in the atmosphere was not determined. However, since 5 volumes of gas were passed through the system before cleavage, it was assumed that the relative humidity was well below 30%.

Measurement of Crack Velocity

The electrical circuit developed by Gilman et al. (49) was extensively modified for this study to accommodate stripes of low resistance. A diagram of the electrical circuit used in this series of tests is shown in Figure 7. A 30 volt-100 milliampere DC power supply was used to supply power to the deflection stripes and the trigger stripe through the circuit. A Tektronix 564B oscilloscope (Tektronix, Inc., Portland, Oregon) with a 2A63 amplifier and a 2B67 time base and a Tektronix 561A oscilloscope with a 3A6 amplifier and a 2B67 time base were connected to the electrical circuit.

Both oscilloscopes were set in the single sweep mode and adjusted to trigger when the trigger stripe on the crystal surface was broken. The trigger test in the circuit allowed simulation of stripe breakage to insure that the oscilloscopes were set properly. The Y-axis sensitivity was adjusted so that the oscilloscope trace would remain on the screen during breakage of all deflection stripes. The storage oscilloscope was set at a sweep rate 10 times slower than that of the other oscilloscope. This was done to increase the probability of observing the breakage of the stripes since the effect of atmosphere and temperature on crack velocity were unknown.

Once the oscilloscopes were triggered by the trigger stripe breakage, the sweep was shifted upward as each deflection stripe was broken, creating a step-like trace. By noting

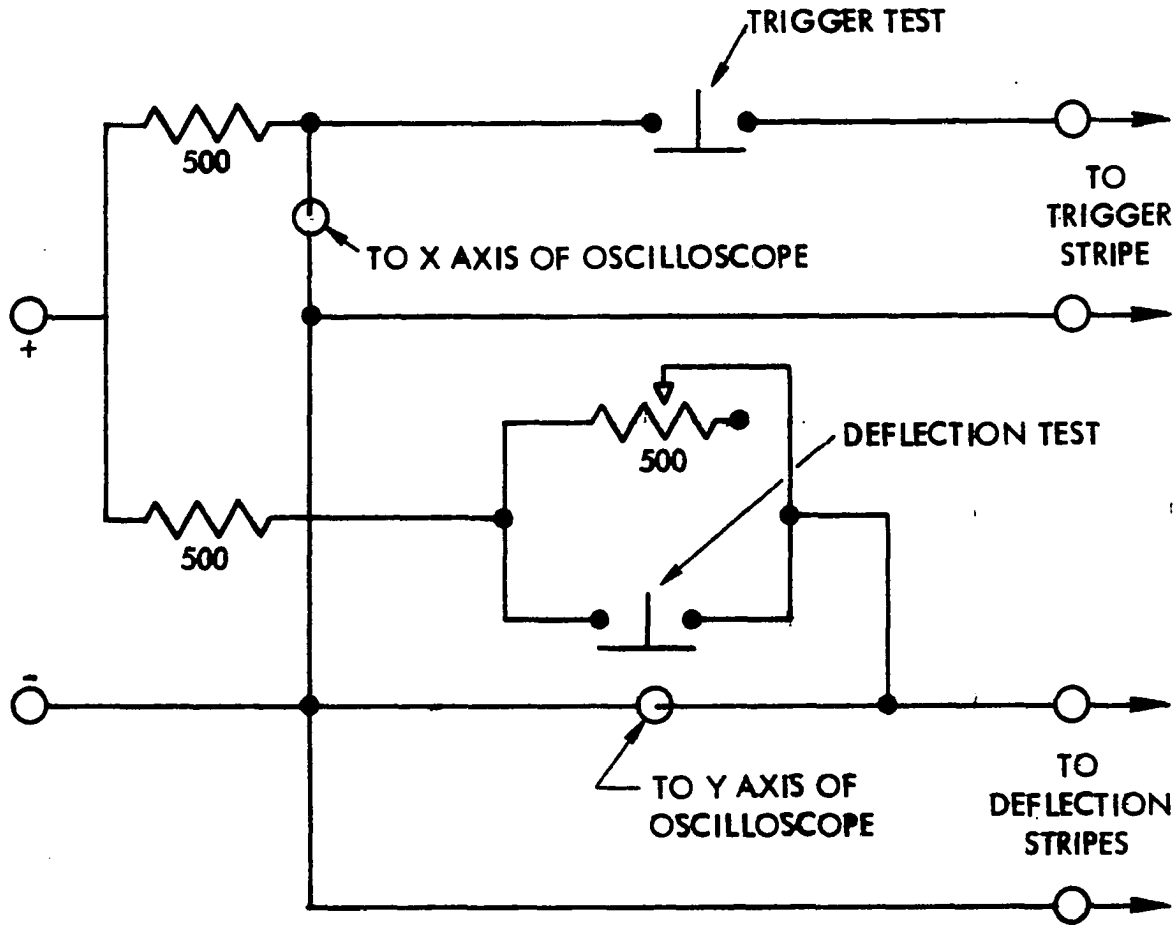

Figure 7. The electrical circuit

elapsed time between steps, it was possible to determine the time required for the cleavage crack to travel from one point to another in the crystal. A typical oscilloscope trace is shown in Figure 8.

Examination of Fracture Surfaces

Usually within 3 minutes after cleavage, one cleavage arm was removed and etched for 10 seconds in a 30 gm/ℓ solution of mercuric chloride in absolute ethanol (75). It was then rinsed in acetone and dried in a stream of nitrogen gas. However, when cleavage was performed at temperatures above 100°C, it was necessary to allow the sample to cool before being etched. Several attempts were made to etch samples while they were still hot. The etchant dried almost immediately upon contact with the surface, leaving deposits which obliterated most surface features.

The etchant produced sharply defined pyramidal shaped pits with sides oriented in the <100> directions. As reported by Long (74) the subgrain boundaries appeared to be more heavily attacked than the interior of the subgrains. The cleavage surface was examined under reflected light with a Zeiss Ultraphot II camera microscope (Carl Zeiss, Oberkochen/ Wuertt., West Germany). Photographs of interesting features were taken.

Due to the rapid attack of moisture in the atmosphere on the cleavage surface, it was found necessary to protect the

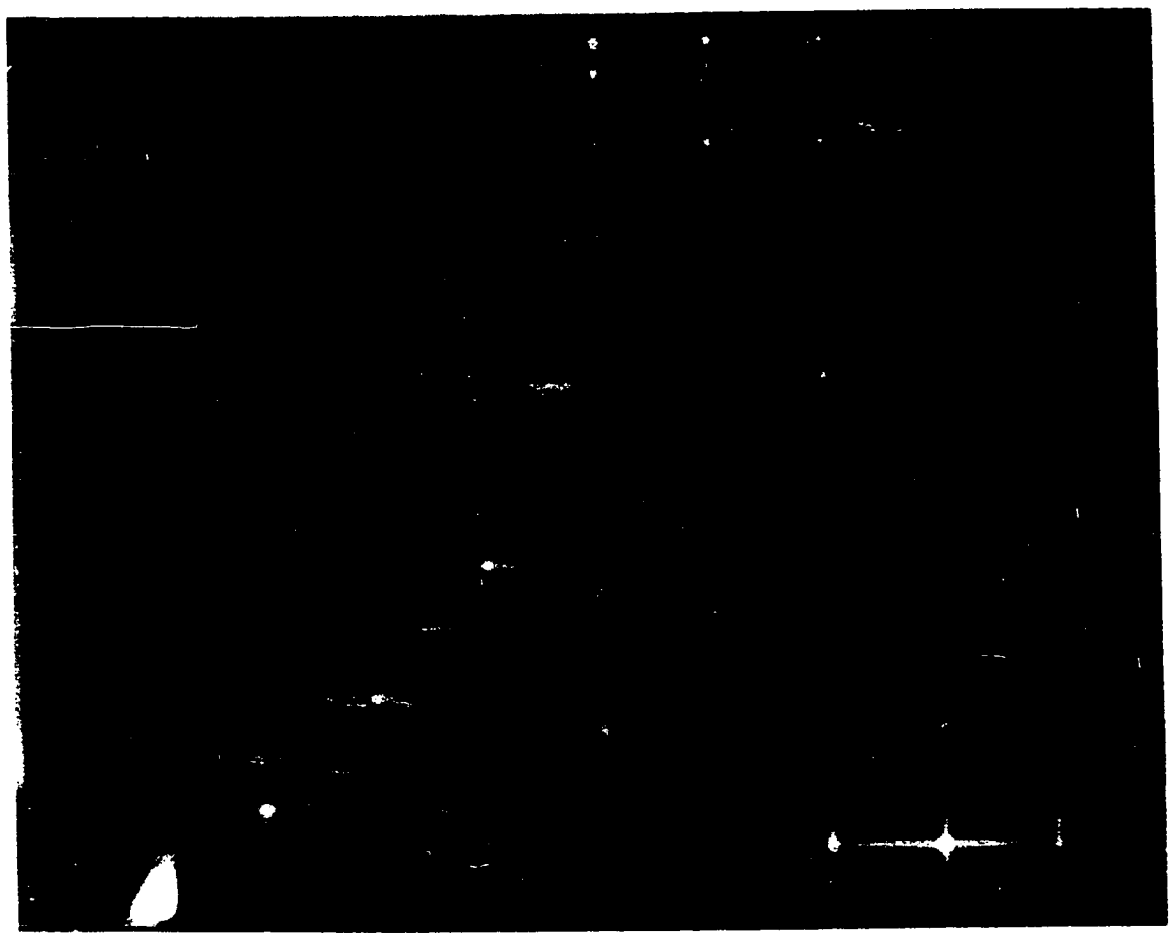

Figure 8. Typical oscilloscope trace

surface while it was being observed microscopically. A layer of gold approximately 50Å in thickness deposited on the surface retarded the attack but did not prevent it. However, if a stream of dry nitrogen was directed across the surface, attack could be prevented indefinitely.

After each crystal was examined the dimensions of each cleavage arm were measured with a standard micrometer. The distance between deflection stripes was measured at the point of breakage with a microscope.

RESULTS AND DISCUSSION

The Range of Crack Velocities

In the crystals of regular geometry (total height = 1.2 cm) the crack velocity averaged over the entire crystal length, or V_A, ranged from about 0.09 V_S to 0.20 V_S. The velocity of sount, V_S, was taken as $(C_{11}/\rho)^{1/2}$ where C_{11} is the elastic modulus in the <100> directions and ρ is the density (49). The values of C_{11} and ρ were taken from a compilation of values (76) obtained from many sources. The temperature dependence of C_{11} and ρ were also taken from the same source. In the crystals with reduced height (total height = 0.8 cm) V_A ranged from about 0.001 V_S to about 0.16 V_S. The averages and ranges of V_A for samples cleaved in nitrogen are shown in Figure 9. The averages and ranges of V_A for samples cleaved in other atmospheres are shown in Table II. The values of V_A for individual specimens can be calculated from data in Appendices B and C.

In the crystals of regular geometry, the crack velocity measured between 2 consecutive deflection stripes, or V_I, ranged from about 0.07 V_S to about 0.34 V_S. In the crystals with reduced height the range was from 0.00 to about 0.32 V_S. The fastest crack speed measured was 1.57×10^5 cm/sec, which is 0.329 V_S. This value was obtained in a crystal cleaved in argon. However, the fastest crack speed in relation to V_S was obtained in a crystal cleaved at 200°C in nitrogen. This

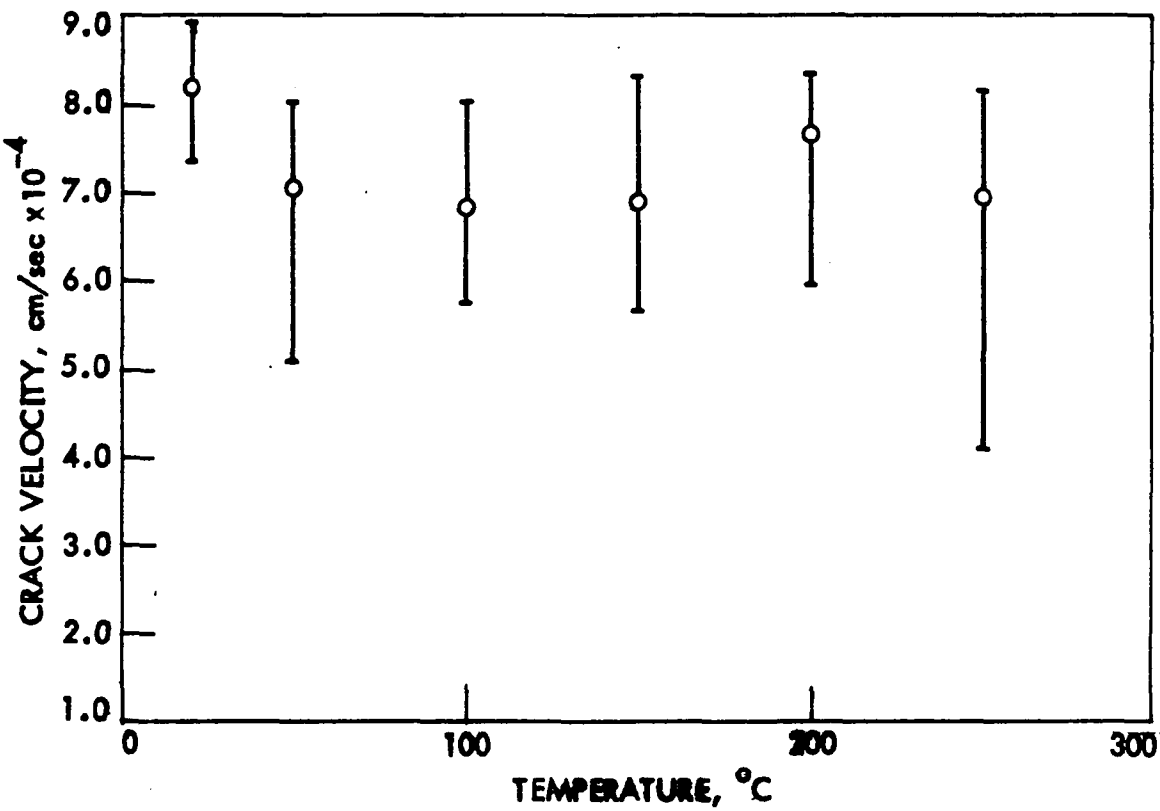

Figure 9. Averages and ranges of V_A for samples cleaved in nitrogen

Table II

The average and ranges of V_A for crystals cleaved in various atmospheres

Atmosphere	Average V_A cm/sec	High V_A cm/sec	Low V_A cm/sec
Argon	8.95×10^4	9.66×10^4	7.74×10^4
Carbon dioxide	7.88×10^4	8.48×10^4	6.93×10^4
Air (regular geometry)	7.53×10^4	8.96×10^4	5.26×10^4
Air (reduced height)	3.72×10^4	7.39×10^4	0.055×10^4
Nitrogen (γ-irradiation)	8.29×10^4	9.51×10^4	7.40×10^4

value was 1.53×10^5 cm/sec, or 0.337 V_S. It is fastest in relation to V_S because V_S decreases with temperature due to the temperature dependence of C_{11}.

The highest values of V_I approach the maximum theoretical crack velocity for NaCl very closely. The velocity limit, which is well below the velocity of sound, was first postulated by Mott (39). He obtained the relation

$$V_C = BV_S\left(1 - \frac{4E\gamma}{\pi\sigma^2 L}\right)^{1/2} \qquad (39)$$

where V_C is crack velocity, B is a constant, V_S is the velocity of sound, E is the elastic modulus, γ is the surface energy, σ is the applied stress, and L is crack length. Roberts and Wells (77) calculated the constant B and obtained a value of 0.38. Experimentally, B has been found to equal 0.31 for a wide range of materials (49), but values as high as

0.40 have been reported (77). It is possible that the highest values of V_I from the current study are slightly high due to experimental error. The fastest crack speed is only 6% greater than 0.31 V_S. Nevertheless, values greater than 0.31 V_S were obtained in 4 different crystals.

Figure 10 shows the variation in V_I with crack length for sample 24. It is a typical example of the way V_I varied in most specimens. Forwood (48) and Gilman et al. (49) have observed that V_I is typically large at the front of the crystal, decreases in the middle of the crystal, and then increases again toward the back. They attribute the increase at the back of the crystal to enhancement of the strain field at the crack tip as the crack approaches a boundary. The oscillation in crack velocity shown in Figure 10 is apparently a common occurrence (48,51). Forwood (48) explains the oscillation in the following manner. As the knife travels at a uniform rate between the 2 cleavage arms of the sample, the arms lose contact with the knife with a resulting decrease in force exerted by the knife. The crack then slows down until the knife can again exert full force on the arms. Burns (51) says there is no reason for the tips on the cleavage arms to lose contact with the knife since they are loaded by the bent arms. He states that one possible cause of velocity oscillation is that the crack travels with flexure waves produced by the knife. The condition necessary to prevent this is that the speed of the knife be less than the maximum determined by Equation 37

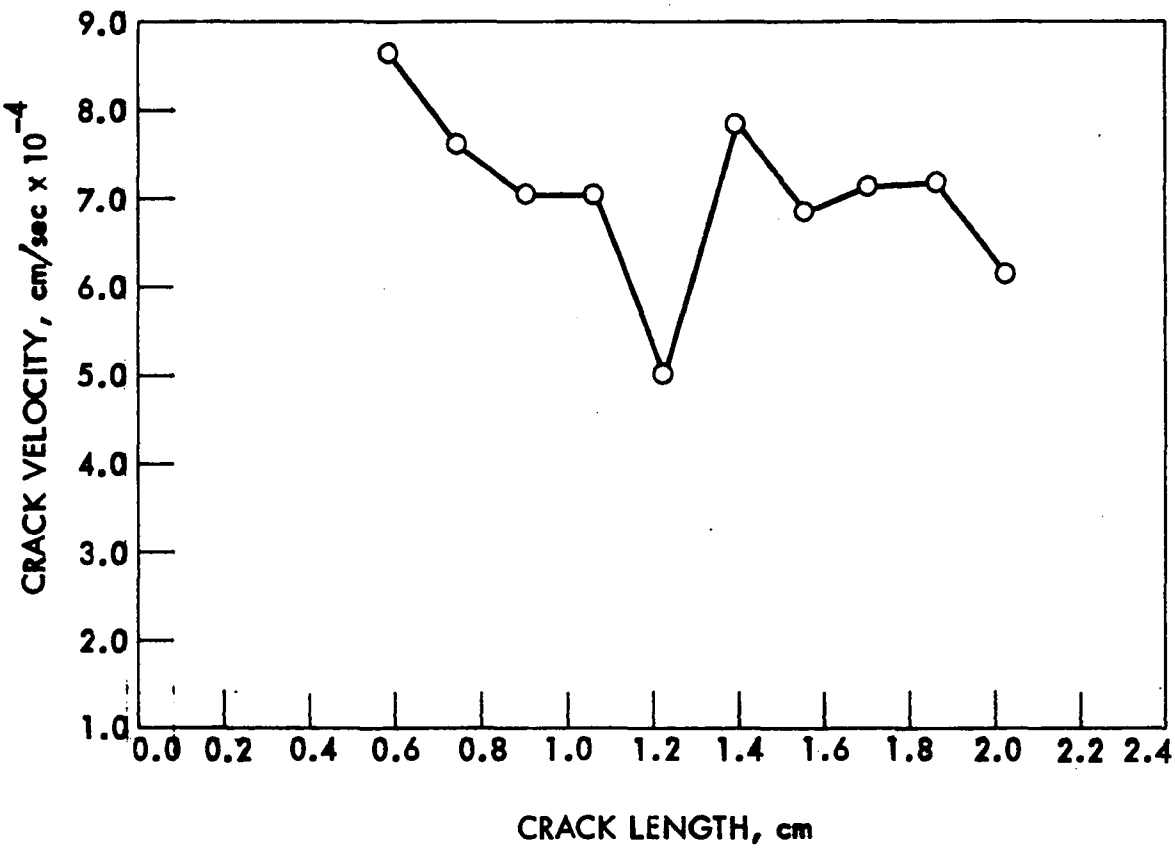

Figure 10. Variation in V_I with crack length for sample 24

in the section on theory. This criterion was applied to the data of this study and was satisfied. On this basis the influence of flexure waves was ruled out as a cause of the oscillation. Gilman et al. (49) state that oscillation can occur because the swiftly moving crack surges ahead until the force supplied by the knife is reduced. If the crack slows down enough it can cause numerous dislocations to be nucleated, slowing it down even more. However, since the arms are being moved apart at constant velocity, the force again builds up and the crack surges ahead again. This appears to be the case which applies to this study. However, the oscillation did not appear to be severe enough for the crack to slow down sufficiently to cause great numbers of dislocations to be nucleated.

Reproducibility of Data

The reproducibility of the crack speed measurements in this study is comparable to that reported by other workers using the dynamical cleavage technique (3,48,49). The ratio of the standard deviation of the average crack speed to the average crack speed for each set of crystals tested under the same conditions was typically less than 13% of the average speed. However, the ratio for samples cleaved at 250°C, the highest temperature at which a group of crystals was cleaved, was 20.8%. Samples with the regular geometry cleaved at room temperature in air had a ratio of 15.3%, while the ratio for samples with reduced height cleaved in air was

76%.

Various factors which could influence data reproducibility are: (1) cleavage under conditions of enhanced plastic flow at the crack tip, (2) use of a damaged cleavage knife, (3) specimen misalignment, (4) lack of precision in stripe breakage, (5) atmospheric effects on NaCl, (6) lack of uniformity in properties from specimen to specimen. Each of these factors is discussed below.

Gilman (4) has found that in quasistatic measurements of surface energy, the use of a wedge gives poor results. This is apparently true even if the wedge is very carefully made and lubricated. However, in dynamical cleavage, wedges have been employed with good success (3,48,49). Gilman's data (49) show that reproducibility is better when the crack speeds are higher than when they are low. This indicates that the quasistatic cleavage method suffers from greater variation in plastic flow at the crack tip than does dynamical cleavage (4). It also shows that conditions producing fast cracks should have greater reproducibility than conditions favoring slow cracks because of the reduced tendency for plastic flow. The tendency for plastic flow should be increased by increasing the temperature and also by reducing the crystal height (i.e. making the crack long with respect to crystal height (34). Thus the reduced precision of measurements made at 250°C and on the samples with reduced height is apparently attributable in part to increased plastic flow at the crack tip.

Great care was taken to reduce experimental error due to any variation in the condition of the cleavage knife. Because the same knife was used to cleave many specimens, it was examined periodically under a microscope and also by running a fingernail across the edge to detect any nicks in the edge. Due to the possibility that there might still be damage which was undetectable, the knife was replaced periodically with a duplicate. A record of which knife was used for each sample was kept and casual observation of the data showed no discernible effect due to knife condition. For instance, there was no trend toward reduced crack speed with prolonged use of a single knife, nor a drastic change in speed when the knife was replaced.

Misalignment of the specimen with respect to the line of travel of the cleavage knife could not be ruled out as a source of experimental error. As mentioned earlier, a tremendous variation in crack speed from specimen to specimen was noted in Kyropoulos-grown samples cut from a single parent block with a string saw. This was due in part to misalignment of the [100] direction in the crystal from the line of travel of the knife by about 2°. Gilman (4) has indicated that the number and height of cleavage steps is a measure of the degree of misalignment. The photomicrographs in Figures 27-29 show that steps on the cleavage surfaces of the Kyropoulos crystals were indeed very large and numerous. Many of the cleavage steps can be related to imperfections such as twist boundaries.

Nevertheless, specimen misalignment was most likely a contributing factor. Comparison with the photomicrographs of the cleavage surfaces of the Stockbarger crystals in Figures 21-26 will show that the difference in step density and height is significant. Another indication of specimen misalignment in the Kyropoulos crystals was the formation of twin <110> cracks at the point of knife impact in about 80% of the crystals. (Similar cracks have also been observed by Wiederhorn (78).) The cracks generally ran about 2 mm into the crystal and were arrested by plastic flow. In several cases the <110> crack shifted to the <100>direction, traveling about 1 cm before stopping. The presence of <110> cracks in the Stockbarger crystals was observed only once in the test crystals.

Failure of the knife to bisect the samples exactly did not appear to produce any variation in crack speed in a consistent manner. When the ratio of the heights of the 2 cleavage arms of a sample was related to the speed, it was found that samples with equal ratios often produced crack speeds at opposite ends of the range of the data. (A ratio of 1.0 represents exact bisection and an increasing ratio represents increasing deviation from bisection).

Forwood (48) has stated that part of the scatter in his data was caused by the deflection stripes having finite width. It is possible that a deflection in the oscilloscope trace may occur before a stripe is completely broken. In this study the width of the deflection stripes was less than 10% of the

distance between the stripes. For this reason it was felt that any error due to deflection before complete stripe breakage would be quite small. Several tests were made to see if a crack could be passed through a crystal without breaking the deflection stripes. This was done by compressing the crystal to hold the sides of the crack together. It was always found that if the crack passed under a stripe, the stripe was broken. It was often impossible to see the break with the naked eye so that the best way to detect breakage was to check the electrical resistance. Because of these tests it was assumed that a great amount of spreading apart of the cleavage arms was not required for stripe breakage. This was a necessary condition for accurate measurement of crack speed.

It was noted that the ratio of the standard deviation of the average V_A to the average V_A for the group of crystals cleaved in air is over twice as large as the ratios for all other atmospheric conditions. The one exception is the ratio for the irradiated crystals cleaved in nitrogen. The ratio for air is only about 1.85 times as large as this ratio. The ratio for the samples with reduced height, which were also cleaved in air is about 10 times as large as the others. The greater scatter of the air data could not be related to a specific cause although less control was exerted on the atmosphere during air testing than at other times. The only control used was maintenance of relative humidity in the range 45%-54%. Machlin and Murray (63) and Class et al. (66) have observed

that mechanical tests on NaCl in air during summer months may give erratic results and they have attributed this to variations in ozone content in the atmosphere after thunderstorms. The samples of regular geometry were cleaved in air on 3 separate days. It was noted that heavy rain occurred on one of the test days but the range of data collected on that day was not significantly different from the data gathered on the other days. The samples with reduced geometry were all cleaved on the same day and rain did not occur on this day. It therefore seems unlikely that thunderstorm activity affected the reproducibility significantly. Although the exact cause of the scatter could not be determined, it was undoubtedly a result of some factor present at the time of cleavage rather than a result of prior exposure to the atmosphere. This was deduced from the fact that all samples cleaved in the various atmospheres were unavoidably exposed to the air prior to being placed in the test atmosphere.

Finally, the perfection of the single crystals was examined. The cleavage surfaces showed the presence of subgrains ranging in number from about $1/mm^2$ to $10/mm^2$. Most of the sub-boundaries appeared to be low angle tilt boundaries since few cleavage steps emanated from them. No correlation between crack speed and the density of sub-boundaries could be made.

Effect of Temperature and Atmosphere on Crack Velocity

The criterion for statistically comparing the various groups of data was passage of the F test. If the averages of 2 sets of data passed the Student "t" test at the $\alpha = 0.05$ level, then a significant difference was said to exist. In cases where the averages and variances were approximately the same, it was assumed that no significant difference in the data existed. Practically, this meant that for the difference between the average V_A's for 2 groups of crystals (V_A is the average crack velocity in a single specimen) to be important, the difference had to be greater than 10%.

Crack velocity in the irradiated crystals was not significantly different from that in the unirradiated crystals. The average V_A for the irradiated crystals was $(8.29 \pm 0.68) \times 10^4$ cm/sec and for the unirradiated crystals cleaved in nitrogen was $(8.21 \pm 0.53) \times 10^4$ cm/sec. Since it is the premise of this study that crack velocity is directly related to fracture energy, these results can be compared to the results of a study made by Gilman (4). Gilman found in the quasistatic measurement of surface energy of LiF that substantial radiation caused little change in surface energy. He justified this by saying that although the bulk properties of a crystal might be changed, relatively few of the bonds at the cleavage plane would be affected and fracture energy is determined mainly by the breakage of these bonds. Wiederhorn

et al. (30) stated that irradiation caused an apparent increase in fracture energy in NaCl (which would mean slower crack speed in this study). This is contrary to what might be expected if a change were to be seen at all. They explained this by saying that plastic flow, which in this case enhanced crack movement, was reduced by the irradiation. The fracture energy appeared to be insensitive to radiation dose from $4x10^6$ rads to $3.4x10^7$ rads although the yield stress was increased by a factor of 4. Reducing the specimen width in soft crystals to about 0.1 cm had about the same effect as irradiation of wider samples.

The average V_A for samples cleaved in argon was (8.95 $\pm$ 0.57) x 10^4 cm/sec. This was not discernibly different from the value obtained in nitrogen. Argon would not be expected to have any effect on crack propagation since it is generally considered to be inert (66). The similarity in the data therefore indicated that nitrogen also has little effect. Gorum et al. (61) have stated that nitrogen embrittles NaCl tested in bending. However others (63) have found no embrittling effect of nitrogen on NaCl and have indicated that the findings of Gorum et al. were due to the presence of NO or O_3 as impurities in the nitrogen gas. Both the argon and nitrogen gases used in this study contained small amounts of oxygen. The argon also contained nitrogen as an impurity. No attempt was made to determine if NO or O_3 were present. It is therefore possible that either NO or O_3 might have

caused embrittlement in crystals cleaved in argon and nitrogen.

The average V_A for crystals cleaved in CO_2 was (7.88 $\pm$ 0.55) x 10^4 cm/sec. This was about 12% less than the value for crystals cleaved in argon and therefore significantly different. However, this was only about 4% less than the average V_A for crystals cleaved in nitrogen. For this reason it was felt that the action of the CO_2 atmosphere was not due to exclusion of NO or O_3, which might have been present in the argon and nitrogen. Gross and Gutshall (79) have found that exposure of NaCl to moist CO_2 causes enhanced ductility during quasistatic measurement of surface energy. Otterson (64) found that crystals aged in moist CO_2 and tested in flexure in air were embrittled unless the crystals were initially free of hydroxyl ions. Aging in dry CO_2 and then testing in air produced no detectable difference from results of testing crystals which had been protected from exposure to CO_2. The results of aging in one atmosphere and then testing in another are not necessarily comparable to testing in the atmosphere used in aging. This is shown by the conflicting data of Gross and Gutshall (79) and Otterson (64). Also, the fact that scatter in the air data of this study is greater than for other atmospheres although all crystals were exposed to air reinforces this assumption. For this reason Otterson's results cannot be considered necessarily contradictory to the results of this study. The manner in which CO_2 might influence crack speed is unknown.

Temperature had only a slight effect on crack velocity in the samples cleaved in nitrogen. As stated earlier the value of V_A at room temperature (22°C) was (8.21 ± 0.53) x 10^4 cm/sec. The values of V_A at 50°C, 100°C, 150°C, 200°C, and 250°C were (7.07 ± 0.91) x 10^4 cm/sec, (6.86 ± 0.84) x 10^4 cm/sec, (6.90 ± 0.84) x 10^4 cm/sec, (7.67 ± 0.75) x 10^4 cm/sec, and (6.95 ± 1.4) x 10^4 cm/sec, respectively. The difference between the average V_A at room temperature and the values at 50°C, 100°C, and 150° was statistically significant. However, the value at 200°C was only 8% less than that at room temperature and could not be said to be discernibly different. The variance of the data from the samples cleaved at 250°C was too great to allow comparisons to be made. Neglecting the room temperature data, the variation in average V_A with increasing temperature was so small that the differences were not significant. The maximum variation was only 10% and this was not enough to satisfy requirements of the "t" test.

The exact effect of temperature on crack velocity is dependent on the crystal quality and on the experimental procedure. If conditions are such that plastic deformation is favored, the effect of temperature will be more pronounced than otherwise. Gilman et al. (49) found no effect of temperature on crack velocity in LiF between -200°C and 25°C. Conversely, Burns and Webb (3) found that the crack velocity in LiF decreased substantially as the temperature was increased from 25°C to 300°C. The difference in their findings may be

due to several reasons. The fact that they used different ranges of temperature is an obvious factor. Gilman et al. (49) also used a greater knife velocity than Burns and Webb (3) and this would make crack velocity less sensitive to temperature. In this study the experiment was designed to reduce the tendency for plastic flow. This was done by using a high knife velocity and using samples with height much greater than those used by Gilman et al. (49) or Burns and Webb (3). This necessarily would have reduced the effect of temperature on crack velocity.

The same conclusions that were drawn from the data for samples cleaved in nitrogen at 22°C could also be made for the data from the irradiated crystals. That is, the irradiated crystals tended to produce higher average crack velocities than crystals cleaved at 50°C, 100°C, and 150°C. This is not surprising since crack speed in the irradiated and unirradiated samples was similar. This was also true of the data from crystals cleaved in argon. In addition, it was possible to say that crack velocity at 200°C tended to be less than for the crystals cleaved in argon. However, such conclusions could not be made about the crystals cleaved in CO_2. The average V_A for these samples was not sufficiently different from the others to satisfy the "t" test.

Calculation of Cleavage Energy

The equation of crack motion which was derived earlier was used to calculate the cleavage energy of the specimens. The computer program shown in Appendix F was used to facilitate computation. The values for several specimens were calculated with the aid of the equation developed by Burns and Webb (3) and compared with values obtained from the newer equation. The former values were always less than the latter because of the neglect of shear effects by Burns and Webb. The values obtained from the two equations converged with increasing crack length because of the decreasing importance of shear.

In a typical crystal the apparent cleavage energy decreased with increasing crack length. This was due to the fact that the crack velocity either remained fairly constant or decreased slowly throughout most of the crystal length. Both the equation of Burns and Webb (2) and the present equation predict that when shear can be neglected the crack velocity should be inversely proportional to crack length so long as the cleavage energy is constant. This is equivalent to saying that the square of the crack length plotted against time would yield a straight line. In the derivation of Burns and Webb's equation it was not necessary to assume such a relationship between crack length and time and so the relationship is not a necessary condition for applicability of the

equation (51). This is also true of the present equation. If the plot of the square of crack length versus time is a curve, the cleavage energy varies continuously during cleavage (2).

In order for the equation of Burns and Webb (2) and the present equation to be applicable, the crack must travel slower than flexure waves sent down the crystal by the knife (51). This condition is met when Equation 37 is satisfied. A condition equivalent to Equation 37 is

$$\frac{L^2}{(t-t_0)} < \frac{X^2}{(t-t_0)} = \frac{\pi}{2\sqrt{3}} \left(\frac{C_{11}}{\rho}\right)^{1/2} (h_1+h_2) \qquad (40)$$

where L is crack length, $(t-t_0)$ is time subsequent to introduction of the cleavage knife into the crystal, X is position of the largest bending moment pulse produced by the knife, C_{11} is the elastic modulus, ρ is the density, and (h_1+h_2) is the total crystal height. If the crack travels with a particular bending moment pulse, the crack position follows the relationship

$$\frac{L_1^2}{(t-t_0)} = \frac{L_2^2}{(t_1-t_0)} \; . \qquad (41)$$

As stated earlier, the crack velocities obtained in this study were fairly constant (i.e. $L_1/(t-t_0) = L_2/(t_1-t_0)$ and not $L_1^2/(t-t_0) = L_2^2/(t_1-t_0)$). Also, the crack velocity was small enough so that Equation 40 was satisfied. Because of this, it was felt that the crack motion was not strongly affected by

the motion of flexure waves.

The values of cleavage energy obtained in this study are plotted in Figures 11-20. The fact that the cleavage energy varied with crack length did not allow the assignment of a single value of cleavage energy to a crystal. However, when the crack length was greater than about 1 cm, the measured cleavage energy was typically between 100 ergs/cm^2 and 400 ergs/cm^2. Estimations of the reversible surface energy of NaCl from atomic theory range from about 77 ergs/cm^2 to about 190 ergs/cm^2 and experimental measurements range up to about 330 ergs/cm^2 (4,6). Thus it can be seen that the experimental values of cleavage energy obtained in this study are reasonable.

Comparison of Figures 14 and 15 shows that there was little difference in the cleavage energy of the irradiated and unirradiated crystals. This was to be expected since there was no significant difference in crack velocity. However most points beyond a crack length of 1 cm in Figure 14 do lie slightly above the corresponding points in Figure 15. While it cannot be said that the difference is significant, the fact that the cleavage energies of the irradiated crystals are slightly higher is in agreement with the findings of Wiederhorn et al. (30). They attributed this to the absence of enhanced crack growth from plastic flow, which was found in soft crystals. Such enhanced crack growth gave very low

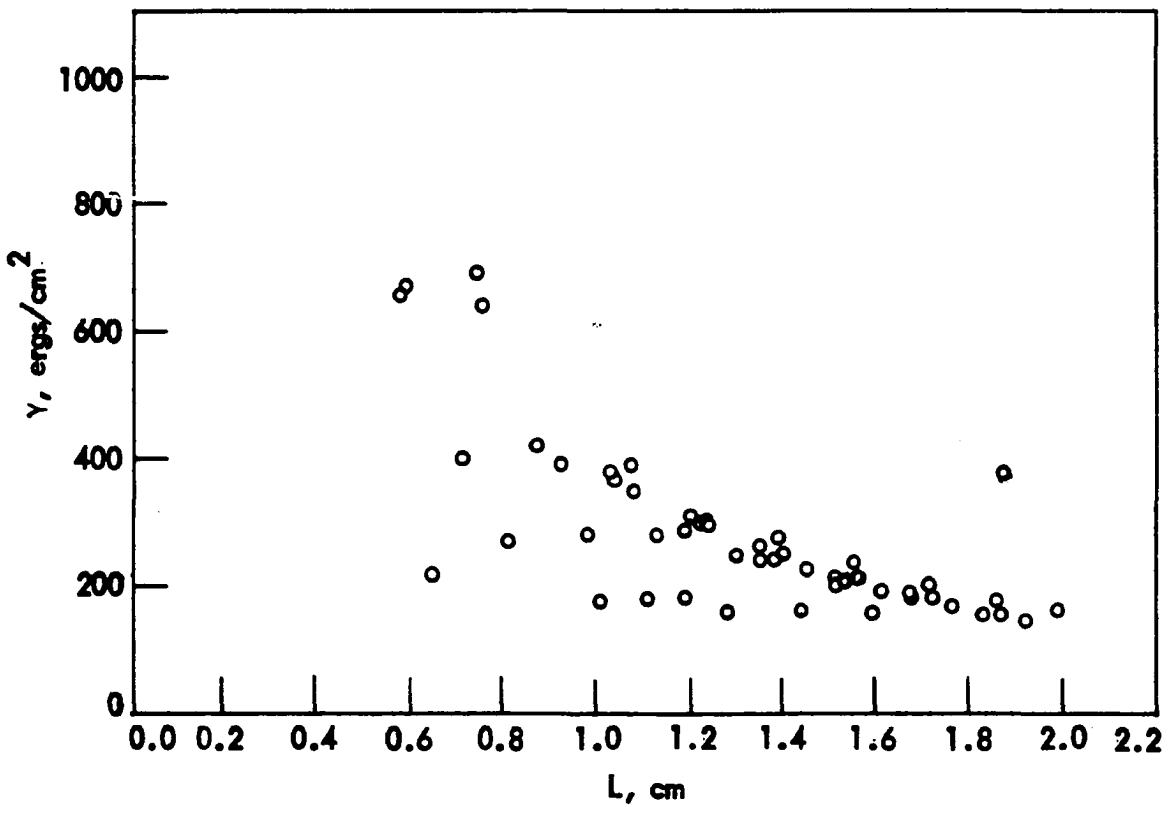

Figure 11. Cleavage energy of samples of regular geometry cleaved in air

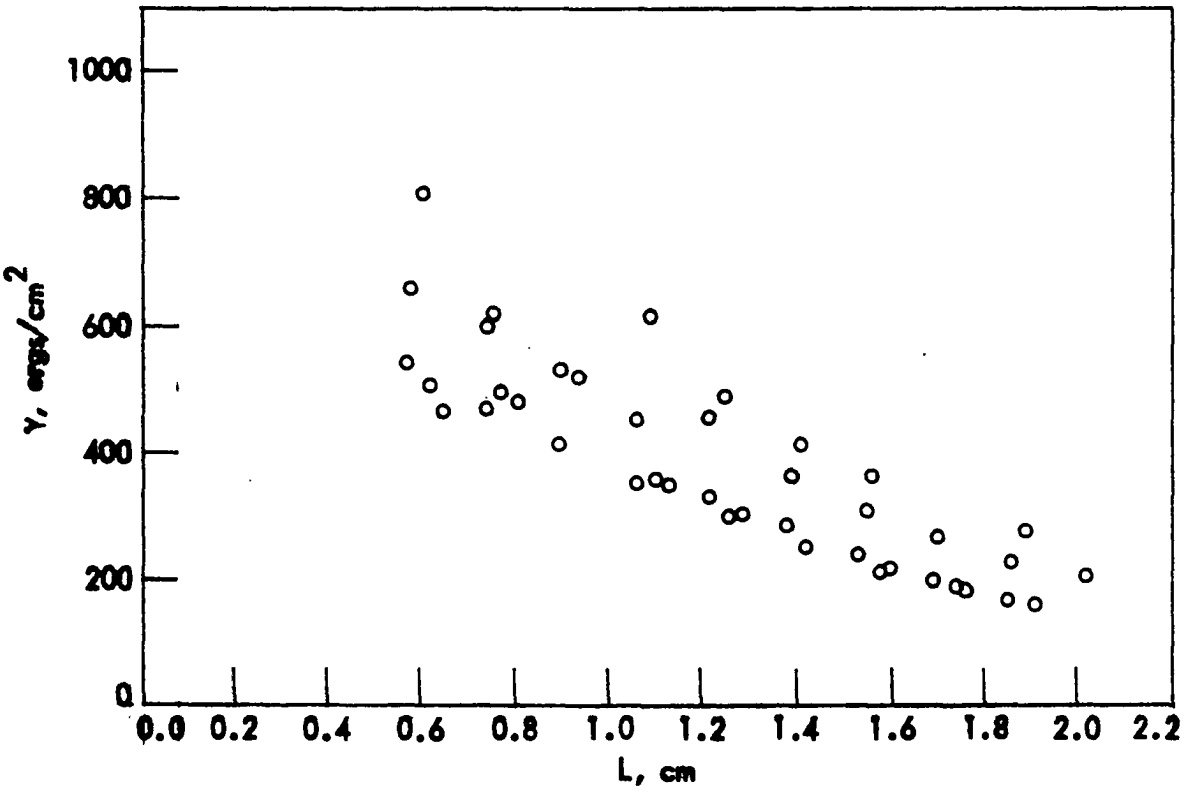

Figure 12. Cleavage energies of samples cleaved in CO_2

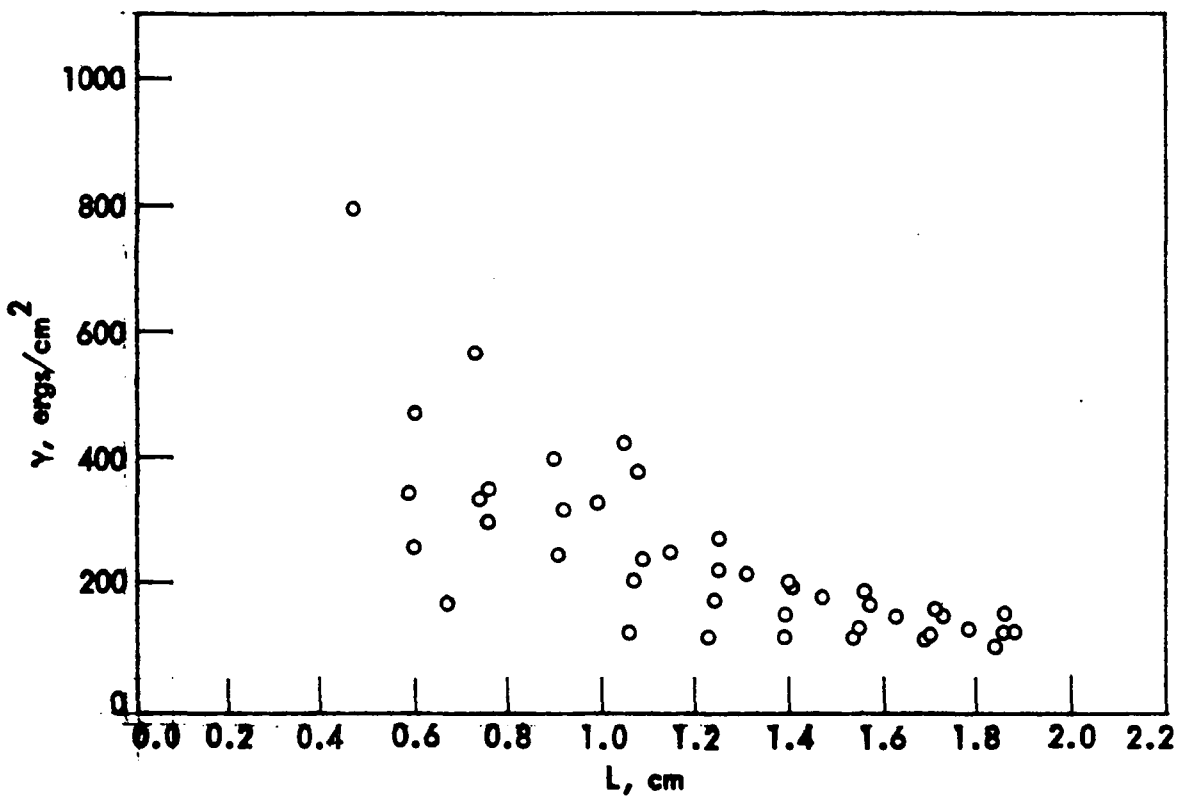

Figure 13. Cleavage energies of samples cleaved in argon

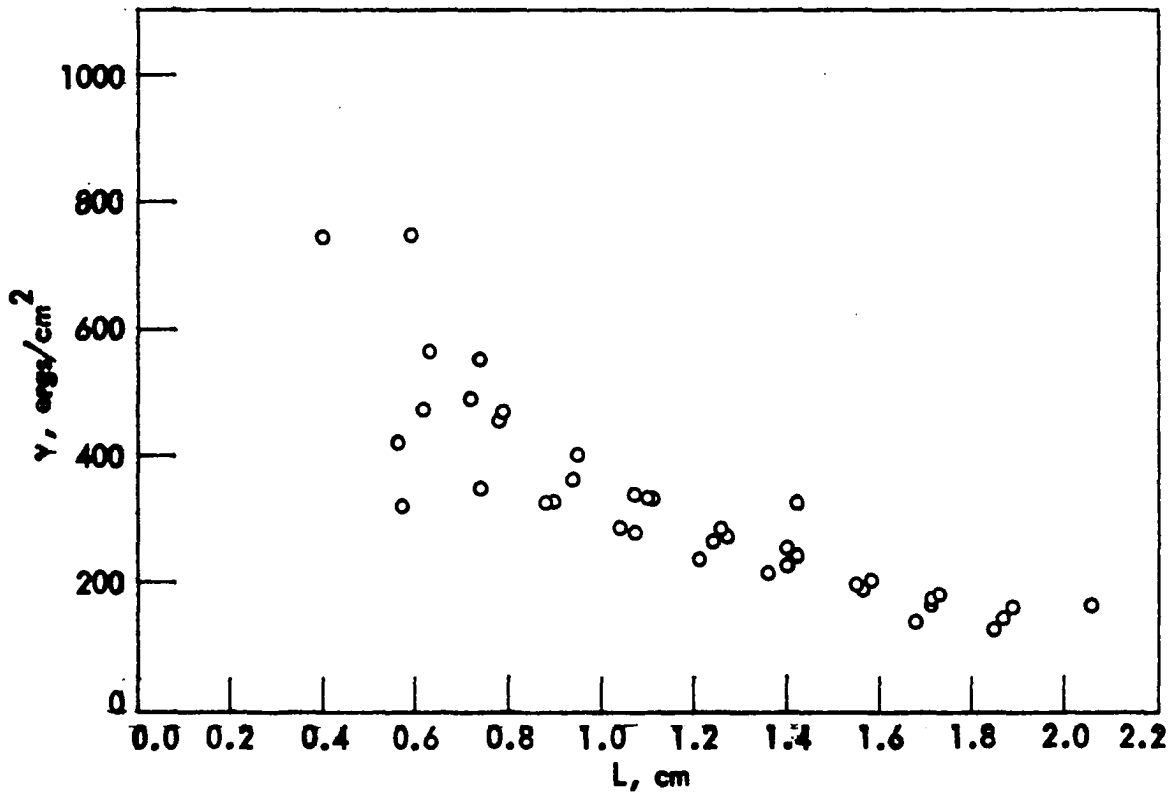

Figure 14. Cleavage energies of γ-irradiated samples

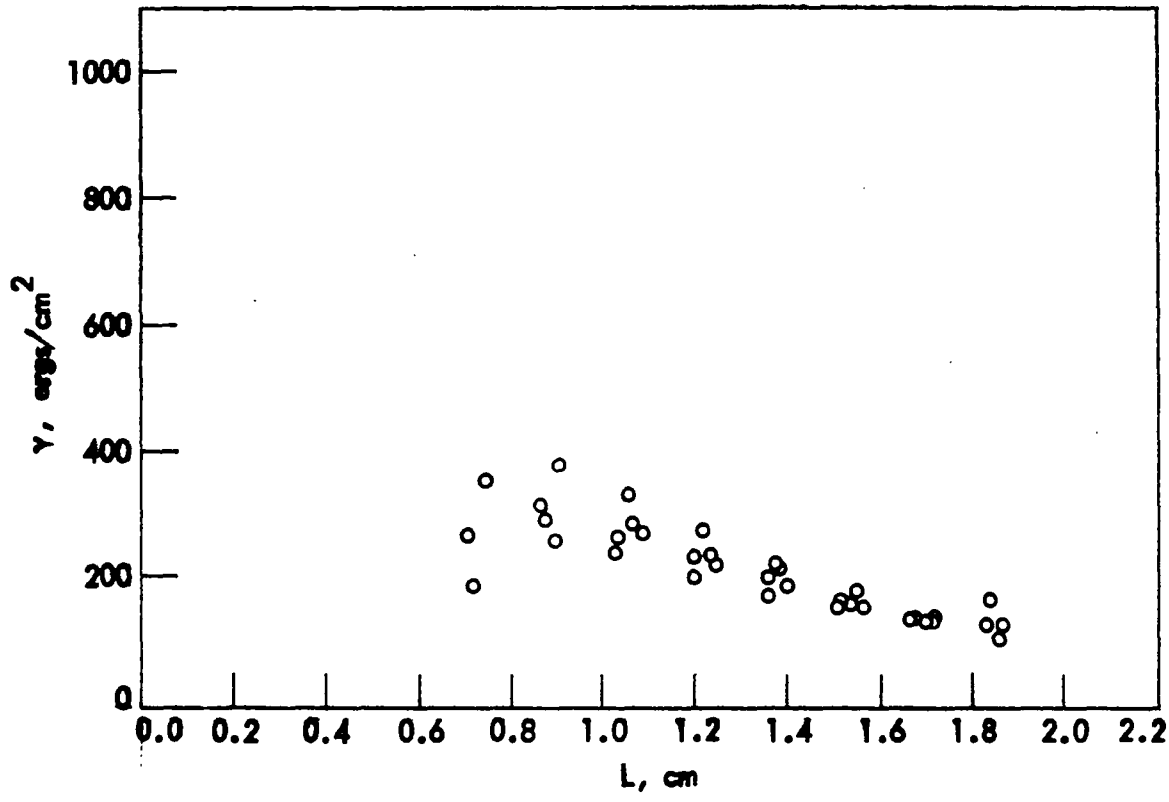

Figure 15. Cleavage energies of samples cleaved in nitrogen at 22°C

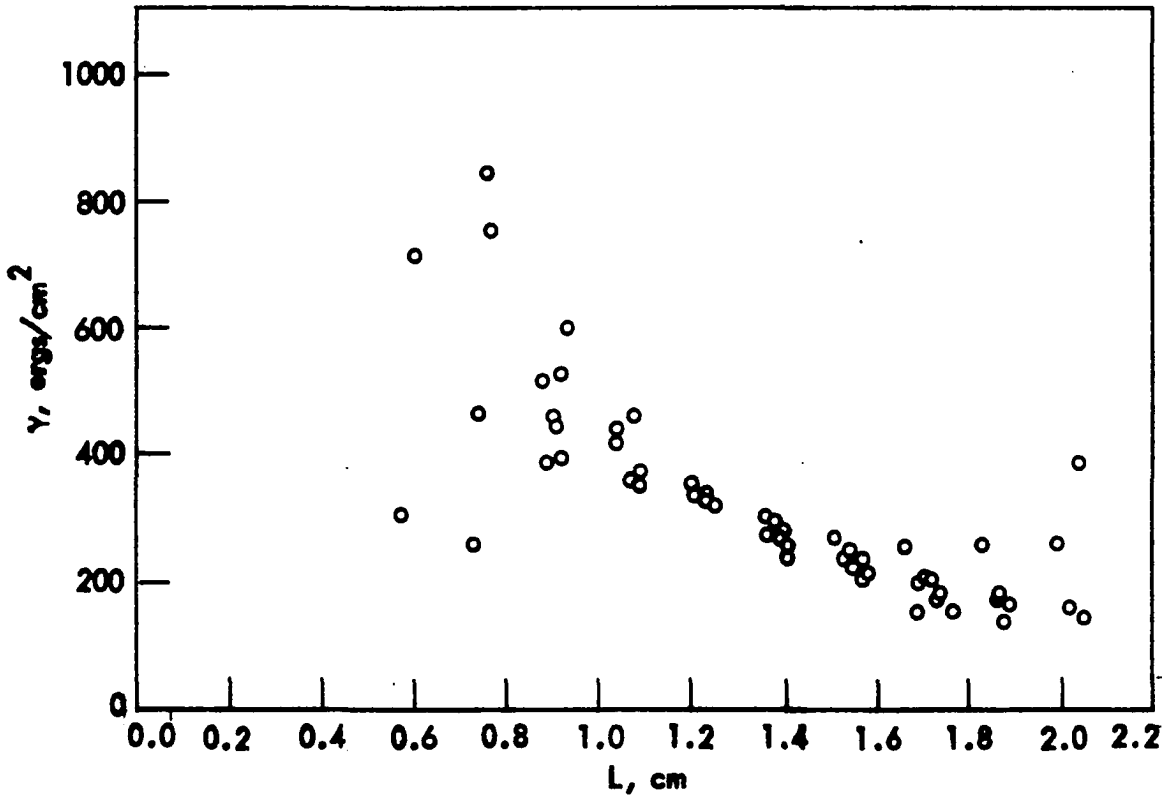

Figure 16. Cleavage energies of samples cleaved in nitrogen at 50°C

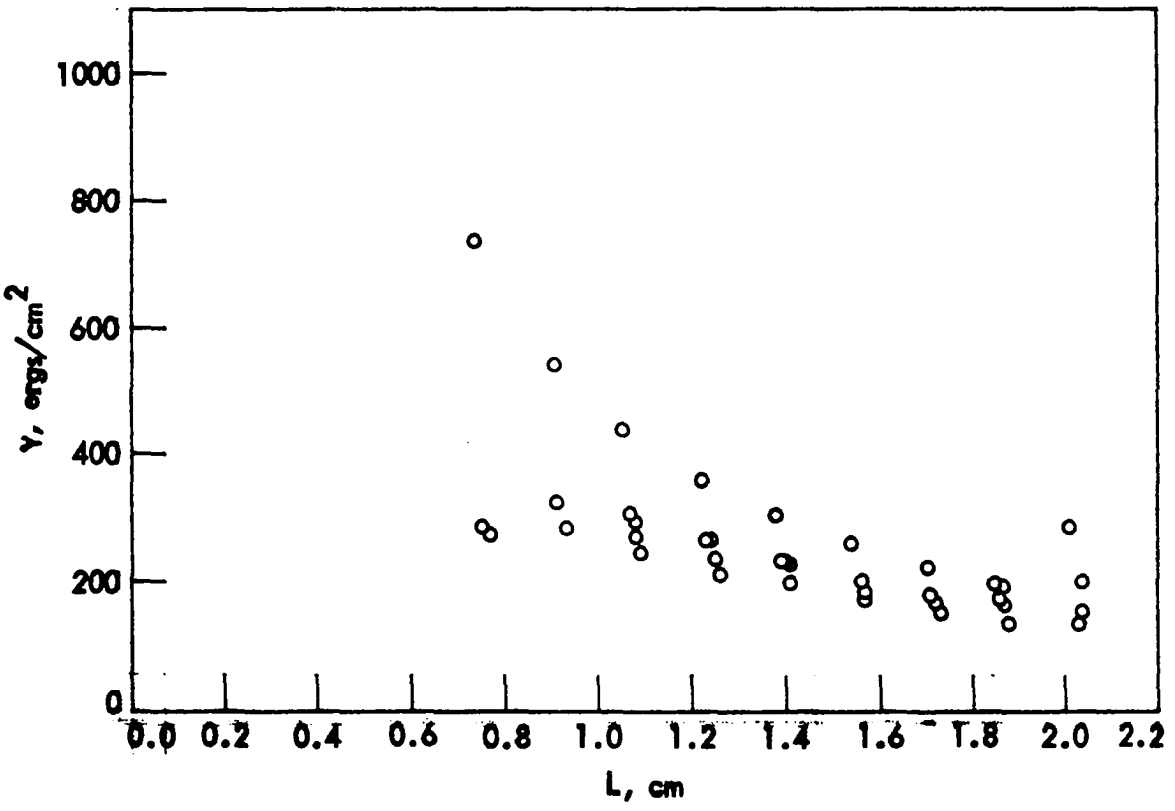

Figure 17. Cleavage energies of samples cleaved in nitrogen at 100°C

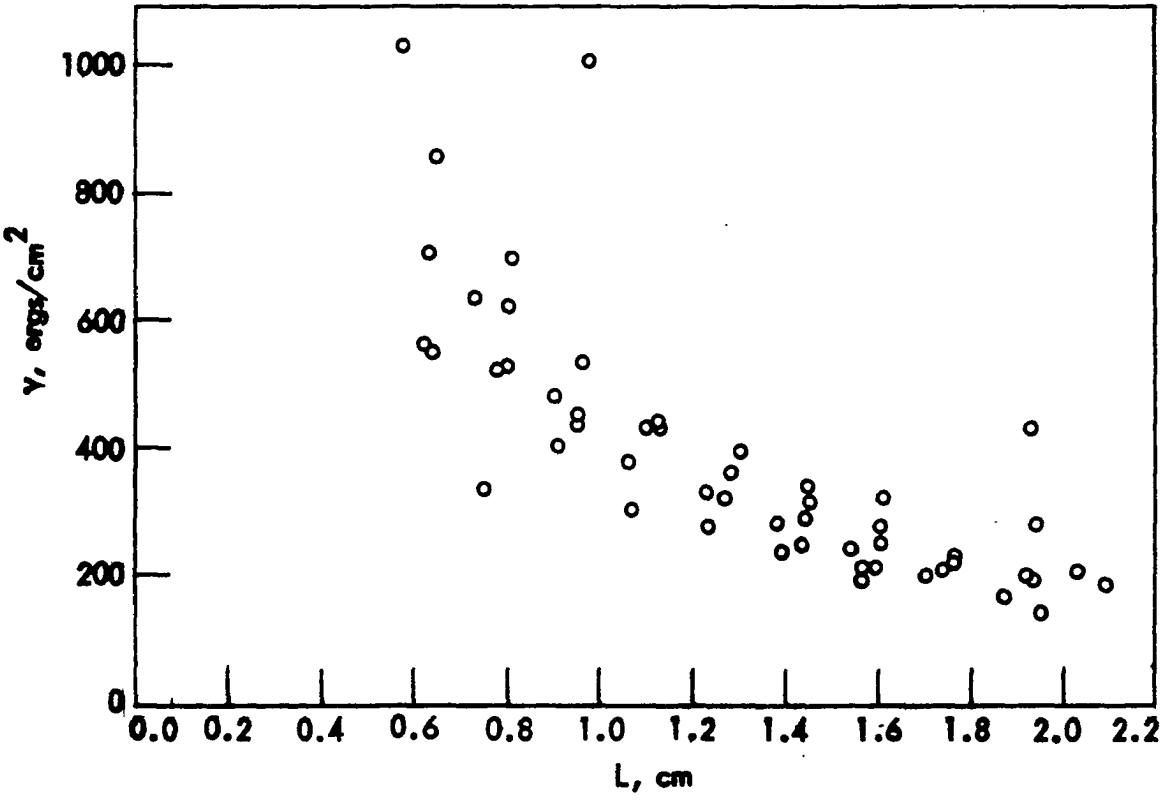

Figure 18. Cleavage energies of samples cleaved in nitrogen at 150°C

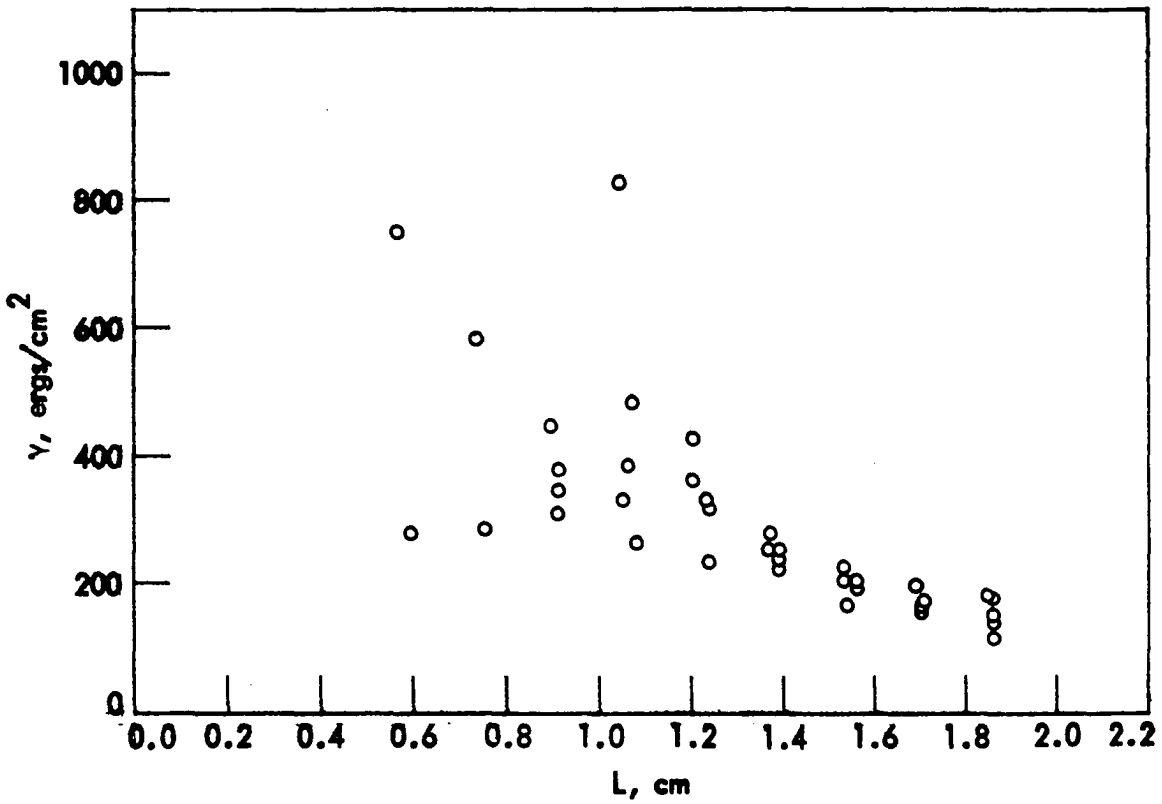

Figure 19. Cleavage energies of samples cleaved in nitrogen at 200°C

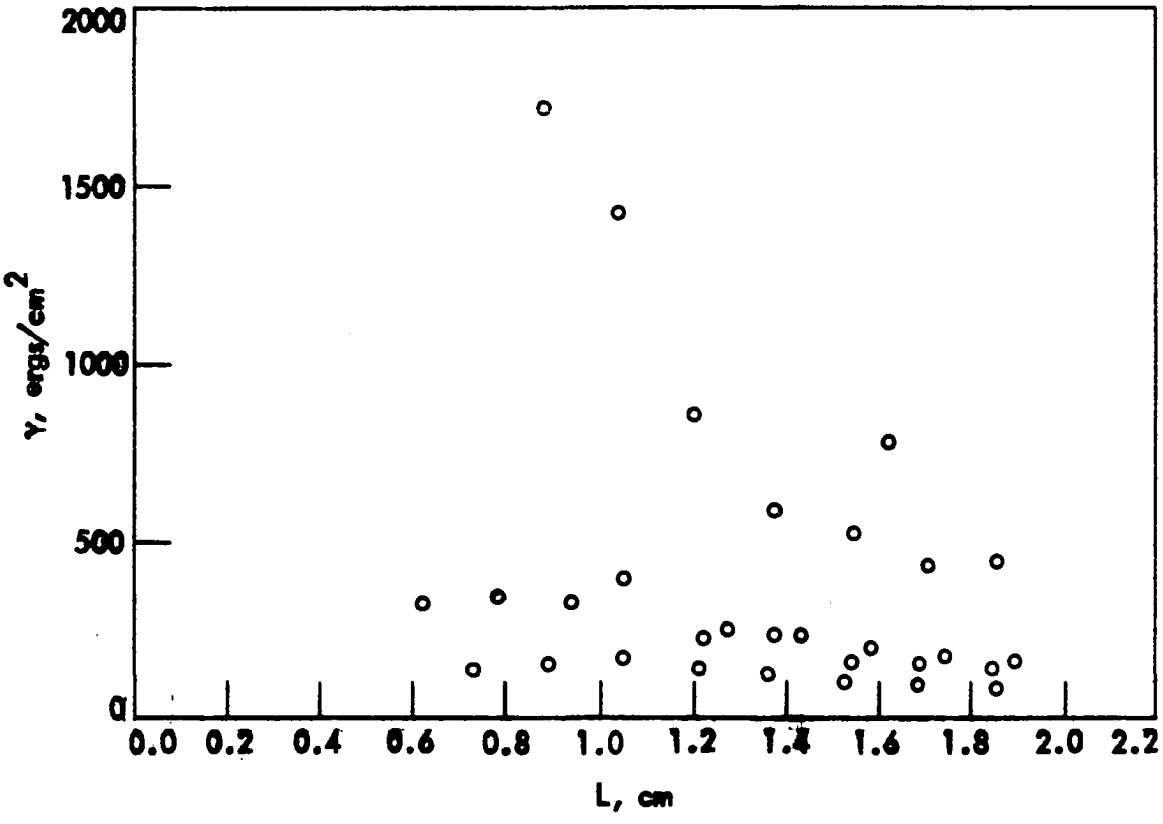

Figure 20. Cleavage energies of samples cleaved in nitrogen at 250°C

cleavage energy values by the quasistatic method. Figure 21 shows a photomicrograph of sections of the cleavage surface of an irradiated crystal. The density of etch pits is very much less than that on the surface of the unirradiated crystal shown in Figure 22. It thus appears that much less plastic flow occurred in the irradiated crystal, precluding the possibility of enhanced crack growth. However, the density of cleavage steps on the irradiated crystal surface is about the same as on the unirradiated crystal surface. Formation of these cleavage steps would have contributed significantly to the cleavage energy since they were probably formed by shear rather than by secondary cleavage (1,26).

There appeared to be no difference in the cleavage energy of crystals cleaved in argon and nitrogen at room temperature. For crack lengths greater than about 1 cm, the cleavage energy of crystals cleaved in CO_2 was noticeably greater than that of crystals cleaved in argon or nitrogen. The reason for the difference has not been determined. As mentioned earlier, Gross and Gutshall (79) found that the cleavage energy of NaCl crystals cleaved in CO_2 saturated with water vapor was greater than that of crystals cleaved in vacuum, probably because of plastic blunting of the crack tip. However, in this study the water content of the CO_2 was much less and Otterson (64) has found that dry CO_2 has no effect on NaCl.

The effect of temperature on the cleavage energy was

Figure 21. Photomicrograph of portion of cleavage surface of an irradiated sample, 60X. Direction of cleavage is from bottom to top

Figure 22. Photomicrograph of portion of cleavage surface of a crystal cleaved in CO_2, 150X. Direction of cleavage is from bottom to top

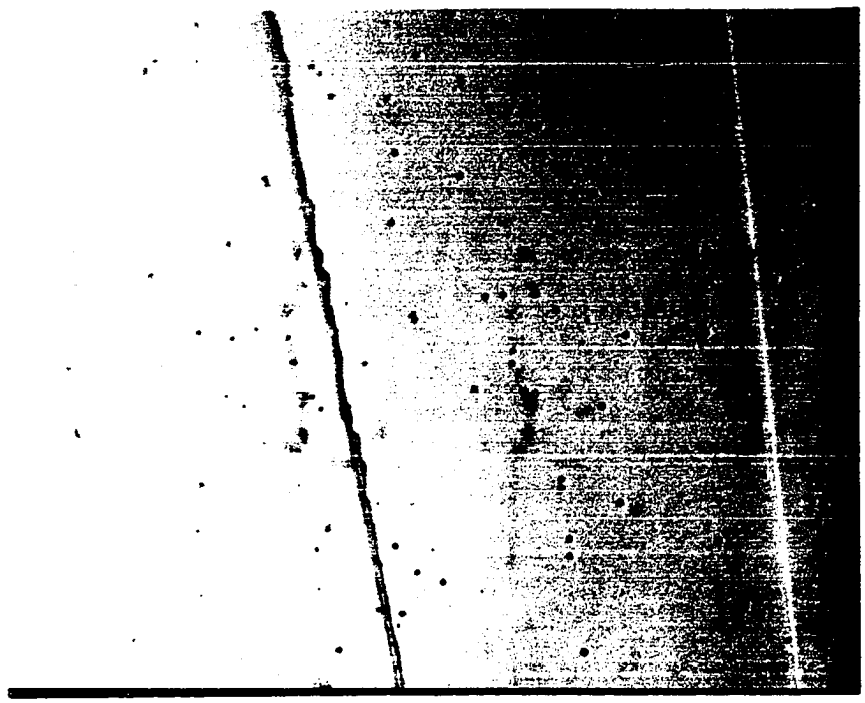

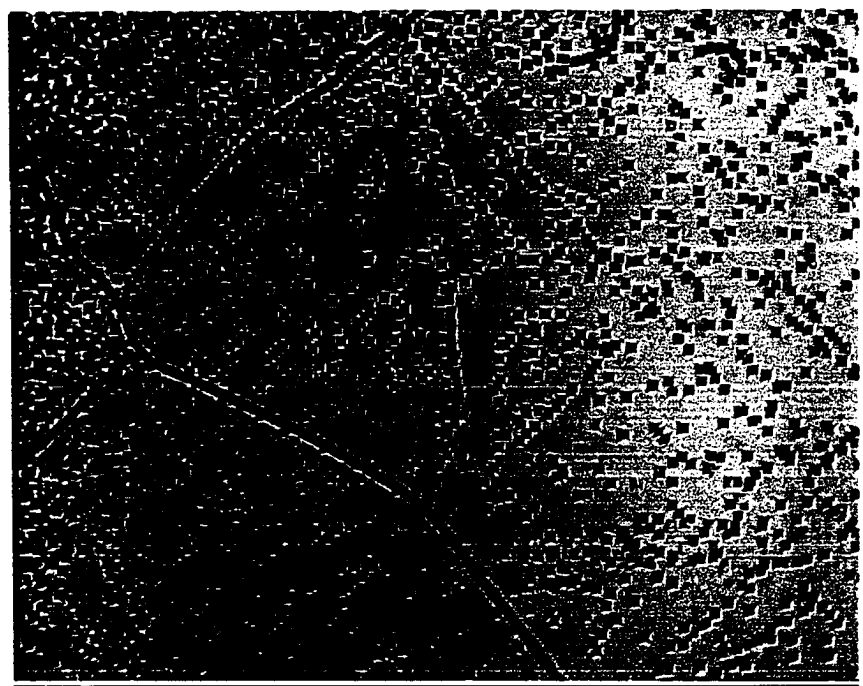

negligible. The cleavage energy of crystals cleaved at 22°C appeared to be slightly less than for crystals cleaved at higher temperatures. However, there was considerable overlap of the data so that no changes in cleavage energy with increasing temperature could be detected. The scatter in the data obtained at 250°C was considerably greater than that obtained at lower temperatures, presumably due to increased ease of plastic flow at the crack tip.

The small effect of temperature on the cleavage energy may be surprising in view of the fact that Burns and Webb (3) found a significant temperature dependence in LiF. The difference in the results can be attributed to the different sample dimensions used. Burns and Webb used long slender crystals. However, crystals with large height were used in this study to reduce the tendency for plastic flow and this would have reduced the effect of temperature.

Examination of Fracture Surfaces

In general, the dislocation etch pits on the (010) cleavage surfaces of the crystals were distributed in several ways. Narrow bands of etch pits lying either parallel or perpendicular to the [100] direction of cleavage were usually present. Occasionally, slip bands lying at 45° to the [100] direction were present. These showed the presence of slip on the {101} and $\{\bar{1}01\}$ planes, which are normally considered to be inactive during cleavage (1). Subgrain boundaries always con-

sisted of very closely spaced etch pits. Finally, numerous etch pits were scattered over the surface without any apparent crystallographic pattern.

The slip bands lying at 45° to the [100] direction were generally more prevalent toward the rear of the crystal. They appeared to be formed by compression from the small pivot block against which the rear of the crystal rested. Slip on both the {101} and {$\bar{1}$01} planes typically occurred simultaneously.

An attempt was made to see if compression by the knife could be responsible for slip band formation. It was found that if the crystal was compressed slightly by the knife parallel to the (010) cleavage plane, bands of dislocations lying perpendicular to the [100] cleavage direction were formed. The width and spacing of the bands depended upon the amount of compression. When the crystal was compressed in the direction of cleavage but an an angle other than parallel to the cleavage plane, slip in either the {101} or {$\bar{1}$01} planes was activated. Slip on one family of planes appeared to preclude slip on the other. The width and spacing of the bands formed in this manner also depended upon the amount of compression. Compression apparently did not cause formation of bands parallel to the [100] cleavage direction.

For crack velocities greater than about 1×10^4 cm/sec variations in velocity did not appear to significantly affect the density of dislocations. No correlation between etch pit

density and crack velocity could be made. The density of etch pits was much greater than could be accounted for by interaction with the cleavage crack, according to the results of Gilman et al. (49) and Burns and Webb (3). Evidence for the assumption that the majority of dislocations were formed by processes (such as compression) extraneous to cleavage was found in examination of the irradiated crystals. The density of etch pits on the cleavage surface of sample 55, an irradiated crystal, was only about 450 etch pits/cm^2. However, the crack velocity was no greater than that for unirradiated crystals with much greater dislocation densities. Gilman et al. (49) stated that plastic deformation occurs in significant amounts in LiF only when the crack velocity is below the ductile-brittle transition velocity (about 0.03 V_S). Burns and Webb (3) have shown that dislocation interaction with a cleavage crack persists to velocities almost 10 times as fast as the transition velocity. However, the amount of deformation decreases rapidly with increasing crack speed. They state that dislocations which interact with high speed cracks lie very close to the cleavage surface and are easily pulled through the surface by image stresses.

Although most of the dislocation etch pits observed could not be attributed to crack nucleated dislocations, there was strong evidence that some nucleation of dislocations did occur in NaCl at crack velocities well above 5×10^4 cm/sec. Figure 23 shows part of the cleavage surface of a crystal

Figure 23. Photomicrograph of portion of cleavage surface of sample number 35, 240X. Direction of cleavage is from bottom to top

Figure 24. Photomicrograph of part of cleavage surface of sample number 70, 60X. Direction of cleavage is from bottom to top

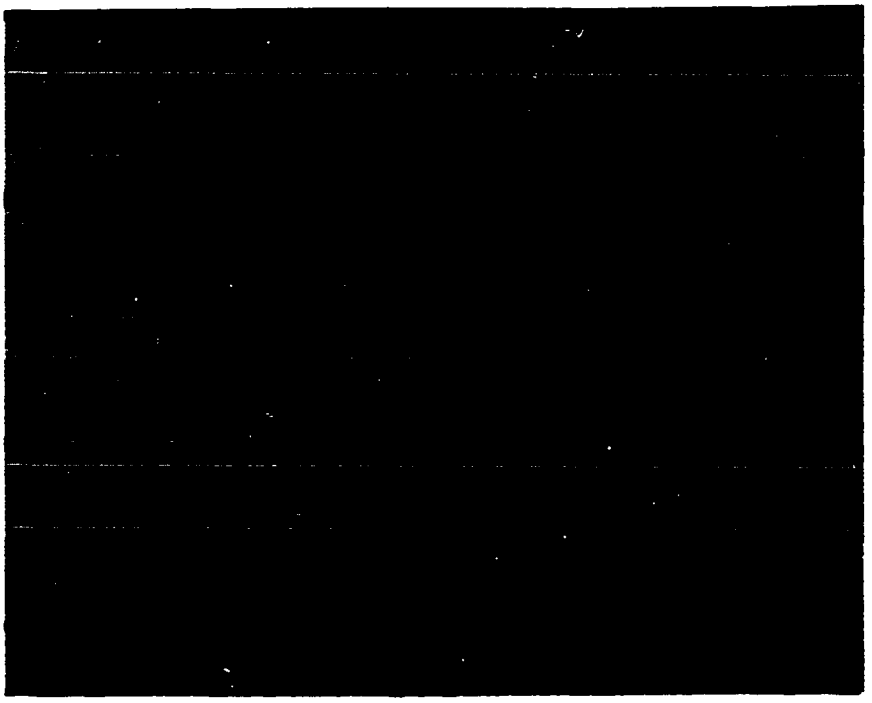

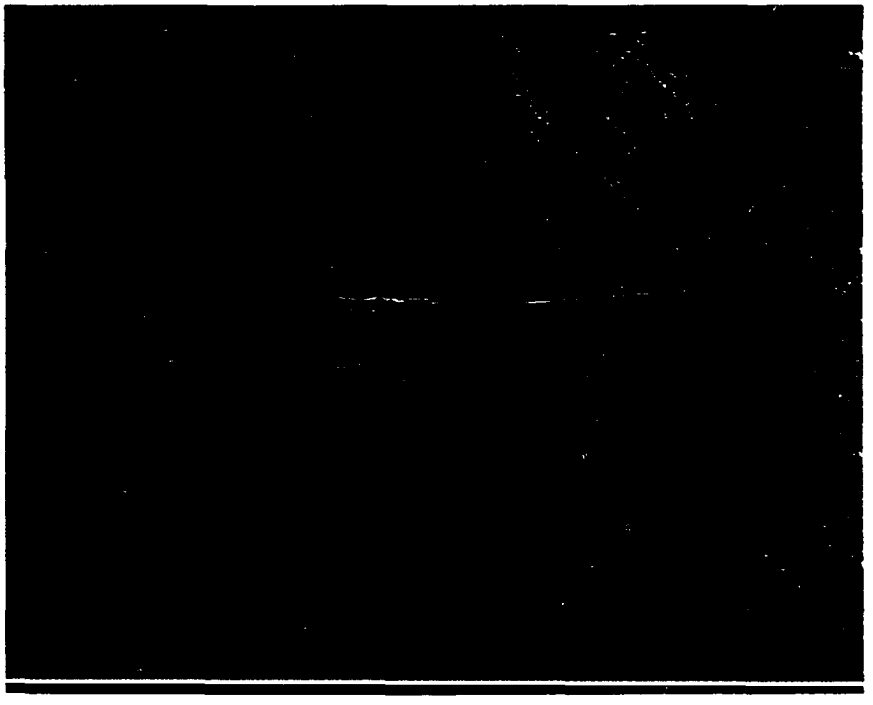

where the crack velocity was (8.0-8.4)x10^4 cm/sec, or about 0.17 V_S. The flat bottomed pits lying along cleavage steps indicate that crack nucleated dislocations have glided out of the surface during etching. Gilman et al. (49) say that the first crack nucleated dislocations to form lie along cleavage steps. This is probably because stresses are higher there than elsewhere. In this study flat bottomed pits were commonly observed to lie along steps, even in crystals where crack velocity was greater than 9x10^4 cm/sec. This was especially true for crystals cleaved at temperatures greater than room temperature.

In cases where the crack velocity falls below the transition velocity, dislocations are driven deeper into the crystal and are not as easily lost through the cleavage surface. Figure 24 is a photomicrograph of part of the cleavage surface of sample 70. The crack velocity was about 600 cm/sec (0.001 V_S). The dislocation density is much greater than that shown in Figure 22, which shows part of the surface of a crystal where crack velocity was about 7.8x10^4 cm/sec. It was also possible to detect points on the cleavage surfaces where the crack hesitated. In the crystals of regular geometry (height = 1.2 cm) such points of hesitation were found only at the front of the crystal near the point of knife impact. However in the crystals with reduced height (height = 0.8 cm) crack stoppage also occurred in the rear of the crystal. This indicated that the tendency for plastic deformation was greater in

the narrow crystals. Figure 25 shows a point of hesitation in a sample of regular geometry. Behind the crack front are rows of etch pits lying parallel to the direction of cleavage. This is a feature resulting from plane stress conditions at the crack tip (30). Figure 26 shows a point of crack stoppage in a crystal with reduced height. The point of hesitation is approximately 2/3 of the crystal length away from the front. The crack velocity in this region could not be determined since the oscilloscope trace sweep was completed before the next deflection stripe beyond the region was broken. A velocity of 640 cm/sec was taken as an upper limit. This value is probably too high since the dislocation etch pit density is even greater than that shown in Figure 24.

Figures 27-29 show parts of the cleavage surfaces of several Kyropoulos crystals. They are presented mainly to show the great difference in perfection between the Stockbarger crystals and the Kyropoulos crystals. This poor quality of the Kyropoulos crystals was a major factor in the great variance in crack speeds. Figure 27 shows the cleavage surface of a crystal cleaved at 100 °C in nitrogen. Figure 28 shows some of the cleavage step patterns that were formed. The mechanisms of step formation have been described by several workers (53,80,81), but Gilman (53) has given a particularly good explanation. The descriptions of step formation mentioned here are largely his. Figure 28A illustrates the effects of 2 different screw dislocation configurations on

Figure 25. Photomicrograph of part of cleavage surface of a crystal cleaved in air, 150X. Direction of cleavage is from bottom to top

Figure 26. Photomicrograph of part of cleavage surface of a crystal with reduced height cleaved in air, 60X. Direction of cleavage is from bottom to top

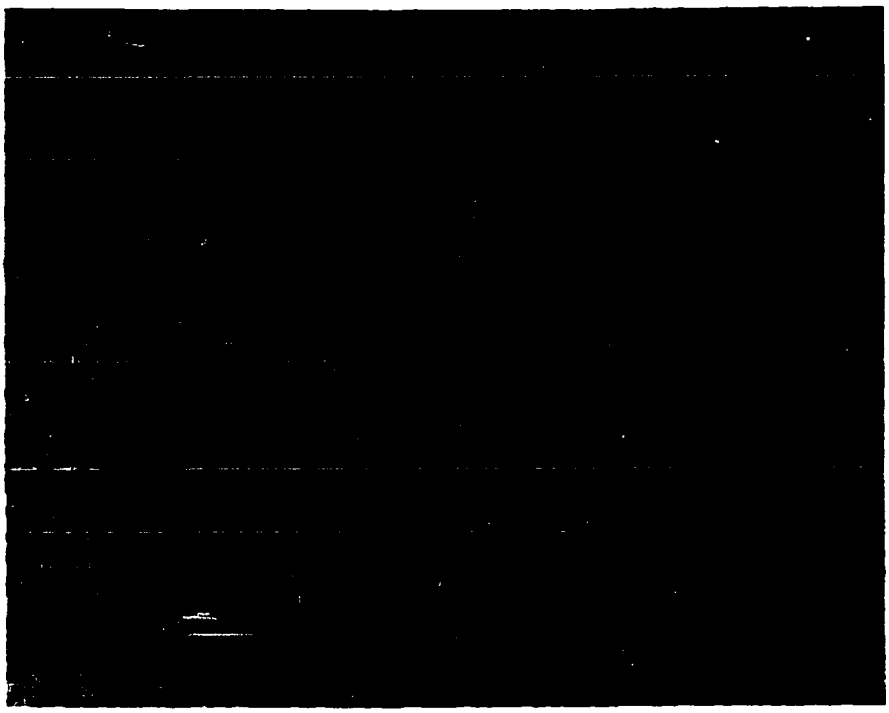

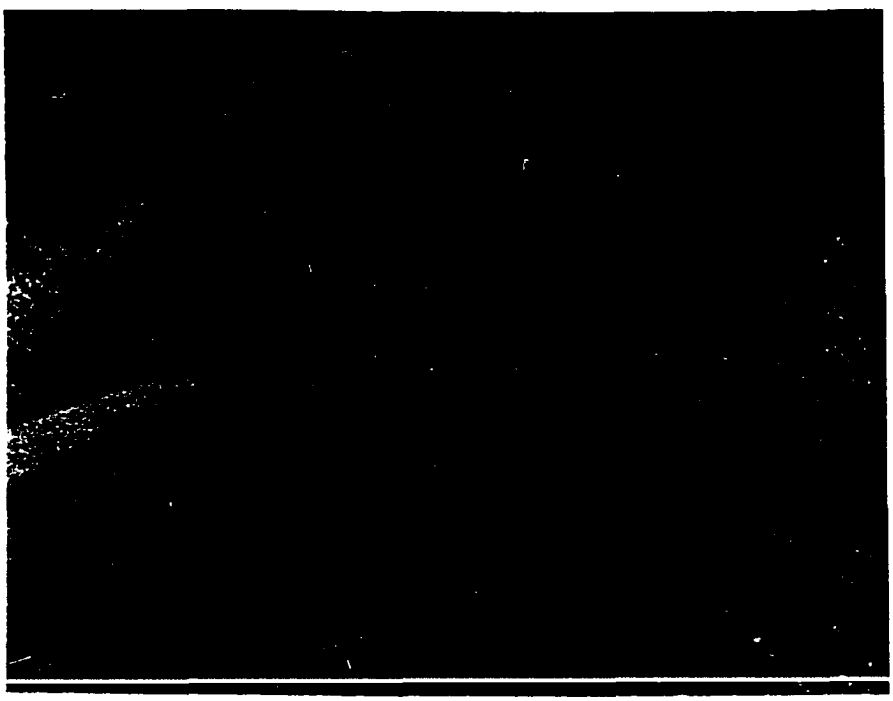

Figure 27A. Photomicrograph of part of cleavage surface of a Kyropoulos-grown NaCl crystal, 60X, reduced 50% in reproduction. Area shown is 20.0 mm from front of crystal. Arrow shows direction of cleavage

Figure 27B. Photomicrograph of a section of the cleavage surface of the same crystal, 60X, reduced 50% in reproduction. Area shown is 13.0 mm from front of crystal. Arrow shows direction of cleavage

Figure 27C. Photomicrograph of a section of the cleavage surface of the same crystal, 60X, reduced 50% in reproduction. Area shown is 3.5 mm from front of crystal. Arrow shows direction of cleavage

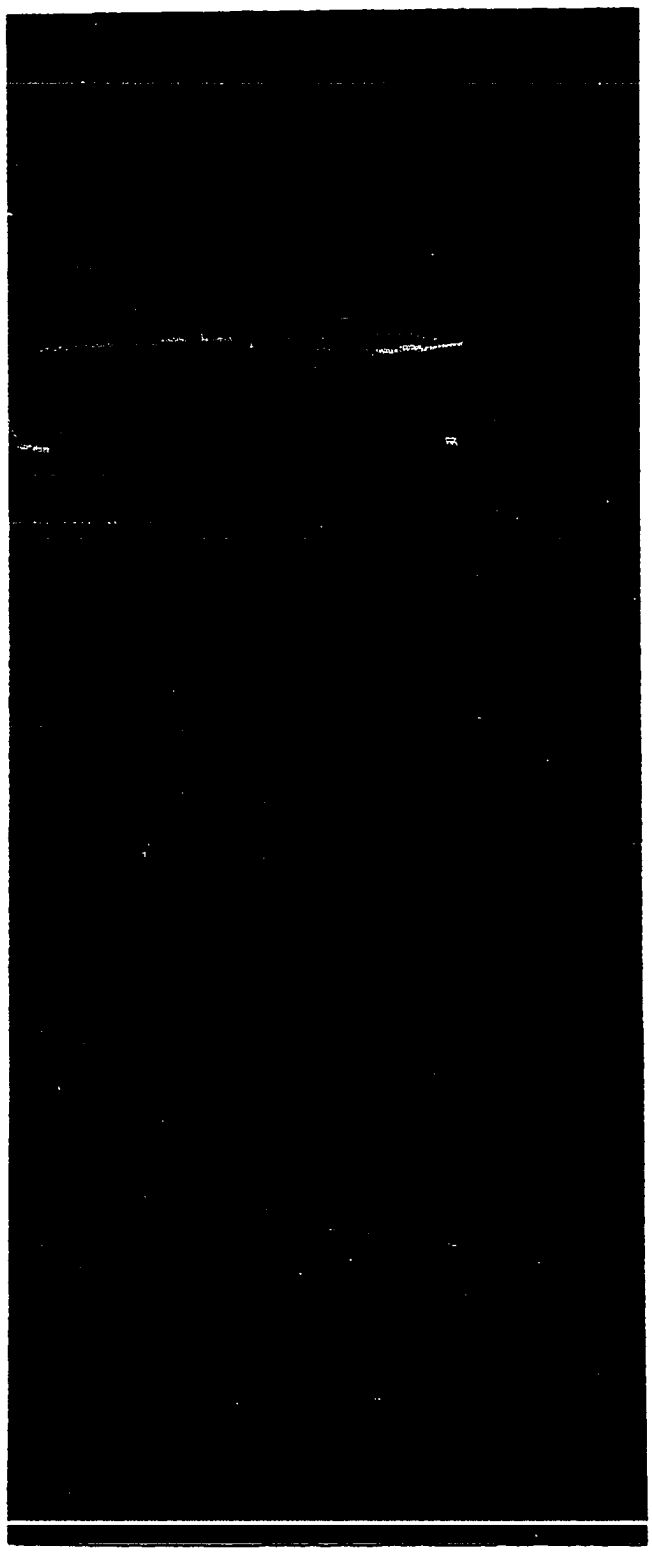

Figure 28A. Photomicrograph of part of cleavage surface of a Kyropoulos-grown NaCl crystal cleaved in nitrogen, 60X, reduced 50% in reproduction. Arrow shows direction of cleavage

Figure 28B. Photomicrograph of part of cleavage surface of a Kyropoulos-grown NaCl crystal cleaved in argon, 60X, reduced 50% in reproduction. Arrow shows direction of cleavage

Figure 28C. Photomicrograph of part of cleavage surface of a Kyropoulos-grown NaCl crystal cleaved in nitrogen, 60X, reduced 50% in reproduction. Arrow shows direction of cleavage

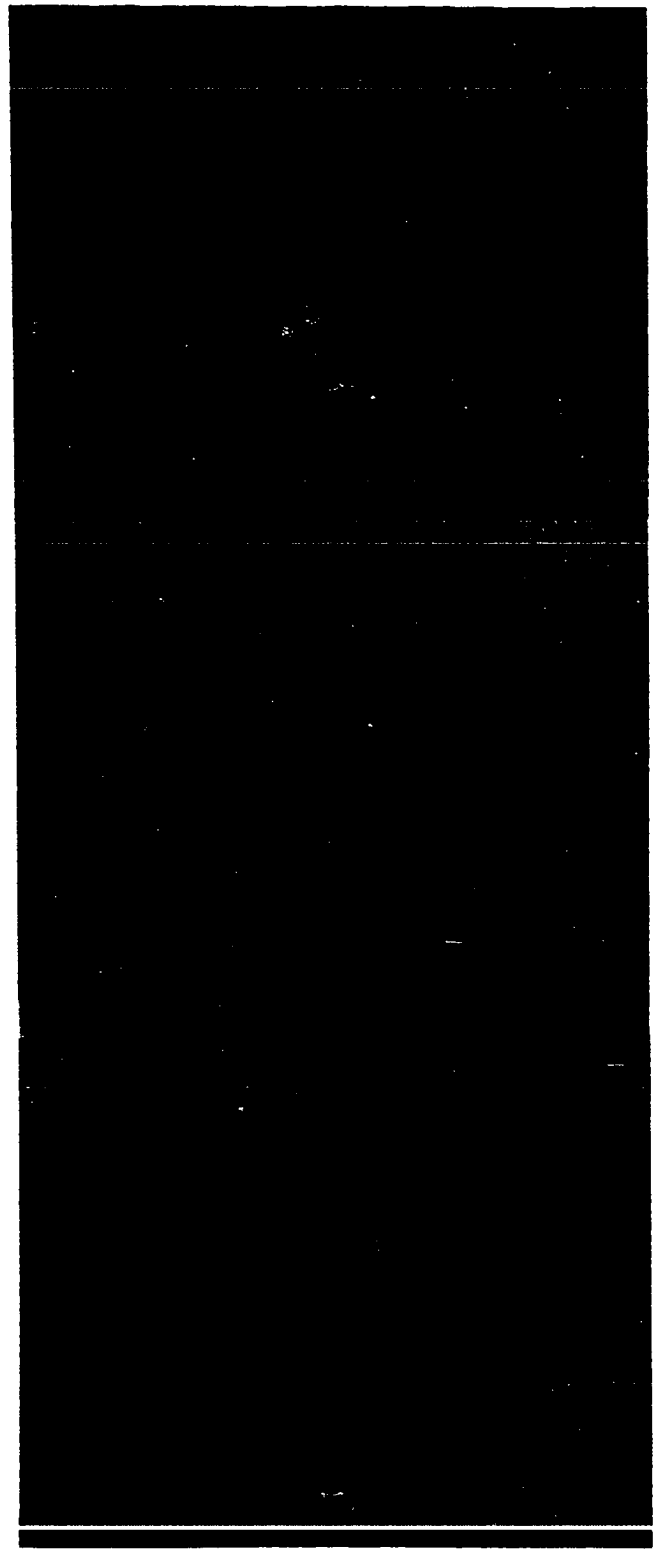

Figure 29A. Photomicrograph of part of cleavage surface of a Kyropoulos-grown NaCl crystal, unetched, 60X, enlarged 10% in reproduction. Arrow shows direction of cleavage

Figure 29B. Photomicrograph of the same surface shown in Figure 29A, etched, 60X, enlarged 10% in reproduction

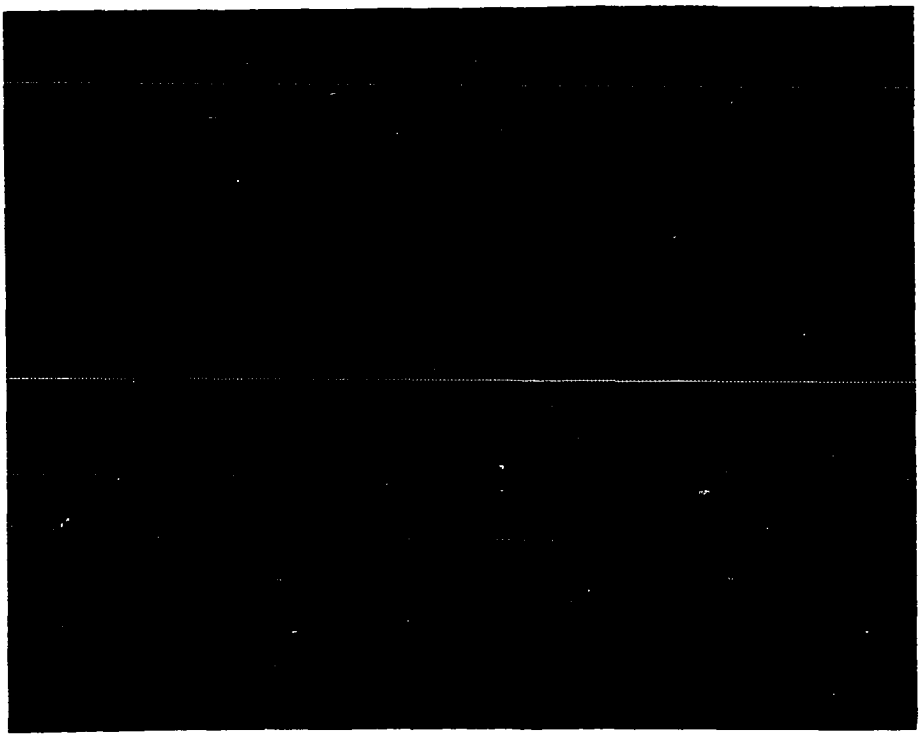

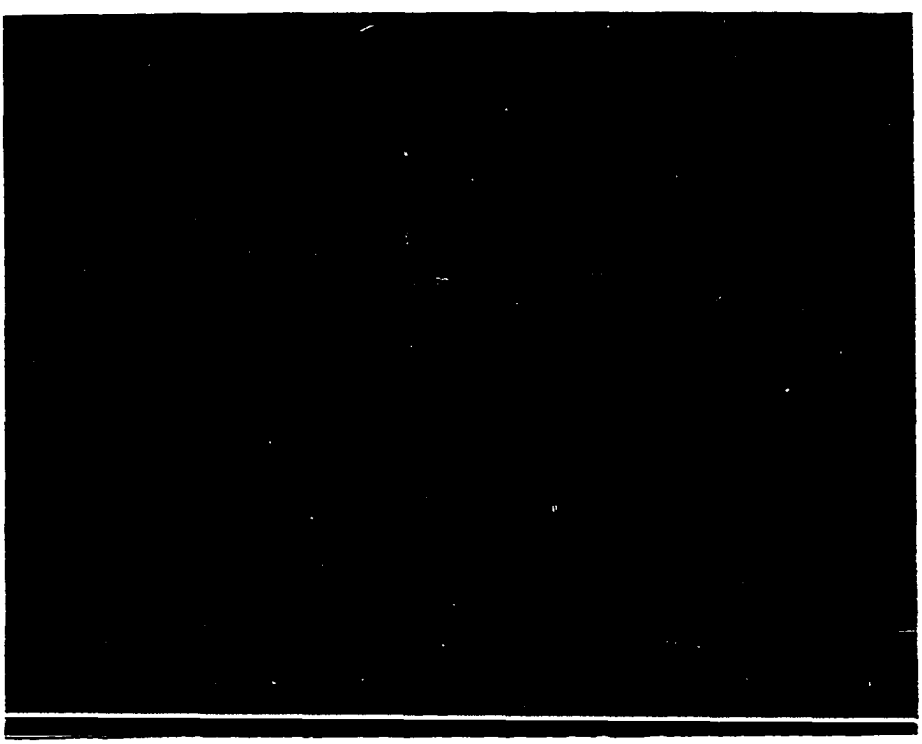

fracture surface morphology. In the left upper portion of the photograph are many vees pointing in the direction of crack propagation. These were formed when the crack intersected closely spaced pairs of right and left handed screw dislocations, creating pairs of steps which ran together. Beyond the vees is the so-called "river pattern". This was formed when the crack intersected a group of screw dislocations which were all right or left handed (twist boundary).

Figures 28B and 28C are examples of the cleavage step patterns formed when a crack intersects sub-boundaries. Figure 28B shows a tilt and a mixed tilt-twist boundary. In the upper left corner of the photograph are 2 simple tilt boundaries. The cleavage steps emanating from the lower portion of the second boundary indicate that this is a tilt-twist boundary (80). Figure 28C also shows a tilt-twist boundary.

It was generally observed that cleavage steps were formed by interaction of screw dislocations with the crack. Gilman (53) has shown that local concentrations of edge dislocations usually have no effect on step formation. However, if the concentration is uniformly high, a characteristically ragged type of step is formed which has no relation to crystallographic directions. The exact reason such steps are formed is unknown. A possible cause may be the presence of locally high stresses in a strain hardened region of the crystal. Figures

29A, B show the steps produced by edge dislocations. Figure 29A shows the surface prior to etching and Figure 29B shows the same surface after it was etched.

CONCLUSIONS

(1) The cleavage energy of NaCl in this study was typically 100-400 ergs/cm^2.

(2) Cleavage of NaCl in a carbon dioxide atmosphere causes the cleavage energy to be greater than if testing is performed in argon or nitrogen.

(3) Cleavage of NaCl in air can produce erratic results, especially if other test conditions are conducive to plastic flow. The scatter in data is not directly attributable to atmospheric humidity or to thunderstorm activity.

(4) For crack velocities greater than about 1×10^4 cm/sec, variations in velocity do not significantly affect the density of dislocations produced by cleavage.

(5) Cleavage crack-dislocation interaction in NaCl persists at room temperature for crack velocities at least as great as 9×10^4 cm/sec.

(6) Large doses of γ-irradiation have only a slight effect on crack velocity and cleavage energy if all other test conditions favor high crack velocity.

(7) Increasing the test temperature from 22°C to 250°C has negligible effect on cleavage energy if all other test conditions favor high crack velocity.

(8) Equation 35 can be used to calculate the cleavage energy of double cantilevered crystals when shear contributes significantly to the cleavage energy.

LITERATURE CITED

1. J. J. Gilman, "Propagation of Cleavage Cracks in Crystals," J. Appl. Phys., 27 [11] 1262-69 (1956).

2. S. J. Burns and W. W. Webb, "Fracture Surface Energies and Dislocation Processes During Dynamical Cleavage of LiF. I. Theory," J. Appl. Phys., 41 [5] 2078-85 (1970).

3. S. J. Burns and W. W. Webb, "Fracture Surface Energies and Dislocation Processes During Dynamical Cleavage of LiF. II. Experiments," J. Appl. Phys., 41 [5] 2086-99 (1970).

4. J. J. Gilman, "Direct Measurements of the Surface Energies of Crystals," J. Appl. Phys., 31 [12] 2209-18 (1960).

5. W. D. Kingery, Introduction to Ceramics; p. 191. John Wiley and Sons, Inc., New York, 1960.

6. J. C. Duga, "Surface Energy of Ceramic Materials," Tech. Rept. DCIC 69-2, June 1969; U.S. Clearinghouse Fed. Sci. Tech. Inform., AD, 1969, AD-691-019, 85 pp.

7. V. D. Kuznetsov, Surface Energy of Solids. Her Majesty's Stationery Office, London, 1957.

8. S. J. Gregg, "The Surface of Solids and Its Significance in the Laboratory," Silicated Ind., 25 [6] 283-88 (1960).

9. J. R. Partington, An Advanced Treatise on Physical Chemistry, Vol. 3. Longmans and Company, New York, 1949.

10. G. C. Benson, H. P. Schrieber, and F. Van Zeggeren, "An Experimental Determination of the Surface Enthalpy of Sodium Chloride," Can. J. Chem., 34 [11] 1553-56 (1956).

11. J. J. Bikerman, The Science of Adhesive Joints. Academic Press, New York, 1968.

12. R. J. Good, L. A. Girifalco, and G. Kraus, "A Theory for Estimation of Interfacial Energies. II. Application to Surface Dynamics of Teflon and Graphite," J. Phys. Chem., 62 [11] 1418-21 (1958).

13. G. R. Lester, "Contact Angles of Liquids at Deformable Solid Surfaces," J. Colloid Sci., 16 [4] 315-26 (1961).

14. L. G. Eberhart, "The Critical Surface Tension of Sapphire," J. Phys. Chem., 71 [1]] 4125-26 (1967).

15. R. J. Good and L. A. Girifalco, "A Theory for Estimation of Surface and Interfacial Energies. III. Estimation of Surface Energies of Solids from Contact Angle Data," J. Phys. Chem., 64 [5] 561-65 (1960).

16. J. N. S. Kwong, J. T. Adams, Jr., J. F. Johnson, and E. L. Piret, "Energy-New Surface Relationship in Crushing. I," Chem. Eng. Progr., 45 [8] 508-16 (1949).

17. J. T. Adams, J. F. Johnson, and E. L. Piret, "Energy-New Surface Relationship in the Crushing of Solids. II," Chem. Eng. Progr., 45 [11] 655-60 (1949).

18. J. F. Johnson, J. Axelson, and E. L. Piret, "Energy-New Surface Relationship in the Crushing of Solids. III," Chem. Eng. Progr., 45 [12] 708-15 (1949).

19. H. Udin, A. J. Shaler, and John Wulff, "The Surface Tension of Copper," Trans. AIME, 185 [2] 186-90 (1949).

20. J. W. Obreimoff, "The Splitting Strength of Mica," Proc. Roy. Soc., London, Ser. A, 127 [5] 290-97 (1930).

21. P. J. Bryant, L. H. Taylor, and P. L. Gutshall; pp. 21-26 in Transactions of the Tenth National Vacuum Society. Edited by George H. Bancroft. The Macmillan Company, New York, 1963.

22. F. P. Bowden; pp. 1-25 in Fundamentals of Gas-Surface Interactions. Edited by H. Saltsburg, J. N. Smith, and M. Rogers. Academic Press, New York, 1967.

23. R. J. Jaccodine, "Surface Energy of Germanium and Silicon," J. Electrochem. Soc., 110 [6] 524-26 (1963).

24. P. L. Gutshall and G. E. Gross, "Surface Energy of NaCl and MgO in Vacuum," J. Appl. Phys., 36 [8] 2459-60 (1965).

25. D. A. Shockey and G. W. Groves, "Effect of Water on Toughness of MgO Crystals," J. Am. Ceram. Soc., 51 [6] 299-303 (1968).

26. D. A. Shockey and G. W. Groves, "Origin of Water-Induced Toughening in MgO Crystals," J. Am. Ceram. Soc., 52 [2] 82-85 (1969).

27. W. F. Brace and J. B. Walsh, "Some Direct Measurements of the Surface Energy of Quartz and Orthoclase," Am. Mineralogist, 47 [9] 1111-22 (1962).

28. S. M. Wiederhorn, "Moisture Assisted Crack Growth in Ceramics," Intern. J. Fracture Mech., 4 [2] 171-77 (1968).

29. G. E. Gross and P. L. Gutshall, "Evidence of a Dislocation Feeding Mechanism for Crack Reinitiation in F-Colored NaCl," Intern. J. Fracture Mech., 1 [2] 131-34 (1965).

30. S. M. Wiederhorn, R. L. Moses, and B. L. Bean, "Plastic Deformation and the Fracture Surface Energy of Sodium Chloride," J. Am. Ceram. Soc., 53 [1] 18-23 (1970).

31. A. S. Tetelman and A. J. McEvily, Jr., Fracture of Structural Metals, John Wiley and Sons, Inc., New York, 1960.

32. J. J. Gilman, "Nucleation of Dislocation Loops by Cracks in Crystals," Trans. AIME, 209 [4] 449-54 (1957).

33. S. M. Wiederhorn, A. M. Shorb, and R. L. Moses, "Critical Analysis of the Theory of the Double Cantilever Method of Measuring Fracture Surface Energies," J. Appl. Phys., 39 [3] 1569-72 (1968).

34. A. R. C. Westwood and T. T. Hitch, "Surface Energy of {100} Potassium Chloride," J. Appl. Phys., 34 [10] 3085-89 (1963).

35. A. E. Glauberman, "The Theory of Surface Energy of Heteropolar Crystals," Zh. Fizi. Khim., 23 [2] 124-130 (1949).

36. A. R. C. Westwood and D. L. Goldheim, "Cleavage Surface Energy of {100} Magnesium Oxide," J. Appl. Phys., 34 [11] 3335-39 (1963).

37. J. E. Lennard-Jones and P. A. Taylor, "Some Theoretical Calculations of the Physical Properties of Certain Crystals," Proc. Roy. Soc., London, Ser. A, 109 [11] 476-507 (1925).

38. J. P. Berry, "Determination of Fracture Surface Energies by the Cleavage Technique," J. Appl. Phys., 34 [1] 62-68 (1963).

39. N. F. Mott, "Fracture of Metals: Theoretical Considerations," Engineering, 165 [1] 16-18 (1948).

40. J. J. Benbow and F. C. Roesler, "Experiments on Controlled Fractures," Proc. Phys. Soc., London, Sect. B, 70 [2] 201-211 (1957).

41. N. L. Svenson, "The Variation of Fracture Energy of Brittle Plastics with Temperature," Proc. Phys. Soc., London, 77 [4] 876-84 (1961).

42. J. J. Benbow, "Stable Crack Propagation in Plastics," Proc. Phys. Soc., London, 78 [11] 970-78 (1961).

43. G. E. Gross and P. L. Gutshall, "A Study of the Physical Basis of Mechanical Properties of Ceramics," Tech. Rept. AFML-TR-66-66, July 1966; U.S. Clearinghouse Fed. Sci. Tech. Inform., AD, 1966, AD486701, 48 pp.

44. G. E. Gross and P. L. Gutshall, "A Study of the Physical Basis of Mechanical Properties of Ceramics," Tech. Rept. AFML-TR-65-97, July 1965; U.S. Clearing House Fed. Sci. Tech. Inform., AD, 1965, AD475010, 22 pp.

45. Peter P. Gillis, "Surface Energy Determinations by Cleavage," J. Appl. Phys., 71 [12] 4125-26 (1967).

46. J. P. Berry, "Some Kinetic Considerations of the Griffith Criterion for Fracture. I," J. Mech. Phys. Solids, 8 [8] 194-206 (1960).

47. J. P. Berry, "Some Kinetic Considerations of the Griffith Criterion for Fracture. II," J. Mech. Phys. Solids, 8 [8] 207-216 (1960).

48. C. T. Forwood, "The Work of Fracture in Crystals of Sodium Chloride Containing Cavities," Phil. Mag., 17 [4] 657-667 (1968).

49. J. J. Gilman, C. Knudsen, and W. P. Walsh, "Cleavage Cracks and Dislocations in LiF Crystals," J. Appl. Phys., 29 [4] 601-07 (1958).

50. Peter P. Gillis and J. J. Gilman, "Double-Cantilever Mode of Crack Propagation,: J. Appl. Phys., 35 [3] 647-58 (1964).

51. S. J. Burns, "Fracture Surface Energies from Dynamical Cleavage Analysis," Phil. Mag., 25 [1] 131-138 (1972).

52. V. M. Finkel', A. M. Savel'ev, I. N. Voronov, and A. S. Khmelevshii, "Damping of High Velocity Cracks by Slip Bands," Soviet Phys.-Solid State, 12 [1] 204-06 (1970).

53. J. J. Gilman, "Creation of Cleavage Steps by Dislocation," Trans. AIME, 212 [6] 310-15 (1958).

54. J. Washburn, A. E. Gorum, and E. R. Parker, "Cause of Cleavage Fractures in Ductile Materials," Trans. AIME, 215 [4] 230-37 (1959).

55. A. J. Forty, "The Generation of Dislocations During Cleavage," Proc. Roy. Soc., London, Ser. A, 242 [11] 392-99 (1957).

56. S. J. Burns and W. W. Webb, "Plastic Deformation During Cleavage of LiF," Trans. AIME, 236 [8] 1165-74 (1966).

57. J. J. Gilman, "Cleavage Steps on Zinc Monocrystals: Their Origins and Patterns," Trans. AIME, 203 [11] 1252-55 (1955).

58. A. V. Granato; pp. 117-157 in Dislocation Dyanmics. Edited by A. R. Rosenfield, G. T. Hahn, A. L. Bement, Jr., and R. L. Jaffee. McGraw-Hill Book Company, New York, 1968.

59. R. J. Stokes, T. L. Johnston, and C. H. Li, "The Relationship between Plastic Flow and Fracture in Magnesium Oxide Single Crystals," Phil. Mag., 4 [8] 920-32 (1959).

60. V. M. Finkel', A. M. Savel'ev, L. B. Zuev, S. V. Serebryakov, Yu M. Kurobov, and I. B. Zueva," The Interaction of a Crack with Dislocation Boundaries," Soviet Phys.-Solid State, 7 [5] 1130-37 (1965).

61. A. E. Gorum, E. R. Parker, and J. A. Pask, "Effect of Surface Conditions on Room Temperature Ductility of Ionic Crystals," J. Am. Ceram. Soc., 41 [5] 161-64 (1958).

62. R. C. Robbins, R. D. Cadle, D. L. Elkhart, "The Conversion of Sodium Chloride to Hydrogen Chloride in the Atmosphere," J. Meteorol., 16 [2] 53-56 (1959).

63. E. S. Machlin and G. T. Murray, "Role of Surfaces in Plastic Flow of NaCl Single Crystals," J. Appl. Phys., 30 [11] 1731-32 (1959).

64. D. A. Otterson, "Influence of Room Temperature Atmospheric Reaction Products on the Ductility of NaCl," J. Chem. Phys., 38 [7] 1481-86 (1963).

65. R. J. Stokes, T. L. Johnston, and C. H. Li, "Environmental Effects on the Mechanical Properties of Ionic

Solids with Particular Reference to the Joffe Effect," Trans. AIME, 218 [8] 655-62 (1960).

66. W. H. Class, E. S. Machlin, and G. T. Murray, "Embrittlement of NaCl by Surface Compound Formation," Trans. AIME, 221 [8] 769-75 (1961).

67. G. T. Murray, "Brittle-Ductile Transition Temperature in Ionic Crystals," J. Am. Ceram. Soc., 43 [6] 330-34 (1960).

68. E. Aerts and W. Dekeyser, "Gases in Rocksalt and the Joffe Effect," Acta Met., 4 [5] 557-58 (1956).

69. A. Joffe, The Physics of Crystals. McGraw-Hill Book Co., Inc., New York, 1928.

70. F. I. Metz and R. A. Lad, "The Effect of Substrate on the Crystallization of Metallic Films," J. Phys. Chem., 60 [3] 277-80 (1960).

71. R. A. Lad, "Crack Formation in Sodium Chloride Single Crystal Surfaces," J. Appl. Phys., 23 [7] 800-01 (1952).

72. C. A. Stearns, A. E. Pack, R. A. Lad, "Factors Affecting the Ductility and Strength of NaCl Single Crystals Tested in Flexure," J. Appl. Phys., 31 [2] 231-34 (1960).

73. A. R. C. Westwood and M. H. Kamdar, "Concerning Liquid Metal Embrittlement, Particularly of Zinc Monocrystals by Mercury," Phil. Mag., 8 [5] 787-804 (1963).

74. S. A. Long, "Effects of Grain Boundary Orientation on the Room Temperature Ductility of Sodium Chloride," M.S. Thesis, Iowa State University of Science and Technology, Ames, Iowa, 1962.

75. P. R. Moran, "Dislocation Etch Techniques for Some Alkali Halide Crystals," J. Appl. Phys., 29 [12] 1768-69 (1958).

76. Gene Simmons and Herbert Wang, Single Crystal Elastic Constants and Calculated Aggregate Properties, A Handbook, p. 90. The M.I.T. Press, Cambridge, Mass., 1971.

77. D. K. Roberts and A. A. Wells, "The Velocity of Brittle Fracture," Engineering, 178 [12] 820-821 (1954).

78. S. M. Wiederhorn, "Fracture on (110) Planes in LiF," J. Appl. Phys., 34 [8] 2125-34 (1963).

79. G. E. Gross and P. L. Gutshall, "A Study of the Physical Basis of Mechanical Properties of Ceramics," Tech. Rept. ASD-TDR-63-605, Pt. II. April 1964, U.S. Clearinghouse Fed. Sci. Tech. Inform., AD, 1964, AD606963, 30 pp.

80. P. B. Hirsch, "Mosaic Structure," Progr. Metal Phys., 6 236-339 (1956).

81. J. A. Kies, A. M. Sullivan, and G. R. Irwin, "Interpretation of Fracture Markings," J. Appl. Phys., 21 [7] 716-720 (1950).

APPENDIX A. DIMENSIONS OF CLEAVAGE SPECIMENS

Sample No.	Height 1	Height 2	Width	Total length
Specimens cleaved at room temperature in nitrogen				
1	0.592 cm	0.580 cm	0.290 cm	2.090 cm
2	0.625	0.507	0.312	2.000
3	0.674	0.538	0.277	1.940
9	0.646	0.626	0.281	2.001
15	0.626	0.604	0.478	1.962
Specimens cleaved at 50°C in nitrogen				
14	0.685 cm	0.626 cm	0.476 cm	2.117 cm
16	0.650	0.604	0.304	2.104
18	0.672	0.628	0.315	2.060
20	0.648	0.614	0.276	2.110
26	0.680	0.571	0.347	2.150
33	0.659	0.553	0.347	2.020
77	0.663	0.610	0.508	2.090
Specimens cleaved at 100°C in nitrogen				
4	0.696 cm	0.606 cm	0.253 cm	2.120 cm
5	0.621	0.597	0.286	2.120
12	0.672	0.574	0.289	1.973
17	0.669	0.613	0.302	2.140
19	0.689	0.601	0.436	2.126
Specimens cleaved at 150°C in nitrogen				
27	0.684 cm	0.570 cm	0.231 cm	2.020 cm
28	0.680	0.625	0.248	2.020
31	0.625	0.622	0.255	2.090
32	0.660	0.614	0.539	2.010
34	0.622	0.604	0.328	2.180
39	0.659	0.635	0.252	2.010
Specimens cleaved at 200°C in nitrogen				
48	0.674 cm	0.554 cm	0.424 cm	1.920 cm
49	0.764	0.550	0.384	1.950
50	0.641	0.641	0.477	2.090
52	0.721	0.609	0.478	1.990
59	0.701	0.584	0.504	2.000

Specimens cleaved at 250°C in nitrogen

60	0.644 cm	0.606 cm	0.544 cm	1.990 cm
61	0.690	0.659	0.506	2.020
62	0.694	0.635	0.551	1.880
63	0.586	0.528	0.497	1.930

Specimen cleaved at 300°C in nitrogen

78	0.700 cm	0.605 cm	0.446 cm	1.970 cm

Specimens cleaved in carbon dioxide

22	0.690 cm	0.675 cm	0.288 cm	1.986 cm
23	0.669	0.621	0.256	2.012
24	0.659	0.591	0.227	2.140
25	0.680	0.590	0.216	2.015
38	0.634	0.624	0.372	2.100

Irradiated specimens cleaved in nitrogen

53	0.778 cm	0.553 cm	0.468 cm	1.960 cm
54	0.724	0.534	0.409	1.940
55	0.666	0.664	0.357	1.970
57	0.562	0.550	0.310	2.010
58	0.669	0.649	0.413	2.150

Specimens cleaved in argon

41	0.637 cm	0.601 cm	0.350 cm	2.000 cm
42	0.650	0.575	0.552	1.940
43	0.674	0.614	0.546	2.040
44	0.666	0.633	0.574	1.940
45	0.683	0.564	0.492	1.950
46	0.756	0.594	0.468	1.910

Specimens (regular geometry) cleaved in air

29	0.610 cm	0.574 cm	0.240 cm	1.990 cm
30	0.656	0.565	0.212	1.960
35	0.730	0.672	0.482	2.080
37	0.656	0.579	0.371	2.050
40	0.650	0.649	0.332	2.080
76	0.652	0.648	0.304	2.090
36	0.692	0.659	0.390	2.080

Specimens (reduced height) cleaved in air

64	0.410 cm	0.396 cm	0.370 cm	1.910 cm
65	0.423	0.343	0.296	1.910
66	0.447	0.392	0.438	1.850
67	0.365	0.348	0.391	2.090
68	0.413	0.356	0.396	1.780
69	0.386	0.337	0.393	2.000
70	0.404	0.339	0.318	1.950
71	0.398	0.331	0.317	1.950
72	0.457	0.309	0.303	1.800
73	0.447	0.349	0.498	1.930

APPENDIX B. CUMULATIVE DISTANCES BETWEEN DEFLECTION STRIPES

Remarks	Specimens cleaved at room temperature in nitrogen				
Sample No.	1	2	3	9	15
	Cumulative distance between deflection stripes (cm)				
Stripe No.					
Trigger	0.110*	0.100	0.090	0.120	0.240
1	0.270	0.270	0.240	0.440	0.400
2	0.430	0.420	0.400	0.600	0.550
3	0.590	0.580	0.560	0.790	0.720
4	0.750	0.740	0.710	1.090	0.880
5	0.910	0.900	0.870	1.250	1.040
6	1.070	1.060	1.030	1.410	1.200
7	1.240	1.220	1.200	1.580	1.360
8	1.390	1.380	1.360	1.730	1.520
9	1.550	1.540	1.510	1.880	1.680
10	1.720	1.700	1.670		1.830
11	1.880	1.860	1.840		
12	2.010				

Remarks	Specimens cleaved at 50°C in nitrogen						
Sample No.	14	16	18	20	26	33	77
	Cumulative distance between deflection stripes (cm)						
Stripe No.							
Trigger	0.270*	0.240	0.270	0.290	0.280	0.260	0.290
1	0.420	0.410	0.430	0.440	0.440	0.410	0.440
2	0.580	0.570	0.580	0.600	0.600	0.570	0.600
3	0.740	0.720	0.740	0.770	0.760	0.730	0.760
4	0.900	0.880	0.910	0.930	0.920	0.890	0.920
5	1.070	1.040	1.070	1.090	1.090	1.040	1.080
6	1.230	1.200	1.230	1.250	1.260	1.210	1.240
7	1.380	1.360	1.390	1.400	1.410	1.370	1.410
8	1.540	1.510	1.550	1.570	1.580	1.530	1.570
9	1.700	1.660	1.710	1.720	1.740	1.690	1.730
10	1.860	1.830	1.860	1.870	1.890	1.850	1.880
11	2.020	1.990		2.040	2.050	2.010	2.040
12							

*The front of the crystal is at 0.000 cm.

Remarks	Specimens cleaved at 100°C in nitrogen				
Sample No.	4	5	12	17	19
Stripe No.	Cumulative distance between deflection stripes (cm)				
Trigger	0.090*	0.120	0.440	0.290	0.280
1	0.260	0.290	0.600	0.340	0.340
2	0.410	0.440	0.760	0.510	0.490
3	0.570	0.600	1.080	0.670	0.650
4	0.730	0.770	1.240	0.930	0.810
5	0.900	0.930	1.390	1.090	0.970
6	1.050	1.080	1.560	1.260	1.130
7	1.220	1.250	1.710	1.410	1.300
8	1.380	1.410	1.860	1.570	1.460
9	1.540	1.570		1.730	1.510
10	1.700	1.720		1.880	1.770
11	1.850	1.870		2.040	1.930
12	2.010	2.040			

Remarks	Specimens cleaved at 150°C in nitrogen					
Sample No.	27	28	31	32	34	39
Stripe No.	Cumulative distance between deflection stripes (cm)					
Trigger	0.340*	0.320	0.280	0.260	0.340	0.300
1	0.490	0.480	0.430	0.320	0.490	0.450
2	0.650	0.630	0.590	0.480	0.640	0.620
3	0.810	0.800	0.750	0.630	0.800	0.780
4	0.980	0.960	0.910	0.800	0.950	0.950
5	1.300	1.120	1.070	0.960	1.120	1.100
6	1.450	1.280	1.230	1.130	1.280	1.270
7	1.610	1.440	1.390	1.280	1.450	1.430
8	1.940	1.600	1.560	1.440	1.600	1.590
9		1.760	1.710	1.600	1.760	1.740
10		1.930	1.870	1.750	1.920	1.900
11			2.030		2.090	
12						

Remarks: Specimens cleaved at 200°C in nitrogen

Sample No.	48	49	50	52	59
Stripe No.	Cumulative distance between deflection stripes (cm)				
Trigger	0.250*	0.430	0.280	0.250	0.270
1	0.410	0.590	0.430	0.400	0.430
2	0.560	0.740	0.590	0.560	0.580
3	0.730	0.910	0.750	0.730	0.750
4	0.880	1.060	0.910	0.890	0.910
5	1.040	1.230	1.080	1.050	1.070
6	1.200	1.390	1.240	1.200	1.240
7	1.370	1.540	1.390	1.370	1.390
8	1.530	1.700	1.560	1.530	1.560
9	1.700	1.860	1.710	1.690	1.710
10	1.860	1.950	1.860	1.850	1.860
11	1.920		2.030		
12					

Remarks: Specimens cleaved at 250°C in nitrogen

Sample No.	60	61	62	63
Stripe No.	Cumulative distance between deflection stripes (cm)			
Trigger	0.250*	0.310	0.260	0.250
1	0.400	0.460	0.410	0.410
2	0.570	0.620	0.570	0.570
3	0.730	0.780	0.730	0.730
4	0.880	0.940	0.890	0.890
5	1.040	1.100	1.050	1.050
6	1.200	1.270	1.220	1.210
7	1.370	1.430	1.370	1.360
8	1.540	1.580	1.540	1.520
9	1.700	1.740	1.690	1.680
10	1.850	1.890	1.840	1.850
11				
12				

Remarks	Specimen cleaved at 300°C in nitrogen
Sample No.	78
Stripe No.	Cumulative distance between deflection stripes (cm)
Trigger	0.280*
1	0.440
2	0.600
3	0.760
4	0.920
5	1.080
6	1.240
7	1.400
8	1.560
9	1.710
10	1.880
11	
12	

Remarks	Specimens cleaved in carbon dioxide				
Sample No.	22	23	24	25	38
Stripe No.	Cumulative distance between deflection stripes (cm)				
Trigger	0.290*	0.330	0.280	0.300	0.250
1	0.440	0.490	0.430	0.460	0.410
2	0.610	0.650	0.580	0.620	0.570
3	0.770	0.810	0.740	0.770	0.740
4	0.930	0.970	0.900	0.940	0.900
5	1.090	1.130	1.060	1.100	1.060
6	1.250	1.290	1.220	1.260	1.220
7	1.410	1.440	1.390	1.420	1.380
8	1.560	1.600	1.550	1.580	1.530
9	1.720	1.760	1.700	1.740	1.690
10	1.890	1.930	1.860	1.910	1.850
11			2.020		
12					

Remarks	Irradiated specimens cleaved in nitrogen				
Sample No.	53	54	55	57	58
Stripe No.	Cumulative distance between deflection stripes (cm)				
Trigger	0.270*	0.240	0.300	0.250	0.300
1	0.430	0.400	0.470	0.410	0.450
2	0.590	0.560	0.630	0.570	0.620
3	0.740	0.720	0.790	0.740	0.780
4	0.910	0.880	0.950	0.900	0.940
5	1.070	1.040	1.110	1.070	1.100
6	1.240	1.210	1.270	1.240	1.260
7	1.400	1.360	1.420	1.400	1.420
8	1.550	1.520	1.580	1.560	1.580
9	1.710	1.680	1.750	1.710	1.730
10	1.880	1.850	1.910	1.870	1.890
11					2.060
12					

Remarks	Specimens cleaved in argon					
Sample No.	41	42	43	44	45	46
Stripe No.	Cumulative distance between deflection stripes					
Trigger	0.290*	0.260	0.340	0.280	0.250	0.270
1	0.440	0.420	0.500	0.440	0.410	0.420
2	0.600	0.590	0.670	0.600	0.580	0.580
3	0.760	0.740	0.820	0.760	0.730	0.740
4	0.920	0.910	0.990	0.920	0.900	0.900
5	1.090	1.070	1.150	1.080	1.050	1.060
6	1.250	1.240	1.310	1.250	1.220	1.230
7	1.410	1.390	1.470	1.400	1.370	1.390
8	1.570	1.550	1.630	1.560	1.530	1.540
9	1.730	1.700	1.780	1.710	1.700	1.690
10	1.880	1.860	1.950	1.860	1.860	1.840
11						
12						

Remarks	Specimens (regular geometry) cleaved in air						
Sample No.	29	30	35	36	37	40	76
Stripe No.	Cumulative distance between deflection stripes (cm)						
Trigger	0.320*	0.260	0.270	0.250	0.330	0.230	0.280
1	0.470	0.420	0.430	0.400	0.490	0.390	0.440
2	0.630	0.580	0.590	0.550	0.650	0.550	0.590
3	0.790	0.740	0.750	0.710	0.810	0.710	0.750
4	0.950	0.900	0.910	0.870	0.980	0.870	0.920
5	1.110	1.220	1.070	1.030	1.130	1.040	1.080
6	1.280	1.380	1.230	1.200	1.300	1.190	1.240
7	1.440	1.530	1.390	1.350	1.450	1.350	1.400
8	1.590	1.870	1.550	1.510	1.610	1.510	1.560
9	1.750		1.710	1.670	1.760	1.670	1.720
10			1.860	1.830	1.920	1.830	1.870
11							
12							

Remarks	Specimens (reduced height) cleaved in air					
Sample No.	64	65	66	67	68	69
Stripe No.	Cumulative distance between deflection stripes (cm)					
Trigger	0.070*	0.060	0.090	0.120	0.130	0.120
1	0.220	0.210	0.250	0.280	0.290	0.280
2	0.370	0.360	0.420	0.440	0.450	0.440
3	0.530	0.520	0.580	0.590	0.610	0.590
4	0.680	0.670	0.730	0.750	0.760	0.750
5	0.850	0.840	0.890	0.920	0.930	0.920
6	1.010	1.000	1.050	1.080	1.090	1.080
7	1.170	1.160	1.210	1.240	1.250	1.240
8	1.330	1.320	1.380	1.400	1.400	1.400
9	1.490	1.480	1.540	1.560	1.560	1.570
10	1.640	1.630	1.700	1.720	1.720	1.720
11	1.810	1.780	1.850	1.870	1.780	1.870
12						

Remarks	Specimens (reduced height) cleaved in air			
Sample No.	70	71	72	73
Stripe No.	Cumulative distance between deflection stripes (cm)			
Trigger	0.120*	0.100	0.140	0.120
1	0.270	0.270	0.300	0.280
2	0.430	0.430	0.450	0.440
3	0.580	0.580	0.610	0.590
4	0.740	0.740	0.770	0.750
5	0.910	0.900	0.940	0.920
6	1.060	1.060	1.100	1.080
7	1.230	1.220	1.260	1.240
8	1.380	1.390	1.410	1.400
9	1.540	1.540	1.570	1.560
10	1.690	1.710	1.740	1.720
11	1.860	1.870		1.870
12				

APPENDIX C. CUMULATIVE TIMES FOR CRACK TRAVEL BETWEEN DEFLECTION STRIPES

Remarks: Specimens cleaved at room temperature in nitrogen

Sample No.	1	2	3	9	15
	Cumulative time for crack travel between deflection stripes				
Stripe No.					
Trigger					
1					
2					0.00
3	0.00*		0.00	0.00	1.27
4	1.84	0.00	1.41	3.68	3.43
5	4.22	2.06	3.52	5.53	5.33
6	6.07	5.10	5.15	7.21	7.28
7	8.23	7.58	7.10	9.05	9.18
8	10.39	9.80	8.89	10.90	10.75
9	12.24	11.15	10.78	12.69	12.32
10	13.43	13.05	12.62		14.27
11		14.41	17.32		
12					

Remarks: Specimens cleaved at 50°C in nitrogen

Sample No.	14	16	18	20	26	33	77
	Cumulative time for crack travel between deflection stripes						
Stripe No.							
Trigger							
1		0.00		0.00			
2		1.24	0.00	1.95	0.00	0.00	
3	0.00*	--	1.84	4.66	2.71	1.52	0.00
4	4.00	5.89	4.12	6.88	4.12	4.12	2.50
5	--	8.11	6.07	7.97	6.56	6.88	5.10
6	8.38	10.06	8.39	10.13	--	9.26	7.16
7	10.44	12.22	10.23	12.19	11.05	11.32	8.84
8	12.50	14.44	12.13	14.30	13.21	13.76	10.95
9	14.34	17.20	13.59	16.30	15.21	15.88	12.84
10	16.02	21.10	15.91	18.36	17.53		14.19
11	18.51	25.30		31.66	19.59		
12							

*Time is in microseconds. The zero time denotes the stripe at which time measurement began.

Remarks	Specimens cleaved at 100°C in nitrogen				
Sample No.	4	5	12	17	19
	Cumulative time for crack travel between deflection stripes				
Stripe No.					
Trigger					
1					
2					0.00
3	0.00*	0.00	0.00		1.52
4	2.33	1.73	7.30	0.00	3.58
5	4.61	3.79	9.57	2.06	5.75
6	6.61	5.85	11.52	4.27	7.81
7	8.89	8.13	13.74	6.43	10.09
8	11.11	10.79	15.85	8.59	12.15
9	13.33	12.47	18.50	10.65	14.04
10	15.39	14.74		12.65	16.42
11	17.45	19.07		16.59	17.89
12	25.10	23.46			

Remarks	Specimens cleaved at 150°C in nitrogen					
Sample No.	27	28	31	32	34	39
	Cumulative time for crack travel between deflection stripes					
Stripe No.						
Trigger						
1	0.00*	0.00		0.00	0.00	0.00
2	2.44	1.90	0.00	2.33	1.84	1.89
3	4.93	4.28	1.73	3.96	4.17	3.95
4	10.13	6.61	4.21	6.02	6.33	6.11
5	12.67	8.83	6.05	7.86	9.41	8.71
6	15.11	10.94	8.38	10.30	--	10.44
7	18.55	12.83	10.60	12.29	14.71	11.95
8	25.75	15.05	13.20	14.51	17.15	14.01
9		17.37	15.42	16.29	19.31	16.88
10		19.86	17.53	18.40	21.53	
11			23.43		25.05	
12						

Remarks	Specimens cleaved at 200°C in nitrogen				
Sample No.	48	49	50	52	59
	Cumulative time for crack travel between deflection stripes				
Stripe No.					
Trigger					
1			0.00	0.00	
2		0.00	1.24	1.89	0.00
3		2.30	--	3.89	1.68
4	0.00*	4.96	4.91	5.67	4.17
5	4.06	7.72	6.86	7.19	7.69
6	6.34	9.35	8.86	10.12	9.26
7	8.45	10.33	11.02	11.31	10.99
8	10.40	12.87	13.29	13.47	12.89
9	12.46	14.00	15.29	15.59	--
10	16.52		17.07	18.03	16.03
11					
12					

Remarks	Specimens cleaved at 250°C in nitrogen			
Sample No.	60	61	62	63
	Cumulative time for crack travel between deflection stripes			
Stripe No.				
Trigger				
1		0.00		
2		1.35		0.00
3	0.00*	3.08		1.35
4	4.50	5.02	0.00	3.19
5	9.26	--	2.54	5.46
6	11.86	9.02	4.33	7.30
7	14.52	11.24	6.87	9.24
8	18.79	13.08	8.38	11.13
9	21.99	15.14	10.66	13.13
10	27.34	17.52	12.88	15.67
11				
12				

Remarks	Specimen cleaved at 300°C in nitrogen
Sample No.	78
	Cumulative time for crack travel between deflection stripes
Stripe No.	
Trigger	
1	
2	
3	
4	
5	
6	0.00*
7	5.62
8	8.38
9	10.62
10	19.43
11	
12	

Remarks	Specimens cleaved in carbon dioxide				
Sample No.	22	23	24	25	38
	Cumulative time for crack travel between deflection stripes				
Stripe No.					
Trigger					
1	0.00*	0.00	0.00	0.00	0.00
2	2.00	1.63	1.73	1.68	1.62
3	--	3.69	3.83	3.58	3.51
4	--	--	6.10	6.34	5.46
5	9.05	7.69	8.37	7.74	7.41
6	11.00	9.75	11.56	9.74	9.84
7	13.16	--	13.72	11.58	11.90
8	15.32	13.38	16.04	13.42	13.63
9	--	15.11	18.14	15.70	15.30
10	20.04		20.36	17.65	16.97
11			22.96		
12					

Remarks	Irradiated specimens cleaved in nitrogen				
Sample No.	53	54	55	57	58
	Cumulative time for crack travel between deflection stripes				
Stripe No.					
Trigger					
1	0.00*	0.00	0.00	0.00	0.00
2	1.95	1.60	1.68	1.46	1.62
3	3.62	2.70	3.41	3.58	3.46
4	--	4.92	5.25	5.80	5.08
5	7.30	6.05	7.04	8.08	7.14
6	9.08	7.95	8.72	11.00	8.98
7	10.97	9.79	12.24	13.98	10.87
8	12.70	11.79		15.34	12.60
9	14.81	--		17.34	14.44
10		14.49		19.72	16.39
11		16.93			19.80
12					

Remarks	Specimens cleaved in argon					
Sample No.	41	42	43	44	45	46
	Cumulative time for crack travel between deflection stripes					
Stripe No.						
Trigger						
1	0.00*	0.00	0.00	0.00	0.00	
2	1.20	1.46	1.08	1.52	2.16	
3	2.88	3.03	--	2.93	3.84	
4	4.94	4.49	5.30	--	5.57	0.00
5	6.51	6.06	6.76	7.48	8.27	1.35
6	8.63	7.84	8.60	8.89		2.92
7	10.53	9.41	10.17	9.86		4.65
8	12.43	11.03	11.74	12.02		6.49
9	14.43	12.82	13.25	13.53		8.39
10	15.73	15.85		15.97		10.23
11						
12						

Remarks Specimens (regular geometry) cleaved in air

Sample No.	29	30	35	36	37	40	76
	Cumulative time for crack travel between deflection stripes						
Stripe No.							
Trigger							
1		0.00			0.00		0.00
2		1.90			1.19	0.00	1.68
3		4.39			2.97	1.62	3.79
4	0.00*	--	0.00	0.00	5.19	3.68	5.14
5	1.95	9.84	2.16	2.16	7.41	5.84	7.14
6	4.11	11.63	4.11	4.38	9.68	7.35	9.03
7	6.54	13.47	6.33	6.28	11.79	9.13	10.87
8	9.04	27.57	8.33	8.07	13.79	10.91	12.65
9	12.72		10.22	10.13	15.57	12.91	14.43
10			12.06	11.75	17.52	14.80	15.95
11				14.89			
12							

Remarks Specimens (reduced height) cleaved in air

Sample No.	64	65	66	67	68	69
	Cumulative time for crack travel between deflection stripes					
Stripe No.						
Trigger						
1			0.00		0.00	0.00
2		0.00	1.35	0.00	1.84	2.54
3		1.73	3.03	1.79	3.57	5.24
4		4.17	4.87	3.14	5.95	9.04
5	0.00*	6.82	7.25	5.79	8.65	15.90
6	3.08	--	9.57	8.87	11.29	500.00
7	5.62	12.77	12.00	10.66	15.45	
8	7.57	16.18	14.06	13.58	128.45	
9	10.33	17.91	16.60	17.54	--	
10	13.47	18.89		22.64	143.45	
11		30.19		32.48		
12						

Remarks	Specimens (reduced height) cleaved in air			
Sample No.	70	71	72	73
	Cumulative time for crack travel between deflection stripes			
Stripe No.				
Trigger				
1	0.00	0.00		
2	372.00	1.57		
3	472.00	4.01		
4	852.00	5.91		0.00
5		10.41	0.00	2.65
6		16.59	8.00	8.10
7		28.19	10.92	10.48
8		29.98	14.70	11.88
9		--	17.46	14.32
10		--	19.35	
11		865.98		
12				

APPENDIX D. CLEAVAGE ENERGY VALUES FOR INDIVIDUAL SPECIMENS

Sample No.	1	2	3	9	15	14
	Cleavage energy value in ergs/cm^2					
Stripe No.						
Trigger						
1						
2						
3					184	
4	352		264	268	291	461
5	376	257	311	219	261	336
6	285	330	237	184	231	295
7	236	274	200	153	199	252
8	213	220	169	137	162	211
9	177	157	152	123	135	176
10	130	130	131		124	164
11		102	161			
12						

Sample No.	16	18	20	26	33	77	4
	Cleavage energy value in ergs/cm^2						
Stripe No.							
Trigger							
1							
2	306		715				
3	518	469	754	844	261		
4	444	446	601	396	390	529	737
5	358	363	374	350	420	462	544
6	305	331	323	260	338	344	441
7	272	268	283	183	273	243	360
8	258	226	236	168	239	208	306
9	258	154	208	146	202	174	263
10	262	170	185			142	224
11			387				197
12							286

Sample No.	5	12	17	19	27	28
	Cleavage energy value in ergs/cm^2					
Stripe No.						
Trigger						
1						
2					863	710
3				288	701	625
4	278	295		327	1011	537
5	289	268	246	310	397	444
6	272	234	212	269	344	364
7	238	201	199	236	326	294
8	230	181	175	205	281	254
9	183	172	152	179		224
10	168		136	164		197
11	194		154	135		
12	201					

Sample No.	31	32	34	39	48	49
	Cleavage energy value in ergs/cm^2					
Stripe No.						
Trigger						
1						
2		1035	555	569		
3	337	639	531	526		346
4	407	485	455	436		385
5	308	378	435	436	828	333
6	278	331	319	323	430	237
7	241	284	280	249	278	166
8	216	247	235	216	208	156
9	194	204	200	213	163	119
10	167	145	189		178	
11	210					
12						

Sample No.	50	52	59	60	61	62	63
	Cleavage energy value in ergs/cm^2						
Stripe No.							
Trigger							
1							
2	279	752			332		
3	---	584	284		346		141
4	309	450	379	1725	330		159
5	264	333	484	1426	252	399	170
6	235	364	319	859	231	230	142
7	219	255	255	588	202	239	127
8	194	225	203	527	179	167	108
9	173	198	141	439	168	158	95
10	151	182		453		146	88
11							
12							

Sample No.	78	22	23	24	25	38	53
	Cleavage energy value in ergs/cm^2						
Stripe No.							
Trigger							
1							
2		807	465	656	507	541	749
3		---	480	598	497	468	553
4		---	---	529	518	412	---
5		614	350	452	356	351	340
6		487	301	454	300	329	268
7	953	410	---	359	248	281	197
8	469	359	216	306	208	237	176
9	314	273	181	264	188	196	
10	509			227	160	164	
11				205			
12							

Sample No.	54	55	57	58	41	42	43
	Cleavage energy value in ergs/cm^2						
Stripe No.							
Trigger							
1							
2	746	566	324	473	260	343	170
3	425	470	351	461	298	334	328
4	493	403	331	365	314	246	250
5	329	336	282	337	239	207	219
6	291	275	269	286	225	178	181
7	240	330	256	247	196	155	152
8	218		193	208	171	133	132
9	---		167	185	152	121	
10	141		148	164	127	127	
11	130			167			
12							

Sample No.	44	45	46	29	30	35	36
	Cleavage energy value in ergs/cm^2						
Stripe No.							
Trigger							
1							
2	472	792	126		658		
3	351	566	118		694		
4	---	399	118		---		
5	379	425	119	178	297	389	380
6	274		116	159	241	302	311
7	204		108	159	207	278	263
8	189			178	375	236	213
9	162					200	188
10	158					177	155
11							164
12							

Sample No.	37	40	76	64	65	66	67
	Cleavage energy value in ergs/cm^2						
Stripe No.							
Trigger							
1							
2	217		670			208	
3	271	401	640		189	197	148
4	283	421	391		219	180	80
5	283	368	347		182	169	87
6	249	288	295	175	---	147	93
7	225	240	250	123	144	128	70
8	193	203	212	84	131	102	66
9	167	180	181	77	98	91	68
10	145	158	155	75	72		75
11					129		108
12							

Sample No.	68	69	70	71	72	73
	Cleavage energy value in ergs/cm^2					
Stripe No.						
Trigger						
1						
2	301	514	$>1x10^6$	205		
3	200	415	$>1x10^6$	253		
4	193	392	$>1x10^6$	173		
5	165	488		226		125
6	141	243,161		285	91	261
7	148			457	90	167
8	6494			300	95	103
9	---			---	86	83
10	3464			---	68	
11				74,655		
12						

APPENDIX E. COMPUTER PROGRAM FOR SOLVING LAGRANGIAN EQUATION OF CRACK MOTION

```
C.....................................................................
C
C                              PROGRAM-SLEM
C
C
C   PURPOSE-SOLUTION TO A LAGRANGIAN EQUATION OF MOTION FOR CRACK
C        PROPAGATION IN A SPECIMEN WITH THE DOUBLE CANTILEVERED BEAM
C        CONFIGURATION
C
C
C   DESCRIPTION OF PARAMETERS
C
C     ALPHA-INVERSE OF THE BENDING STIFFNESS OF THE BEAMS
C     AK-A GEOMETRY CONSTANT FOR BEAMS, AK=3/2 FOR BEAMS OF RECTANGULAR
C        CROSS-SECTION
C     BETA-INVERSE OF THE SHEARING RESISTANCE OF THE BEAMS
C     CHANGE-INCREMENTAL FRACTION USED TO CHANGE CO
C     CO-VARIANT NUMBER USED AS THE EQUIVALENT OF HO IN CONS IN
C        SOLVING THE EQUATION
C     CONS-THE CONSTANT USED IN THIS FORM OF THE SOLUTION
C     DIFF-THE DIFFERENCE BETWEEN THE 2 CALCULATED ACCELERATIONS (X1,X2)
C     DUFF-STORED VALUE FROM PREVIOUS CALCULATION OF DIFF
C     ELAST-YOUNGS MODULUS
C     GAM-SPECIFIC CLEAVAGE ENERGY OF THE CRYSTAL, INCLUDES THE WORK
C        DONE IN PLASTIC FLOW
C     GSHEAR-SHEAR MODULUS
C     HEIGT1-HEIGHT OF ONE BEAM
C     HEIGT2-HEIGHT OF SECOND BEAM
C     HO-A MATHEMATICAL EXPRESSION FOR THE TOTAL HEIGHT OF BOTH BEAMS
C        DEPENDING ON THE MOMENTS OF INERTIA OF THE INDIVIDUAL BEAMS
C     L-LENGTH OF CRACK
C     LDOT-CRACK VELOCITY
C     RHO-DENSITY OF THE CRYSTAL
C     SHRBM-THE RATIO OF THE SHEAR TERM TO THE BENDING MOMENT TERM
C     SPEED-OUTWARD VELOCITY OF THE LOADED ENDS OF THE BEAMS
C     TTO-ELAPSED TIME OF CLEAVAGE
C     WIDTH-WIDTH OF BEAMS (CRYSTAL HALVES)
```

```
C      X1-ACCELERATION OF THE CRACK AS DERIVED FROM THE EQUATION OF
C         MOTION
C      X2-ACCELERATION OF THE CRACK AS DERIVED FROM A TRIAL SOLUTION
C
C
C    REMARKS-ALL CALCULATIONS ARE IN DOUBLE PRECISION WITH ACCURACY SET
C         BY INTEGER K AT 11 DECIMAL PLACE. THIS VALUE FOR K IS SOMEWHAT
C         ARBITRARY IN DETERMINING WHEN THE 2 ACCELERATIONS ARE EQUAL.
C
C
C    METHOD- THE HORNIER METHOD WAS USED. THIS INVOLVES DIVIDING THE
C         SOLUTION SET INTO 10 EQUAL PARTS AND CHECKING THE DIFFERENCE
C         BETWEEN THE CALCULATED ACCELERATIONS FOR A SIGN CHANGE AND
C         INCREMENTING AT 1/10 THE PREVIOUS STEP SIZE.
C
C.....................................................................
C
      IMPLICIT REAL*8(A-H,L,M,O-Z)
      DO 22 JM=1,10
C    THE NUMBER 10 IN THE PRECEDING STATEMENT IS THE NUMBER OF SETS OF
C         INPUT DATA.
      READ(5,31)ELAST,GSHEAR,AK,WIDTH,HEIGT1,HEIGT2,GAM,RHO,SPEED,CONS
   31 FORMAT(8E10.4)
      WRITE(6,52)WIDTH,HEIGT1,HEIGT2,GAM,RHO,SPEED
   52 FORMAT('0',8E14.7)
      IJ=HEIGT1+16.5
C    THE NUMBER HEIGT1+16.5 IN THE PRECEDING STATEMENT IS THE MAXIMUM
C         CRACK LENGTH FOR WHICH A SOLUTION WILL BE ATTEMPTED.
      DO 2 II=1,IJ
      IF(II.LE.25) GO TO 88
      L=(II-25)*2.0+24.0
      GO TO 92
   88 L=II
   92 L2=L*L
      L3=L**3
      L5=L**5
      L7=L**7
```

```
      L9=L**9
      L11=L**11
      L13=L**13
C
C   CALCULATION OF GEOMETRY COEFFICIENTS
C
      A1=WIDTH*HEIGT1
      A2=WIDTH*HEIGT2
      AI1=(WIDTH*HEIGT1**3)/12.0
      AI2=(WIDTH*HEIGT2**3)/12.0
      AO=(2.0*A1*A2)/(A1+A2)
      AIO=(2.0*AI1*AI2)/(AI1+AI2)
      HO=(AIO/AI1)**2*HEIGT1+(AIO/AI2)**2*HEIGT2
      ALPHA=1.0/(3.0*ELAST*AIO)
      ALPHA2=ALPHA**2
      ALPHA3=ALPHA**3
      BETA=AK/(AO*GSHEAR)
      BETA2=BETA**2
      BETA3=BETA**3
      C1STAR=(WIDTH/(6.0*ELAST)**2)*(HEIGT1*AI2**2+HEIGT2*AI1**2)/(AI1**
     12*AI2**2)
      C2STAR=(AK*WIDTH/(3.0*ELAST*GSHEAR))*(HEIGT1*AI2*A2+HEIGT2*AI1*A1)
     1/(AI1*A1*AI2*A2)
      C3STAR=((AK**2)*WIDTH/GSHEAR**2)*(HEIGT1*A2**2+HEIGT2*A1**2)/(A1**
     12*A2**2)
      ALPBET=(ALPHA*L3+BETA*L)
C
C   COEFFICIENTS OF THE 4 TERMS IN THE LAGRANGIAN EQUATION
C
      TERM4=(3.0*ALPHA*L**2+BETA)/ALPBET**2
      TERM2=((48.0/35.0)*C1STAR*L11*ALPHA2+(228.0/35.0)*C1STAR*ALPHA*BET
     1A*L9+(444.0/35.0)*C1STAR*L7*BETA2-(0.6)*C2STAR*L9*ALPHA2-3.4*C2STA
     2R*ALPHA*BETA*L7+1.6*C2STAR*L5*BETA2+2.0*C3STAR*L7*ALPHA2+(2.0/3.0)
     3*C3STAR*L3*BETA2)/ALPBET**4
      TERM3=((-24.0/35.0)*C1STAR*L13*ALPHA3-(174.0/35.0)*C1STAR*BETA*L11
     1*ALPHA2-(540.00/35.0)*C1STAR*ALPHA*L9*BETA2+(660.0/35.0)*C1STAR*L7
     2*BETA3+(18.0/20.0)*C2STAR*L11*ALPHA3+7.0*C2STAR*BETA*L9*ALPHA2-(21
```

```
     34.0/20.0)*C2STAR*ALPHA*L7*BETA2+0.8*C2STAR*L5*BETA3-5.0*C3STAR*ALP
     4HA3*L9+3.0*C3STAR*ALPHA2*BETA*L7-3.0*C3STAR*ALPHA*BETA2*L5-(1.0/3.
     50)*C3STAR*BETA3*L3)/ALPBET**5
      TERM42=TERM4/TERM2
      TERM32=TERM3/TERM2
      TERM12=1.0/TERM2
      SHRBM=BETA/(ALPHA*L2)
      WRITE(6,51)TERM42,TERM32,TERM12,SHRBM,L,HO
   51 FORMAT('0 TERM42= ',E14.7,' TERM32= ',E14.7,' TERM12= ',E14.7,' SH
     1EAR/BENDING = ',E14.7,' L= ',E14.7/ ' HO= ',E14.7)
C
C    INITIALIZATION OF TERMS USED IN THE ITERATIVE SOLUTION
C
      K=0
      DIFF= 1.0D 00
      DEFF=1.0D 00
      CHANGE=0.9D 00
    3 CHANGE=CHANGE-1.0D 00/10.D 00**K
      K=K+1
   10 IF(CHANGE.GE.1.0D 00) GO TO 12
      IF(K.GE.11) GO TO 12
C
C    EQUALIZATION OF THE 2 EXPRESSIONS FOR ACCELERATION OF THE CRACK
C
      DO 20 I=1,11
      CHANGE=CHANGE+1.0D 00/10.D 00**K
      A=(3.0*ALPHA*L*L+BETA)
      B=(ALPHA*L*L*L+BETA*L)
      CO=CHANGE*10.0*HO
      CONS=2.0*WIDTH*35.0*CO*RHO*SPEED**2/3328
      D=2.0*WIDTH*GAM+CONS
      E=1.0/(6.0*ALPHA*L/(B*B)-2.0*A*A/B**3)
      TTO=(B*B*D/(SPEED*SPEED*A))**0.5
      LDOT=(-2.0*SPEED*E/D**0.5)*(A/B**2)**1.5
      X1=-LDOT*LDOT*TERM32-2.0*LDOT/TTO+10.0*TERM42/RHO-20.*GAM*WIDTH*TE
     1RM12/(SPEED*SPEED*RHO*TTO*TTO)
      X2=6.0*SPEED*SPEED*E*A*A/(B**4*D)+(2.0*SPEED*E*E/D**0.5)*(A/(B*B))
```

```
     1**1.5*(6.0*ALPHA*LDOT/(B*B)-36.0*ALPHA*L*A*LDOT/B**3+6.0*A**3*LDOT
     2/B**4)
       IF(I-2)94,97,94
   94  IF(DEFF)98,97,97
   97  DUFF=DIFF/DABS(DIFF)
   98  DIFF=X2-X1
       DEFF=DUFF*DIFF
       IF(DABS(CHANGE).LT.1.0D-04) GO TO 20
       IF(X2)7,5,5
    5  IF(X1)7,4,4
    7  IF(DEFF)3,4,4
C
C    PRINTOUT FOR EACH ITERATION
C
    4  WRITE(6,40)X1,X2,DIFF,CHANGE,CO,D
   40  FORMAT('0',6D21.14)
   20  CONTINUE
C
C    PRINTOUT FOR A SOLUTION ( WHEN X1=X2)
C
   12  WRITE(6,40)X1,X2,DIFF,CHANGE,CO,L
    2  CONTINUE
   22  CONTINUE
       STOP
       END
$ENTRY
```

APPENDIX F. COMPUTER PROGRAM FOR CALCULATING CLEAVAGE ENERGY OF SPECIMENS

```
C.....................................................................
C
C                PROGRAM FOR CALCULATING CLEAVAGE ENERGY
C
C
C     NOPT IS THE OPTION OF USING CUMULATIVE L,TO,(1) OR DELTA L AND TO,(2)
C     GAMMA IS THE CLEAVAGE SURFACE ENERGY IN ERGS/CM**2
C     C EQUALS THE DISTANCE BETWEEN THE DEFLECTION STRIPES IN CENTIMETERS
C     TO IS THE TIME AFTER BREAKAGE OF THE FIRST DEFLECTION STRIPE IN
C     MICROSECONDS.
C     X IS THE NUMERICAL SOLUTION TO THE FINDX SUBROUTINE IN CENTIMETERS
C     LA EQUALS THE INITIAL CRACK LENGTH IN CENTIMETERS.
C     VE IS VELOCITY OF SEPARATION OF THE ENDS OF THE CRYSTAL
C     TERM EQUALS 1/(LOOT*(2*W)**0.5)
C
C
C
      IMPLICIT REAL*8(A-H,L,O-Z)
      DIMENSION TO(14),GAMMA(14),AVGSPD(14)
      COMMON X(14),C(14),GAM,RHO,WIDTH,AK,E,G,AI1,AI2,AIO,A1,A2,AO,N
      DO 21 IN=1,N
C     IN IS THE NUMBER OF SPECIMENS FOR WHICH CALCULATIONS ARE TO BE
C     MADE
      READ(5,2)E,G,AK,RHO,VCM,GAM,M
C     E IS ELASTIC MODULUS, G IS SHEAR MODULUS, AK IS A SHAPE FACTOR,
C     RHO IS SPECIMEN DENSITY, VCM IS KNIFE EDGE SPEED, GAM IS AN
C     ARBITRARY GAMMA VALUE USED IN THE FINDX SUBROUTINE, AND M IS THE
C     SPECIMEN IDENTIFICATION NUMBER.
    2 FORMAT(6E10.4,I2)
      READ(5,3) WIDTH, HEIG1T,HEIG2T,TL,LA,TMPB,N,NOPT
C     WIDTH, HEIG1T, HEIG2T, AND TL ARE SPECIMEN DIMENSIONS.
C     TMPB IS THE TEST TEMPERATURE.
C     N IS THE NUMBER OF DEFLECTION STRIPES ON THE SPECIMEN.
    3 FORMAT (6F10.7, 2I2)
      READ(5,4)(C(II), II=1,N)
C     C(II) IS CUMULATIVE CRACK LENGTH.
    4 FORMAT(14F5.2)
```

```
      READ (5,4) ( TO(IJ), IJ=1,N)
C     TO(IJ) IS CUMULATIVE TIME.
      E=E-0.0003737*(TMPB-23.0)*1.0E 12
      G=G-0.0000525*(TMPB-23.0)*1.0E 12
C     E AND G ARE WRITTEN THIS WAY TO ACCOUNT FOR TEMPERATURE EFFECTS.
      VE=1.510172*VCM
      AI1 = WIDTH* HEIG1T ** 3/12.0
      AI2 = WIDTH * HEIG2T ** 3/12.0
      AIO = 2.0 * AI1 * AI2 /(AI1 +AI2)
      A1 =WIDTH*HEIG1T
      A2 =WIDTH*HEIG2T
      AO=2.0*A1*A2/(A1+A2)
      ALPHA=1.0/(3.0*E*AIO)
      BETA=AK/(AO*G)
      NOPT=NOPT-1
      IF(IN.GT. 1) GO TO 66
C     THE STATEMENT ABOVE IS USED FOR LABELING THE COMPUTER PRINTOUT.
      WRITE(6,65)
   65 FORMAT('1',40X,' CARBON DIOXIDE PURGED > 5 VOLUMES ')
      GO TO 99
   66 IF(IN.GT. 3) GO TO 95
      WRITE(6,86)
   86 FORMAT('1',30X,'RADIATION HARDENED CRYSTALS WITH PREPURIFIED NITRO
     1GEN PURGED > 5 VOLUMES')
      GO TO 99
   95 WRITE(6,96)
   96 FORMAT('1',50X,'ARGON ATMOSPHERE PURGED > 5 VOLUMES')
   99 WRITE (6,5) E,G,AK,RHO,VE,WIDTH,HEIG1T,HEIG2T,NOPT,M,TL,TMPB
    5 FORMAT('0',10X,'E=',E14.7,10X,' G= ',E14.7,10X,' K= ',E14.7,10X,
     1' DENSITY = ',E14.7//' SPEED= ',E14.7,10X,' WIDTH= ', E14.7,
     210X,' HEIGT 1= ',E14.7,10X, ' HEIGT 2= ',E14.7// ' OPTION= ',I2,
     318X,'CRYSTAL NO.=',I2,18X,'TOTAL LENGTH=',E14.7,15X,'TEMPERATURE='
     4,E14.7)
      WRITE(6,22)AO,AIO
   22 FORMAT('0',40X,'AO=',E14.7,20X,'IO=',E14.7)
      WRITE(6,8)
    8 FORMAT('0',5X,'STRIPE',7X,'TERM ',9X,'L/HT',7X,' L ',11X,' TIME ',
```

```
     115X,' X ',17X,' GAMMA ',14X,'AVGSPD')
      VEVEE=VE
      CALL FINDX(HEIG1T,HEIG2T,VEVEE)
C     FINDX IS A SUBROUTINE FOR FINDING X,A NUMBER DEPENDENT ON THE
C     SPECIMEN DIMENSIONS.
      NN=0; GAMTOT=0.0; ASPD=0.0; IR=1
      DO 23 I=1,N
      IF(C(I).LE.LA) GO TO 17
      IF(TO(I).LE.0.0) GO TO 24
C     IF A DEFLECTION STRIPE IS NONCONDUCTIVE TO IS SET EQUAL TO ZERO
C     SO THAT IR GOES TO 2.
      NN=NN+1
      J=I-IR
      AVGSPD(I)=(C(I)-C(J))/((TO(I)-TO(J))*1.0E-06)
      TERM=1.0/(AVGSPD(I)*(2.0*WIDTH)**0.5)
      IF (NOPT.EQ.1) GOTO 6
      TOT=(TO(I)-TO(J))*1.0E-06
      GO TO 14
    6 C(J)=C(M)
      TOT =  TO(I)*1.0E-06
   14 GAMMA(I)=VE*VE*TOT*TOT*(3.0*ALPHA*C(I)**2+BETA)*(3.0*ALPHA*C(J)**2
     1+BETA)/(2.*WIDTH*((ALPHA*C(I)**3+BETA*C(I))*DSQRT(3.0*ALPHA*C(J)**
     22+BETA)-(ALPHA*C(J)**3+BETA*C(J))*DSQRT(3.0*ALPHA*C(I)**2+BETA))**
     32)-35.0*RHO*VE*VE*X(I)/3328
      ASPD=ASPD+AVGSPD(I)
      GAMTOT=GAMTOT+GAMMA(I)
      LF=C(I)/(HEIG1T+HEIG2T)
      WRITE(6,9)I,TERM,LF,C(I),TO(I),X(I),GAMMA(I),AVGSPD(I)
    9 FORMAT(' ',7X,I2,4X,E14.7,4X,F5.2,6X,F5.2,6X,E14.7,10X,F5.2,13X,F1
     10.3,12X,F10.3)
      SIG=(C(N)-C(M))/(TO(N)*1.0E-06)
C     SIG IS AVERAGE CRACK SPEED.
      IR=1
      GO TO 23
   24 IR=IR+1
      GO TO 23
   17 M=I
```

```
C      I IS STRIPE NUMBER OF STRIPE WHERE TIME MEASUREMENT BEGINS.
   23 CONTINUE
      SIGMA=ASPD/NN
C     SIGMA IS MEAN SPEED.
      GAMT=GAMTOT/NN
C     GAMT IS MEAN CLEAVAGE ENERGY.
      WRITE(6,77)GAMT,SIGMA,SIG
   77 FORMAT('0',16X,'THE MEAN GAMMA='F10.3,7X,'THE MEAN SPEED='F10.3,7X
     1,'THE AVERAGE SPEED='F10.3)
   21 CONTINUE
      STOP; END
      SUBROUTINE FINDX(HEIGT1,HEIGT2,SPEED)
      IMPLICIT REAL*8(A-H,L,O-Z)
      COMMON X(14),C(14),GAM,RHO,WIDTH,AK,E,G,AI1,AI2,AIO,A1,A2,AO,N
      ELAST=E
      GSHEAR=G
      DO 2 JJ=1,N
      L=C(JJ)
   92 L2=L*L
      L3=L**3
      L5=L**5
      L7=L**7
      L9=L**9
      L11=L**11
      L13=L**13
      ALPHA=1.0/(3.0*ELAST*AIO)
      ALPHA2=ALPHA**2
      ALPHA3=ALPHA**3
      BETA=AK/(AO*GSHEAR)
      BETA2=BETA**2
      BETA3=BETA**3
      C1STAR=(WIDTH/(6.0*ELAST)**2)*(HEIGT1*AI2**2+HEIGT2*AI1**2)/(AI1**
     12*AI2**2)
      C2STAR=(AK*WIDTH/(3.0*ELAST*GSHEAR))*(HEIGT1*AI2*A2+HEIGT2*AI1*A1)
     1/(AI1*A1*AI2*A2)
      C3STAR=((AK**2)*WIDTH/GSHEAR**2)*(HEIGT1*A2**2+HEIGT2*A1**2)/(A1**
     12*A2**2)
```

```
      ALPBET=(ALPHA*L3+BETA*L)
      TERM4=(3.0*ALPHA*L**2+BETA)/ALPBET**2
      TERM2=((48.0/35.0)*C1STAR*L11*ALPHA2+(228.0/35.0)*C1STAR*ALPHA*BET
     1A*L9+(444.0/35.0)*C1STAR*L7*BETA2-(0.6)*C2STAR*L9*ALPHA2-3.4*C2STA
     2R*ALPHA*BETA*L7+1.6*C2STAR*L5*BETA2+2.0*C3STAR*L7*ALPHA2+(2.0/3.0)
     3*C3STAR*L3*BETA2)/ALPBET**4
      TERM3=((-24.0/35.0)*C1STAR*L13*ALPHA3-(174.0/35.0)*C1STAR*BETA*L11
     1*ALPHA2-(540.00/35.0)*C1STAR*ALPHA*L9*BETA2+(660.0/35.0)*C1STAR*L7
     2*BETA3+(18.0/20.0)*C2STAR*L11*ALPHA3+7.0*C2STAR*BETA*L9*ALPHA2-(21
     34.0/20.0)*C2STAR*ALPHA*L7*BETA2+0.8*C2STAR*L5*BETA3-5.0*C3STAR*ALP
     4HA3*L9+3.0*C3STAR*ALPHA2*BETA*L7-3.0*C3STAR*ALPHA*BETA2*L5-(1.0/3.
     50)*C3STAR*BETA3*L3)/ALPBET**5
      TERM42=TERM4/TERM2
      TERM32=TERM3/TERM2
      TERM12=1.0/TERM2
      SHRBM=BETA/(ALPHA*L2)
      K=0
      DIFF= 1.0D 00
      DEFF=1.0D 00
      CHANGE=0.9D 00
    3 CHANGE=CHANGE-1.0D 00/10.D 00**K
      K=K+1
   10 IF(CHANGE.GE.1.0D 00) GO TO 12
   15 IF(K.GE.11) GO TO 12
      DO 20 I=1,11
      CHANGE=CHANGE+1.0D 00/10.D 00**K
      CO=2.0*WIDTH*HEIGT1*70.*CHANGE
      A=(3.0*ALPHA*L*L+BETA)
      B=(ALPHA*L*L*L+BETA*L)
      D=2.0*GAM*WIDTH+CO
      E=1.0/(6.0*ALPHA*L/(B*B)-2.0*A*A/B**3)
      TTO=(B*B*D/(SPEED*SPEED*A))**0.5
      LDOT=(-2.0*SPEED*E/D**0.5)*(A/B**2)**1.5
      X1=-LDOT*LDOT*TERM32-2.0*LDOT/TTO+10.0*TERM42/RHO-20.*GAM*WIDTH*TE
     1RM12/(SPEED*SPEED*RHO*TTO*TTO)
      X2=6.0*SPEED*SPEED*E*A*A/(B**4*D)+(2.0*SPEED*E*E/D**0.5)*(A/(B*B))
     1**1.5*(6.0*ALPHA*LDOT/(B*B)-36.0*ALPHA*L*A*LDOT/B**3+6.0*A**3*LDOT
```

```
      2/B**4)
         IF(I-2)94,97,94
   94 IF(DEFF)98,97,97
   97 DUFF=DIFF/DABS(DIFF)
   98 DIFF=X2-X1
         DEFF=DUFF*DIFF
         IF(DABS(CHANGE).LT.1.0D-04) GO TO 20
    7 IF(DEFF)3,4,4
    4 X(JJ)=CO*3328/(70.0*WIDTH*SPEED*SPEED*RHO)
   20 CONTINUE
   12 GO TO 2
    2 CONTINUE
      RETURN; END
$ENTRY
```

ACKNOWLEDGEMENTS

The author is indebted to Dr. John T. Jones and Dr. Thomas D. McGee for their encouragement and participation in many helpful discussions throughout the course of this study, to Mr. William Determan for his valuable assistance in sample preparation and computer analysis, and to Miss Verna Thompson for typing the manuscript. The financial support provided by Aerospace Research Laboratories, Office of Aerospace Research, United States Air Force, under contract number F33615-68-C-1034 is gratefully acknowledged.